MAX-PLANCK-INSTITUT FÜR PLASMAPHYSIK

GARCHING BEI MÜNCHEN

Elastic Processes in Hydrogen-Helium Plasmas: Collison Data

P. Bachmann[1], H.J. Belitz[2]

IPP 8/2 June 1993

[1] Max-Planck-Institut für Plasmaphysik, D-10117 Berlin, Germany
[2] Institut für Plasmaphysik, Forschungszentrum Jülich GmbH, D-52425 Jülich, Germany

Die nachstehende Arbeit wurde im Rahmen des Vertrages zwischen dem Max-Planck-Institut für Plasmaphysik und der Europäischen Atomgemeinschaft über die Zusammenarbeit auf dem Gebiete der Plasmaphysik durchgeführt.

Elastic Processes in Hydrogen-Helium Plasmas: Collision Data

P. Bachmann[1], H.J. Belitz[2]

[1] Max-Planck-Institut für Plasmaphysik, D-10117 Bereich Berlin, EURATOM Association, Hausvogteiplatz 5-7, Berlin, Germany

[2] Institut für Plasmaphysik, Forschungszentrum Jülich GmbH, Association EURATOM-KFA, Postfach 1913, D-52425 Jülich, Germany

June 8, 1993

Abstract

This report is intended to provide collision data and data fits for implementing elastic collisions between neutrals and ions in neutral gas transport codes.

Classical methods are employed to calculate cross sections and collision rates for elastic collisions between neutral atoms or molecules and ions. The algorithm for deriving all relevant data needed for kinetic description such processes in a background plasma with Maxwellian ion velocity distribution is presented. Data fits for these quantities are presented for hydrogenic and helium species. Furthermore data fits for the Ω integrals needed in a hydrodynamic description are given. The implementation of such processes into kinetic Monte Carlo neutral gas transport models is described.

Contents

1 Introduction

Neutral gas transport studies in tokamak plasmas have routinely been carried out in the past by employing analytical, numerical and Monte Carlo methods. Until recently, inelastic processes such as ionization, dissociation and charge exchange have been considered exclusively. The need to establish a high recycling regime near divertor targets to allow efficient impurity control and ash removal has focused attention on high density, low temperature boundary plasmas. Under such conditions, however, elastic collisions between neutrals and ions become more important. They are, essentially, thermalization and backscattering (i.e. momentum transfer-) processes for neutral particles penetrating a plasma and they are relevant up to plasma temperatures of about 10 to $20eV$.

Therefore, neglecting them is a very good approximation in model calculations addressing neutral gas transport properties in early limiter or divertor tokamaks and they often are irrelevant even for present day divertor plasma conditions. However, in some recent divertor tokamak experiments, as e.g. in DIII-D, JET, and ASDEX Upgrade (refs.[26], [27], [14]) such low temperatures and sufficiently large densities have been measured. Moreover, such conditions are presently considered necessary for achieving acceptable particle and energy removal efficiencies and simultaneously tolerably low surface erosion. Next generation divertor concepts will focus on such conditions, as for example the so called "charge exchange divertor" for ITER ([21]). Therefore, it is timely to implement elastic collision processes into the various neutral gas transport models used for evaluating such divertor concepts and for interpretation of data from experiments addressing these issues. In two previous papers the effects of such collision processes have been described. Firstly, in refs. [3], [4] we employed a simple relaxation ansatz, a slab configuration and used analytical methods (verified by independent Monte Carlo solutions of the same model equations). Secondly, in ref. [24] the full linear collision kernel and it's implementation into a general Monte Carlo neutral gas transport algorithm code was briefly summarized, and first exemplary applications to a simulation model for the ASDEX Upgrade divertor was given. In particular, the neutral helium transport was investigated.

In this report, both for reference purposes and for providing the basis for extending the model to other elastic collision processes we derive a complete and consistent set of data needed to simulate such process from first principles. Discussion is restricted to the

classical theory of binary collisions. Thus all quantities are then directly derived from the interaction potential field, and from the laws of energy and momentum conservation.

All data needed for implementing elastic neutral-ion collisions will be derived, and we will also provide those derived quantities which are useful for a consistent neutral gas - plasma transport calculation (i.e. Maxwellian averaged momentum and energy exchange rates) and which often are missing in atomic and molecular databases (section 3).

A motivation and key consideration in the present paper is to present data in such a format that they may easily implemented in neutral gas transport codes, and, in particular, in kinetic Monte Carlo algorithms. These latter procedures require very frequent evaluation of the scattering angles for collisions between two individual randomly selected particles. The data required and the implementation of this process in general and into the EIRENE code in particular is described in section 4.

Collision data are calculated for binary elastic collisions between neutral particles and ions. Starting point is the interaction potential for the colliding particles which is taken from literature. All information needed in a classical decription is contained in the classical deflection function χ. From this, total cross sections, transport and viscosity cross sections (sections 2) as well as rate coefficients and momentum and energy exchanges rates are derived (section 3). These rates as well as the collision rates needed in a hydrodynamic description (Ω integrals) are fitted to polynomial expressions (section 6).

Whereas the discussion is kept general in sections 2, 3, the following processes will be considered in detail in this paper: $H^+ + H$ [7] (section 5.2), $H^+ + He$ [7], [8], [1] (section 5.3), $H^+ + H_2$ [10] (section 5.4), $He^+ + He$ (section 5.5). However, the procedure outlined here is kept general to permit other collisions to be treated in the same framework.

Results to an ASDEX-Upgrade SOL Plasma model will be published in a forthcoming paper.

2 Classical Collision Kinetics

2.1 Fundamentals

A binary collision event between two particles of masses m_1 and m_2, moving with velocities $\vec{v}_1$ and $\vec{v}_2$ at the points $\vec{r}_1$ and $\vec{r}_2$, respectively, is described within the framework of a classical theory as the motion of a point with the reduced mass m_r and the relative energy E_r in the effective potential field $V_{eff}(r)$:

$$V_{eff} := V(r) + E_r(b/r)^2, \tag{1}$$

$$E_r := m_r v_r^2/2,\ m_r := m_1 m_2/(m_1+m_2),\ v_r :=\mid \vec{v}_1 - \vec{v}_2 \mid,\ r :=\mid \vec{r}_1 - \vec{r}_2 \mid;$$

b is the classical impact parameter and V is the interaction potential field. We define the function

$$\phi(r, b, E_r) := 1 - V_{eff}(r)/E_r \equiv 1 - V(r)/E_r - (b/r)^2. \tag{2}$$

If the equation

$$\phi(r, b, E_r) = 0 \tag{3}$$

has the positiv roots

$$r_i(b, E_r);\ i = 1, ..., n;$$

the distance of closest approach from infinity, r^*, is given by

$$r^* := \begin{cases} max\{r_i\} & ,n \geq 1, \\ 0 & ,\text{otherwise.} \end{cases} \tag{4}$$

The classical deflection function χ is then defined as:

$$\chi(b, E_r) := \pi - 2b \int_{r^*}^{\infty} dr\ r^{-2}\ \phi^{-1/2}. \tag{5}$$

In the classical approach all information needed is contained in this deflection angle χ. Its functional properties depend on the nature of the potential function $V(r)$ which will be discussed in more detail for repulsive and Morse-like potentials in sections 2.2.1, 2.2.2, respectively. Due to attraction χ may become negative, and even, in case of spiraling (see below), χ may range from $-\infty$ to π. The observable scattering angle, θ, ranges from 0 to π and follows directly from χ, e.g. via the relation $\theta = \arccos(\cos(\chi))$.

The differential elastic cross section $\sigma(\theta, E_r)$ is determined by the deflection function (5) with the following relation

$$\sigma(\theta, E_r) := \sum_i b_i \mid db_i/d\chi \mid / \sin\theta \tag{6}$$

where the summation is over the branches $b_i(\chi)$ of the, in general, multivalued function $b(\chi)$. $\sigma^t(\theta, E_r)$ is unbounded if either $\theta = 0$ or $\theta = \pi$ for impact parameters b different from zero ("glory scattering") if the deflection function has a local minimum, i.e. $\partial\chi/\partial b_r = 0$ ("rainbow scattering") for some $b_r > 0$.

The total cross section $\sigma^t(E_r)$, the diffusion cross section $\sigma^d(E_r)$ and the viscosity cross section $\sigma^v(E_r)$ are defined by the following equations, respectively:

$$\sigma^t(E_r) := 2\pi \int_0^\pi d\theta \ \sin\theta \ \sigma(\theta, E_r); \tag{7}$$

$$\sigma^d(E_r) := 2\pi \int_0^\pi d\theta \ \sin\theta \ (1 - \cos\theta) \ \sigma(\theta, E_r) \tag{8}$$

$$= 4\pi \int_0^\infty dbb \ \sin^2\left[\frac{1}{2}\chi(b, E_r)\right]; \tag{9}$$

$$\sigma^v(E_r) := 2\pi \int_0^\pi d\theta \ \sin\theta \ (1 - \cos^2\theta) \ \sigma(\theta, E_r) \tag{10}$$

$$= 2\pi \int_0^\infty dbb \ \sin^2\chi(b, E_r). \tag{11}$$

Inserting (6) into (7) yields the well known result that finite classical total cross sections are obtained only for interaction potentials with finite range. The potentials considered in this paper do not have this property, i.e. the total classical cross section would become infinite. This problem could be dealt with more rigorously in a quantum mechanical treatment only. However, in our strictly classical approach a cut-off angle χ_0 has to be introduced in order to obtain finite results. Clearly, this cross-section is then largely determined by this choice, which therefore must be based on physical arguments. Distinct from the total cross section the diffusion cross section and also the viscosity cross section remains finite at least for potentials which tend to zero at infinity faster than r^{-1} (s. section 2.2.3). In order to define a meaningful cut-off angle χ_0 (s. Appendix 1) we first point out that the diffusion cross section is the physically more relevant quantity since it weights collisions according to their influence on transport effects. We evaluate, therefore, the integral (9) for a decreasing sequence of cut-off angles χ_0 until it does not

change significantly anymore. In particular we require χ_0 to be small enough such that the correct diffusion cross section is accurately represented within about 1 percent by the diffusion cross section obtained with this cut-off angle.

It is shown in section 7 that $\mid \chi_0 \mid = 0.1$ fulfills this criterion for all collision processes considered here.

In Appendix 2 we discuss a semi-classical approach for calculating total cross sections. The numerical results obtained there agree rather satisfactorily with the classical results, thus serving as independent justification for the above choice of the cut-off parameter.

2.2 Numerical Procedure

Within the framework of our classical approach the deflection function χ completely describes the collisions process. To obtain this function we have to compute the integral

$$I(b, E_r) := \int_{r^*}^{\infty} dr \; r^{-2} \; \phi^{-1/2}, \tag{12}$$

in which $\phi(r^*) = 0$. To investigate the convergence of this integral at the lower integration limit we expand the function ϕ at r^* up to the second order:

$$\phi(r) \simeq \phi'(r^*) \; (r - r^*) + \frac{1}{2}\phi''(r^*) \; (r - r^*)^2 + ... \tag{13}$$

We distinguish the following cases:

$$\phi'(r^*) \neq 0; \tag{14}$$

$$\phi'(r^*) = 0 \; , \; \phi''(r^*) \neq 0; \tag{15}$$

$$\phi'(r^*) = 0 \; , \; \phi''(r^*) = 0. \tag{16}$$

The integral (12) is finite only for the first case (14). For the second case (15) it is logarithmically divergent. For the third case (16) it is also divergent, but of higher order. For an interaction potential $V(r)$ for which the condition (15) or (16) is accessible for some values b and E_r, the integral (12) (and therefore the deflection function χ) is unbounded ("capture").

Considering the first case suggests a Gaussian quadrature rule with weighting $(r-r^*)^{1/2}$ for the integral (12). This leads to a Gauss-Mehler quadrature [15] for the integral (12):

$$I = \frac{1}{r^*} \int_0^1 dx \, \frac{1}{\sqrt{1-x}} \sqrt{\frac{1-x}{\phi(r^*/x)}}. \tag{17}$$

We use, instead, the slightly different quadrature rule:

$$I = \frac{1}{r^*} \int_0^1 dx \, \frac{f(x)}{\sqrt{x(1-x)}} \, , \; f(x) := \sqrt{\frac{x(1-x)}{\phi(r^*/x)}}, \tag{18}$$

$$\cong \frac{1}{r^*} \sum_{i=1}^{n} w_i \, f(x_i) \tag{19}$$

because the abscissas x_i and weights w_i are given by closed form expressions [2]:

$$x_i := \left(1 + \cos \frac{2i-1}{2n}\pi\right), \; w_i := \frac{\pi}{n}. \tag{20}$$

This finally leads to the following approximated expression for the deflection function:

$$\chi \cong \pi \left[1 - \frac{2b}{nr^*} \sum_{i=1}^{n} \sqrt{\frac{x_i(1-x_i)}{\phi(r^*/x_i)}}\right]. \tag{21}$$

The evaluation of χ can be carried out very efficiently, with $n = 8$ or $n = 16$ resulting already in approximation errors less than 1 percent (except near "glory"- or "rainbow" scattering). The computational efford is determined by the efficiency of the root finding procedure for r^*. One should note that in a Monte Carlo procedure (see section 4) in general many thousand evaluations of χ (and therefore of r^*) are necessary. Representations which are faster than (21) would be desirable. For an inverse power potential $V(r) \sim r^{-n}$, for instance, an expansion of χ in $V(b)/E_r$ can be carried out, leading to single parametric dependency for the deflection function χ (s. [20], [5]). For the potentials considered in this report, however, analogous formulae do not seem to be known.

In the following we consider two classes of potentials: purely repulsive (Case I) and Morse-like potentials with one repulsive and one attractive component (Case II).

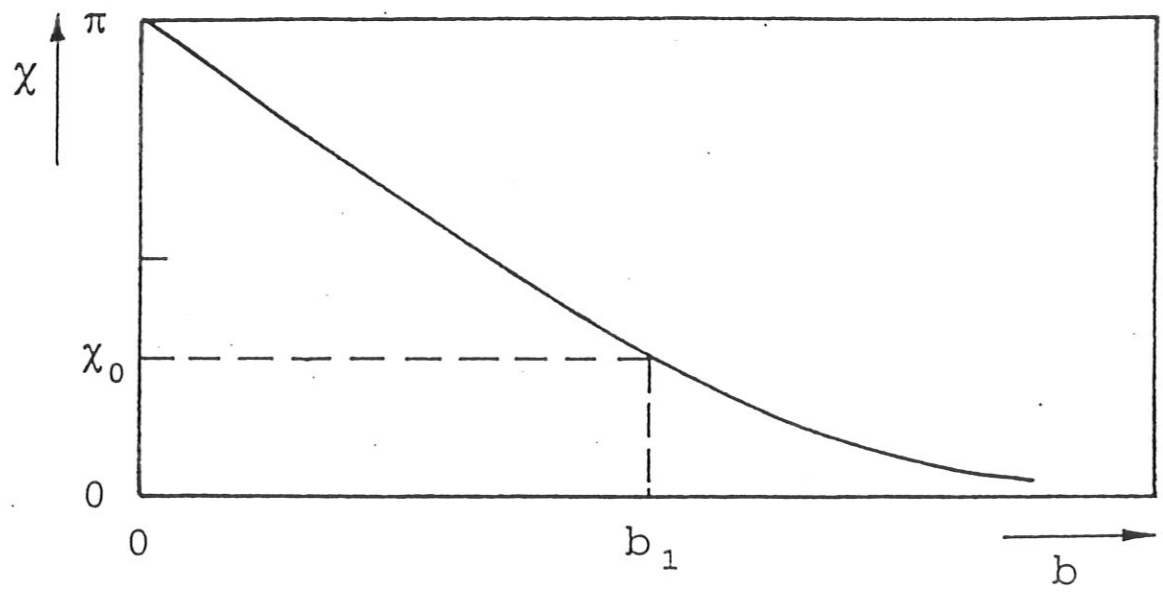

Figure 1: Qualitative behaviour of the classical deflection function χ for Case I (repulsive potential).

2.2.1 Case I: Repulsive Potential

For a repulsive potential the deflection function χ is a one-to-one relation of the impact parameter b. It decreases monotonically from π to 0 with increasing b (Fig. 1) and can very accurately be represented by a two-parameter fit

$$\chi \simeq \sum_{m=0}^{M} \sum_{n=0}^{N} A(m,n)\, b^n\, (\ln E_r)^m, \tag{22}$$
$$b_{min} \leq b \leq b_{max},\ E_{rmin} \leq E_r \leq E_{rmax}$$

with matrix elements $A(m,n)$ obtained by a least square fit procedure (cp. section 5.2).

Performing the integration in eq. (7) from χ_0 to π and using the relation (6) we obtain for the total elastic cross section:

$$\sigma^t(E_r) \cong 2\pi \int_0^{b_1} dbb = \pi b_1^2(E_r), \tag{23}$$

with the maximum impact parameter $b_1(E_r)$ defined by

$$b_1(E_r) := \{b : \chi(b, E_r) = \chi_0\} \tag{24}$$

(cp. Fig. 1). The total cross section $\sigma^t(E_r)$ can be approximated by the two quadratic

fits according to

$$ln\ \sigma^t(E_r) \simeq \sum_{n=0}^{2} a_n\ (\ln E_r)^n, \qquad E_r \leq E_r^*, \tag{25}$$

$$ln\ \sigma^t(E_r) \simeq \sum_{n=0}^{2} b_n\ (\ln E_r)^n, \qquad E_r > E_r^*. \tag{26}$$

The diffusion and viscosity cross sections (8) (10) are calculated by means of the trapezoidal rule and can also be fitted according to (cf. [13]):

$$ln\ \sigma^{d,v}(E_r) \simeq \sum_{n=0}^{N} a_n^{d,v}\ (\ln E_r)^n, \qquad E_{rmin} \leq E_r \leq E_{rmax}. \tag{27}$$

(Cp. sections 5.2 - 5.5.)

2.2.2 Case II: Morse-like Potential

A variety of model potential functions are used in the literature to describe short range repulsive - long range attractive interaction between two particles (cf. [28]). A particular form of such potential functions, which has the advantage of a small number of parameters is the so called Morse potential with a cut-off at the minimum (cf. [18]). It is defined by the formula

$$V(r) := \epsilon \left[e^{2g(1-\rho)} - 2\ e^{g(1-\rho)}\right], \tag{28}$$

$$\rho := \frac{r}{r_m},\ g := \begin{cases} g_1 & \text{for } \rho < 1 \\ g_1 g_2 & \text{for } \rho \geq 1 \end{cases} \tag{29}$$

ϵ is the potential depth, r_m the equilibrium separation (cp. Fig. 2); g_1, g_2 are constants. The greater the value of g the narrower the width of the the potential field. All short range repulsive - long range attractive collision processes considered in this report (sects. 5.3, 5.4,5.5) are described by such Morse-like potential functions. Some characteristic features of this potential function (28) are:

Finite value at

$$r = 0 : V(0) = \epsilon \left(e^{2g} - 2\ e^{g}\right); \tag{30}$$

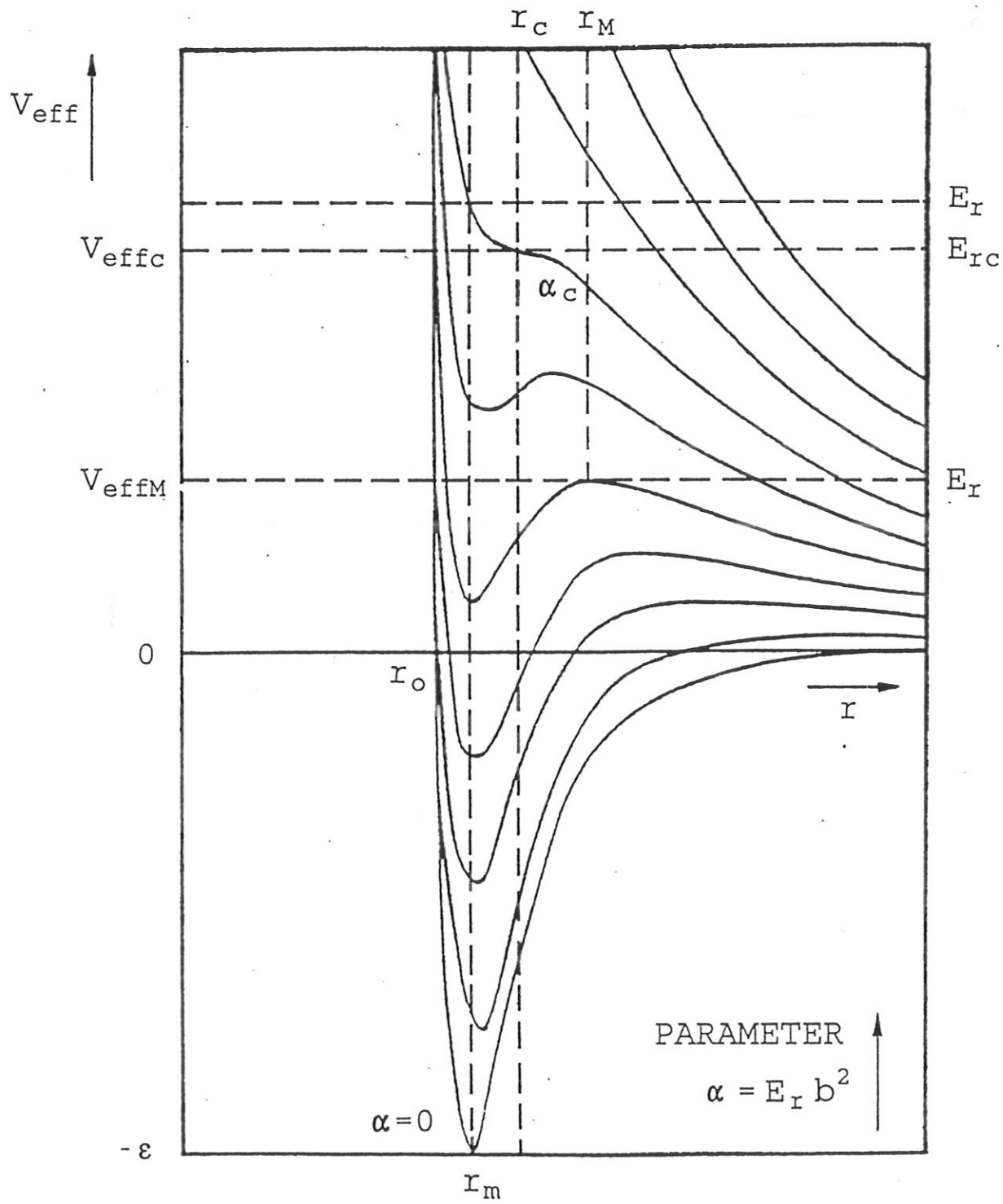

Figure 2: Effective potential V_{eff} for Case II (eq. (33)) as function of r for different values of α which increases upwards.

one root

$$r_0 := r_m \left(1 - \frac{\ln 2}{g}\right), \; V(r_0) = 0; \tag{31}$$

one minimum at

$$r_m : V'(r_m) = 0, \; V(r_m) = -\epsilon; \tag{32}$$

one point of inflection at

$$r_w := r_m \left(1 + \frac{\ln 2}{g}\right), \; V''(r_w) = 0, \; V'(r_w) = \frac{\epsilon g}{2r_m}, \; V(r_w) = -\frac{3\epsilon}{4}. \tag{33}$$

To compute the deflection function χ by means of eq. (21) the roots r^* of eq. (3) have to be determined. In order to discuss this, we rewrite eq. (3) as

$$V_{eff} \equiv V(r) + \frac{\alpha}{r^2} = E_r, \quad \alpha := E_r b^2 \tag{34}$$

(α is proportional to the square of the angular momentum). If there are more than one solutions of (34), r^* is understood to be the largest one. Typical curves of the effective potential (34) are displayed in Fig. 2 with α being the parameter. It can be seen that there exists a "critical" curve with the "critical" parameter $\alpha_c := E_{rc} b_c^2$ such that all curves with $0 < \alpha < \alpha_c$ have one maximum, one minimum and one point of inflection which coincide at the critical curve. For $\alpha > \alpha_c$ the effective potential decreases monotonically with increasing r and approaches 0 at ∞. In this case the potential acts purely repulsive and can be treated as Case I. For $\alpha \leq \alpha_c$ "orbiting solutions" may appear, which differ fundamentally from those ones of Case I. These orbiting solutions lead to singularities in the deflection function χ which correspond physically to the mutual capture of colliding particles. The classical orbiting condition is that the equation (34) has multiple roots leading to divergent integrals for χ. This is the case when the relative energy E_r coincides with the maximum value of V_{eff}: $E_r = V_{eff}(r_M)$ with $r_M(\alpha)$ denoting the separation at the maximum of V_{eff}. Of course, at the maximum point $r_M(\alpha)$ the condition (15) holds, while the eqs. (16) determine the critical distance r_c and the other critical parameters r_c, E_{rc} and b_c.

These critical parameters can be determined as follows:
Assume that the relative energy E_r is given. We then seek a solution of both equations $V_{eff} = E_r$ and $V'_{eff} = 0$ with $V(r)$ given by eq. (28). We obtain the equation

$$E_r = h(r) := V(r) + \frac{r}{2} V'(r) \tag{35}$$

that defines the auxiliary function $h(r)$ and represents the equation to be solved. The root r_M of this equation can, in general, only be found numerically. When such a solution r_M is known, the corresponding impact parameter b_M follows from

$$b_M = r_M \sqrt{1 - V(r_M)/E_r}, \tag{36}$$

and furthermore: $\alpha_M \equiv E_r b_M^2$. For Morse-like potential functions (28) $h(r)$ has one maximum at the critical separation r_c. I.e. there exists a critical energy E_{rc} above which eq. (35) has no solutions. If r_c is known the other critical parameters follow according to

$$E_{rc} = \epsilon \frac{(p-3)\,(p^2-3p+3)}{(2p-3)^2} \tag{37}$$

with $p := r_c g/r_m$ and

$$b_c = \frac{p r_c}{\sqrt{p^2-3p+3}}, \tag{38}$$

and, finally, $\alpha_c \equiv E_{rc} b_c^2$.

In Fig. 3 the dependence of the separation at the maximum r_M on the relative energy E_r for R2 is shown. On the basis of these quantities we can now discuss the procedure to find the distance r^* of closest approach.

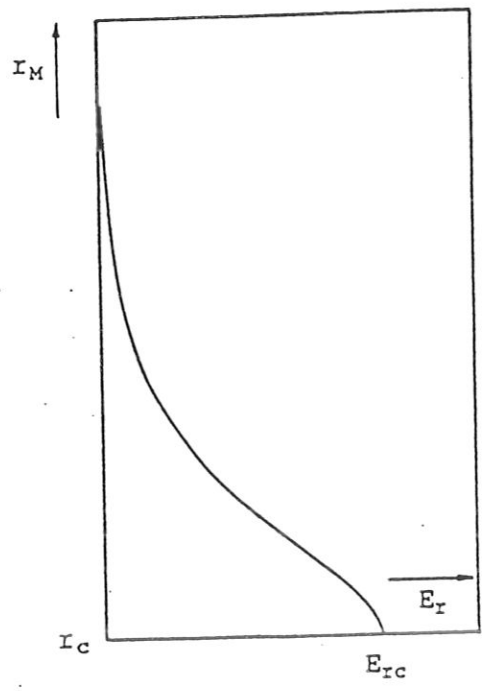

Figure 3: Dependence of the separation at the maximum r_M on the relative energy E_r for R2 $H^+ + He$.

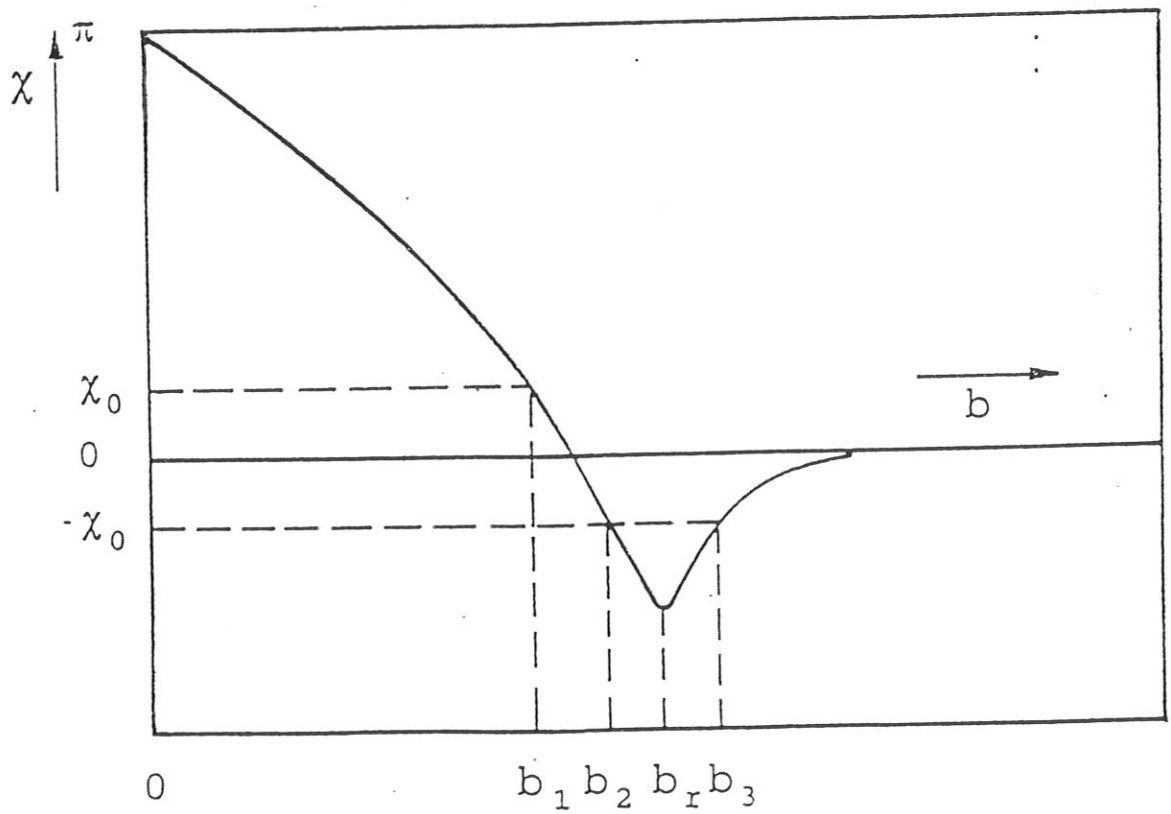

Figure 4: Qualitative behaviour of the classical deflection function χ for a Morse-like potential (Case II).

r^* Discussion ($C(r^*)$):

We try to find the roots r^* in dependence of the collision parameter b and the relative energy E_r under the condition to keep the numerical computation time as low as possible. Assume that the characteristic distances $r_0 < r_m < r_w < r_c < b_c$ and the critical energy E_r are given for each collision process. We define $\mu := \sqrt{E_{rc}/E_r}$.

Independent from the value of the relative energy E_r it is:

(i) $0 \leq b \leq r_0$:

1 root r^* with $b \leq r^* \leq r_0$.

(ii) $r_0 < b \leq r_w$:

1 root r^* with $r_0 < r^* \leq r_w$.

For $b > r_w$ it is:

(iii) $\mu < 1 \wedge \mu b_c < r_w$:

1 root r^* with $r^* > r_0$.

(iv) $\mu < 1 \wedge \mu b_c > r_w$:

(iva) $r_w < b < \mu b_c$:

1 root r^* with $r_0 < r^* < r_c$.

(ivb) $b \geq \mu b_c$:

1 root r^* with $r^* > r_0$.

(v) $\mu > 1 (\mu b_c > r_w)$:

(va) $r_w < b < \mu b_c$:

1, 2, or 3 roots r_i with $r^* := max\{r_i\} > r_w$.

(vb) $b \geq \mu b_c$:

1 root r^* with $r^* \geq r_c$.

(va) can be simplified furthermore if $r_M(E_r)$ (cp Fig. 3) is known.

In summarising the above results, we note: each collision process described by the Morse-like potential eqs. (28), (29) is determined by the 9-parameter set $\vec{R}$:

$$\vec{R} = (\epsilon, g_1, g_2, r_m, r_0, r_w, r_c, b_c, E_{rc}). \tag{39}$$

The first four parameters define the potential field. r_0, r_w are given by eqs. (31), (33), respectively. The last three parameters (numerical calculation) are interrelated by eqs. (37), (38). So for each collision process $\vec{R}$ the deflection function $\chi(b, E_r)$ can be calculated by Gauss-Mehler integration (21) with a numerically determined r^* by means of the

above procedure $C(r*)$. The qualitative behaviour of this deflection function is shown in Fig. 4. χ is no longer a one-to-one relation of b. Several classical trajectories may contribute to the same scattering angle χ: the positive angles correspond to net repulsion and the negative angles to net attraction. In Fig. 4 the three different impact parameters b_1, b_2, b_3 correspond to the same observable scattering angle χ_0. The *rainbow scattering* results from a minimum of the deflection function χ for low energies at the rainbow point $(b_r, \chi_r), \chi_r(E_r) := \chi(b_r, E_r)$. For relative energies smaller than the critical energy $E_r < E_{rc}$ rainbow scattering corresponds to mutual capture: $(b_r, \chi_r) \equiv (b_M, -\infty)$.

For Case II the cross section is no longer given by the expression (23) which is valid only for Case I. It has to be changed as follows.

We start by introducing one further characteristic energy E_{r0} which is defined as that energy where the three points b_2, b_r, b_3 coincide (s. Fig. 4):

$$b_i(E_r) := \{b :\mid \chi(b, E_r) \mid = \chi_0 \wedge b_1 \leq b_2 \leq b_3\}, i = 1, 2, 3, \tag{40}$$

$$E_{r0} := \{E_r : \chi_r(E_r) = -\chi_0\}. \tag{41}$$

For relative energies E_r not less than E_{r0} the total cross section is (as in Case I) given by πb_1^2 (eqs. (23), (24)). Otherwise ($E_r < E_{r0}$), it has to be changed to

$$\sigma^t(E_r) \cong 2\pi \left(\int_0^{b_1} dbb + \int_{b_2}^{b_3} dbb \right) = \pi \left(b_1^2 - b_2^2 + b_3^2 \right). \tag{42}$$

If b_3 is very large compared to b_1, b_2 the rainbow scattering dominates and the total cross section is approximately given by $\sigma^t \simeq \pi b_3^2$. With increasing relative energy E_r the minimum χ_r will be less pronounced and $b_3 \to b_2$. In this limit this results in $\sigma^t \to \pi b_1^2$, which, indeed, is the result for $E_r \geq E_{r0}$. So finally we can define the total cross section as follows:

$$\sigma^t(E_r) := \pi \begin{cases} b_1^2 & \text{for} \quad E_r \geq E_{r0}, \\ b_1^2 - b_2^2 + b_3^2 & \text{for} \quad E_r < E_{r0}. \end{cases} \tag{43}$$

Indeed, this cross section is a continuous function of the relative energy. In particular, there is no cut-off at E_{r0} in our cross section results as it was the case in those of refs. [7], [8] (s. Fig. 8 where one result of [7] is also included). Moreover, extending the definition of E_{r0} such that it is 0 for Case I one sees that the expression (43) includes also this case. Because the functional dependence of the total cross section on E_r is different for both

energy ranges (see section 5). We therefore need two different representations for the two different energy ranges.

Contrary to the total cross section the diffusion and the viscosity cross sections (8), (10) do not have the slowly decreasing high energy tail (see the discussion of the asymptotics following section 2.2.3 and the results in section 5).

The total, diffusion and viscosity cross sections can be approximated by the least square fit

$$ln\ \sigma^{t,d,v}(E_r) \simeq \sum_{n=0}^{N} a_n^{t,d,v}\ (\ln E_r)^n, \qquad E_{rmin} \leq E_r \leq E_{rmax}. \tag{44}$$

Outside the range of validity of the approximation we need asymptotic expressions for the cross sections.

2.2.3 Asymptotic Behaviour of the Cross Sections

We have calculated the cross sections in the energy range of from $0.01eV$ to $100eV$. One needs, however, for the integration involved in evaluation of the collision rates (section 3), the data for the whole energy range $(0, \infty)$. Therefore we now discuss the limiting behaviour of the cross sections for low and high energies, respectively.

(i) $E_r \rightarrow \infty$

For this case the perturbation expression can be derived from eq. (5):

$$\chi(b, E_r \rightarrow \infty) \simeq -\frac{F(b)}{E_r}, \tag{45}$$

$$F(b) := \int_1^\infty dx\ \frac{xV(bx)}{(x^2-1)^{3/2}}. \tag{46}$$

For the following model potential function, which is assumed to give representative asymptotic estimations for both considered Cases I and II,

$$V(r) := \sum_{i=1}^{n} a_1\ e^{-c_i r},\ c_i > 0 \tag{47}$$

F can analytically be expressed as:

$$F(b) = -\ b \sum_{i=1}^{n} a_i c_i\ K_0(bc_i) \tag{48}$$

with K_0 being the modified Bessel function of zeroth order. This results in the closed form expression for the deflection function

$$\chi = \frac{b}{E_r} \sum_{i=1}^{n} a_i c_i K_0(bc_i). \tag{49}$$

If the argument of the modified Bessel function is large, the leading term of the asymptotic expansion [2]

$$K_n(x) \sim \sqrt{\frac{\pi}{2x}}\, e^{-x} \left(1 + O\left(\frac{1}{x}\right)\right) \tag{50}$$

can be used. Considering only the largest term, denoted by l, the following equation

$$\sqrt{\frac{\pi}{2}} \mid a_l \mid \sqrt{bc_l}\, \frac{1}{E_r}\, e^{-bc_l} = \mid \chi_0 \mid \tag{51}$$

has to be solved. Replacing b in the square root by a representative mean value $\bar{b}$, we obtain the solution

$$b_1 = \frac{1}{c_l} \ln \frac{\tilde{E}_r}{E_r}, \quad \tilde{E}_r := \sqrt{\frac{\pi}{2}}\, \frac{\mid a_l \mid \sqrt{\bar{b}c_l}}{\chi_0}. \tag{52}$$

By means of eq. (43) we obtain the asymptotic expression for the total cross section:

$$\sigma^t(E_r \to \infty) \simeq \frac{\pi}{c_l^2} \left(\ln \frac{\tilde{E}_r}{E_r}\right)^2. \tag{53}$$

Defining the constants A, B by

$$A := B \ln \tilde{E}_r, \tag{54}$$

$$B := \frac{\sqrt{\pi}}{c_l}, \tag{55}$$

we arrive at the following asymptotic expression for the total cross section

$$\sigma^t(E_r \to \infty) \simeq (A - B \ln E_r)^2. \tag{56}$$

For the diffusion cross section we obtain the simple relation according to eqs. (9), (45), (46)

$$\sigma^d(E_r \to \infty) = 4\pi \int_0^\infty dbb \sin^2 \frac{1}{2}\chi(b, E_r \to \infty) \tag{57}$$

$$\simeq \pi \int_0^\infty dbb\chi^2(b, E_r \to \infty) \tag{58}$$

resulting in

$$\sigma^d(E_r \to \infty) \simeq \frac{C}{E_r^2}, \tag{59}$$

$$C := \pi \int_0^\infty b\, db\, F^2(b). \tag{60}$$

The diffusion cross section decreases faster than the total cross section for $E_r \to \infty$. An analogous asymptotic expression (59) also holds for the viscosity cross section (10).

If the integral (46) is convergent the deflection function can be estimated to $\chi \sim V(b)/E_r$. For an inverse power law potential $V(r) = \alpha_n r^{-n}$ it is $\chi \sim \alpha_n b^{-n}/E_r$. For $n > 0$ the deflection function is finite and the integral (48) convergent. For the diffusion cross section it results:

$$\sigma^d \sim \int^{\infty} db\, b\, V(b) = (\alpha_n \pi / E_r^2) \int^{\infty} db\, b^{1-2n} \tag{61}$$

which remains finite for $n > 1$. So the diffusion cross section is finite for potentials which tends to zero stronger than r^{-1} at infinity.

(ii) $E_r \to 0$

We use the standard procedure of [13]:

$$\ln \sigma^{t,d,v}(E_r \to 0) \simeq C + D \ln E_r. \tag{62}$$

The various asymptotic estimations (57), (59) and (62) are summarized and generalized to

$$\ln \sigma^{t,d,v} \simeq a_0 + a_1 \ln E_r + a_2 (\ln E_r)^2, \tag{63}$$

where a term of second order in $\ln E_r$ is additionally included. Eq. (63), ideed, is a special case of representations (25), (27), respectively, with $N = 2$. It will be used as standard asymptotic representation. So cross section data for the whole energy range $(0, \infty)$ are presented in this report (section 5).

3 Collision Rates

3.1 Definitions

The deflection function $\chi(b, E_r)$ (5) was the starting point to calculate the total cross section σ^t (7), the diffusion cross section σ^d (8) and the viscosity cross section σ^v (10) which are denoted as follows:

$$\sigma^{(l)}(E_r) := \begin{cases} \sigma^t, & l = 0 \\ 2\pi \int_0^\infty db\ b\ [1 - cos^l\ \chi(b, E_r)], & l > 0. \end{cases} \tag{64}$$

Knowing these cross sections we can calculate the respective collision frequencies $\nu^{(l)}$,

$$\nu^{(l)} := n_\beta v_r \sigma^{(l)}. \tag{65}$$

Let

$$f_{\alpha,\beta}(\vec{v}) \equiv f(\vec{v}_{\alpha,\beta}), \qquad \int d\vec{v}_{\alpha,\beta} f_{\alpha,\beta} = 1. \tag{66}$$

denote the distribution functions of the particles α, β, normalized to 1. The quantity $\vec{g}(\vec{v}_\alpha, \vec{v}_\beta)$, averaged with the distribution function f_β, is written as

$$\langle \vec{g}(\vec{v}_\alpha, \vec{v}_\beta) \rangle_\beta := \int d\vec{v}_\beta\ f_\beta\ \vec{g}(\vec{v}_\alpha, \vec{v}_\beta). \tag{67}$$

Averaging once again, with the distribution function f_α, we write

$$\langle \vec{g}(\vec{v}_\alpha, \vec{v}_\beta) \rangle_{\beta\alpha} := \langle \langle \vec{g}(\vec{v}_\alpha, \vec{v}_\beta) \rangle_\beta \rangle_\alpha. \tag{68}$$

We consider the following quantities (collision rates) (cf. [9]):

(i) rate coefficient:

$$\langle v_r \sigma^{(0)} \rangle \tag{69}$$

(ii) momentum transfer rate:

$$\left(\frac{\delta \vec{p}_\alpha}{\delta t} \right) := -m_r \langle \vec{v}_r \nu^{(1)} \rangle \tag{70}$$

(iii) energy rate:

$$\left(\frac{\delta E_\alpha}{\delta t} \right) := -\kappa_r \langle (E_\alpha - E_\beta + \frac{m_\beta - m_\alpha}{2} \vec{v}_\alpha \vec{v}_\beta) \nu^{(1)} \rangle \tag{71}$$

with $\vec{v}_r \equiv \vec{v}_\alpha - \vec{v}_\beta$, $E_{\alpha,\beta} := \frac{1}{2} m_{\alpha,\beta} v^2_{\alpha,\beta}$, $\kappa_r := 2 m_\alpha m_\beta / (m_\alpha + m_\beta)^2$.

In a kinetic description of neutral particle transport such rates enter, averaged once over the distribution function of the ions according to eq. (67). In hydrodynamic models such expressens enter, averaged twice according to eq. (68).

3.2 Rates for Kinetic Description

For kinetic neutral gas models (e.g. for Monte Carlo algorithms) we need the above mentioned rates for the neutral species α averaged over the distribution function of the ions β. We restrict the discussion in what follows to Maxwellian (no directed velocity) distributions f_β:

$$f_\beta = \left(\sqrt{\pi} a_\beta\right)^{-3} e^{-(v_\beta/a_\beta)^2}, \qquad a_\beta := \sqrt{2T_\beta/m_\beta}. \tag{72}$$

(i) collision rate:

$$R_t := \langle v_r \sigma^{(0)} \rangle_\beta = \tag{73}$$
$$\frac{1}{\sqrt{\pi} v_\alpha a_\beta} \int_0^\infty dv_r \; v_r^2 \; \sigma^{(0)} \left(\frac{m_r}{2} v_r^2\right) \left\{ exp - \left(\frac{v_r - v_\alpha}{a_\beta}\right)^2 \; - \; exp - \left(\frac{v_r + v_\alpha}{a_\beta}\right)^2 \right\}$$

(ii) momentum exchange rate (in one direction):

$$R_{pd} := -m_r \langle v_{r\|} v_r \sigma^{(1)} \rangle_\beta = \frac{m_r}{\sqrt{\pi} v_\alpha a_\beta} \int_0^\infty dv_r \; v_r^2 \; \sigma^{(1)} \left(\frac{m_r}{2} v_r^2\right) \tag{74}$$
$$\left\{ \left(v_r \; - \; \frac{a_\beta^2}{2v_\alpha} \right) exp - \left(\frac{v_r - v_\alpha}{a_\beta}\right)^2 \; + \; \left(v_r \; + \; \frac{a_\beta^2}{2v_\alpha} \right) exp - \left(\frac{v_r + v_\alpha}{a_\beta}\right)^2 \right\}$$

(iii) energy exchange rate:

$$R_{Ed} := -\kappa_r \langle \left(E_\alpha - E_\beta + \frac{m_\beta - m_\alpha}{2} \vec{v}_\alpha \vec{v}_\beta \right) v_r \sigma^{(1)} \rangle = -\frac{\kappa_r}{\sqrt{\pi} v_\alpha a_\beta} \int_0^\infty dv_r v_r^2 \; \sigma^{(1)} \left(\frac{m_r}{2} v_r^2\right) \tag{75}$$
$$\left\{ \left[\frac{m_\alpha}{2} v_\alpha^2 - \frac{m_\beta}{2}(v_\alpha^2 + v_r^2) + \frac{m_\alpha + m_\beta}{2} v_r v_\alpha - \frac{m_\alpha + m_\beta}{4} a_\beta^2 \right] exp - \left(\frac{v_r - v_\alpha}{a_\beta}\right)^2 - \right.$$
$$\left. \left[\frac{m_\alpha}{2} v_\alpha^2 - \frac{m_\beta}{2}(v_\alpha^2 + v_r^2) - \frac{m_\alpha + m_\beta}{2} v_r v_\alpha - \frac{m_\alpha + m_\beta}{4} a_\beta^2 \right] exp - \left(\frac{v_r + v_\alpha}{a_\beta}\right)^2 \right\}$$

These rates can be represented in terms of the following $I^{(l,n)}$ integrals

$$I^{(l,n)}(E_\alpha, T_\beta) := \frac{a_\beta^2}{\sqrt{\pi} v_\alpha} \int_0^\infty d\xi \; \xi^{2+n} \sigma^{(l)}(T_\beta \xi^2) \; \{ e^{-(\xi-\delta)^2} - (-1)^n e^{-(\xi+\delta)^2} \}, \tag{76}$$

$\left(\xi := v_r/a_\beta, \delta := \sqrt{\frac{m_\beta E_\alpha}{m_\alpha T_\beta}} \right)$ by the expressions:

$$R_t = I^{(0,0)}, \tag{77}$$

$$R_{pd} = m_r a_\beta \left(I^{(1,1)} \; - \; \frac{a_\beta}{2v_\alpha} \; I^{(1,0)} \right), \tag{78}$$

$$R_{Ed} = -\kappa_r \left\{ \left(\frac{m_\alpha}{2} v_\alpha^2 - \frac{m_\beta}{2} v_\alpha^2 - \frac{m_\alpha + m_\beta}{4} a_\beta^2 \right) I^{(1,0)} + \frac{m_\alpha + m_\beta}{2} v_\alpha a_\beta I^{(1,1)} - \frac{m_\beta}{2} a_\beta^2 I^{(1,2)} \right\}. \tag{79}$$

The $I^{(l,n)}$ integrals satisfy the equations

$$\delta\ I^{(l,n+1)} = E_\alpha \frac{\partial}{\partial E_\alpha}\ I^{(l,n)} + \left(\frac{1}{2} + \delta^2 \right)\ I^{(l,n)}, \tag{80}$$

$$I^{(l,n+2)} = T_\beta \frac{\partial}{\partial T_\beta} I^{(l,n)} + \frac{n+1}{2} I^{(l,n)} - \delta^2 I^{(l,n)} + 2\delta I^{(l,n+1)} \tag{81}$$

$$= T_\beta \frac{\partial}{\partial T_\beta} I^{(l,n)} + 2E_\alpha \frac{\partial}{\partial E_\alpha} I^{(l,n)} + \left(\frac{n+3}{2} + \delta^2 \right)\ I^{(l,n)}. \tag{82}$$

The various cross sections are included in Monte Carlo transport codes in the form of polynomial fits (section 5). The collision rates which are functional related to the respective cross sections, will also be included as fits (section 6). The variety of different fits of interrelated quantities may lead to inaccuraties in the computation procedure. The relations (77) - (79) allow to reduce the fits, which are necessary for the Monte Carlo description, to down to at least one fit for each l. So sources of inaccurities may be removed. In order to calculate the above mentioned rates we need at least the I Integrals $I^{(0,0)}$ and $I^{(1.0)}$.

3.3 Rates for Hydrodynamic Description

We outline here only the simplest approximations (cf. [9]).

The rates entering a hydrodynamic description are essentially determined by the dependence of the resp. collision frequencies on the relative velocity v_r and the approach of the distribution function for both species α and β. Representing the relative velocity vector $\vec{v}_r := \vec{v}_\alpha - \vec{v}_\beta$ as the sum of the directed ($\vec{u}$) and the random ($\vec{w}$) velocity

$$\vec{v}_r = \vec{u} + \vec{w},\ \vec{u} = \vec{u}_\alpha - \vec{u}_\beta,\ \vec{w} = \vec{w}_\alpha - \vec{w}_\beta \tag{83}$$

and restricting to the case $u << w$, one proceeds by expanding the rates in terms of $\vec{u}$. In what follows, the distribution function $f_{\alpha\beta}$ will be assumed to be isotropic (which corresponds to Grad's 5-moment approximation). We then obtain for the rate coefficient in zeroth approximation the wellknown result

(i) collision rate:

$$R := \langle v_r \sigma^{(0)} \rangle_{\beta\alpha} = \frac{4}{\sqrt{\pi}} a_{\alpha\beta} \int_0^\infty d\xi\ \xi^3\ e^{-\xi^2} \sigma^{(0)}(T_{\alpha\beta}\xi^2) \tag{84}$$

with $\xi := v_r/a_{\alpha\beta}, a_{\alpha\beta}^2 := a_\alpha^2 + a_\beta^2 \equiv 2T_{\alpha\beta}/m_r; T_{\alpha\beta}$ is the effective temperature.
(ii) momentum exchange rate:

$$\langle \vec{v}_r \nu^{(1)} \rangle_{\alpha\beta} \simeq \vec{u}\ \bar{\nu}, \tag{85}$$

$$\bar{\nu} := \frac{8}{3\sqrt{\pi}}\, n_\beta\, a_{\alpha\beta} \int_0^\infty d\xi\ \xi^5\ e^{-\xi^2}\ \sigma^{(1)}(T_{\alpha\beta}\xi^2). \tag{86}$$

(iii) energy exchange rate:

$$\langle \left(\frac{1}{2} m_\alpha v_\alpha^2 - \frac{1}{2} m_\beta v_\beta^2\right) \nu^{(1)} \rangle_{\beta\alpha} \simeq \tag{87}$$

$$\frac{\bar{\nu}}{m_\alpha + m_\beta} \left(T_\alpha - T_\beta + m_\alpha u_\alpha^2 - m_\beta u_\beta u_\beta^2 + (m_\beta - m_\alpha) u_\alpha u_\beta\right).$$

The energy rate is also approximately given in dependence of the averaged collision frequency $\bar{\nu}$. It is related to the diffusion coefficient by [9]

$$D = T_{\alpha,\beta}/m_r \bar{\nu}. \tag{88}$$

The transport coefficients can be expressed in terms of the Ω integrals which are defined analogously to ref. [12] by

$$\Omega^{(l,r)}(T_{\alpha\beta}) := \frac{a_{\alpha\beta}}{2\sqrt{\pi}} \int_0^\infty d\xi\ e^{-\xi^2}\ \xi^{2r+3} \sigma^{(l)}(T_{\alpha\beta}\xi^2) \tag{89}$$

For the diffusion coefficient one obtains

$$D = \frac{3}{16} \frac{T_{\alpha\beta}}{m_r n_\beta} \frac{1}{\Omega^{(1,1)}}. \tag{90}$$

Eq. (90) is the simplest example of the relation of the Ω integrals to the transport coefficients. Furthermore: $R \equiv 8\Omega^{(0,0)}$.

The following relation holds for the Ω integrals [12]:

$$\Omega^{(l,r+1)} = \frac{2r+3}{2} \Omega^{(l,r)} + T_{\alpha\beta} \frac{\partial}{\partial T_{\alpha\beta}} \Omega^{(l,r)}. \tag{91}$$

It allows to calculate the Ω integral of the next order from a given $\Omega^{(l,r)}$ integral. To calculate the transport coefficients for diffusion, thermal diffusion, viscosity and thermal conductivity one needs the following Ω intergrals: $\Omega^{(1,1)}, \Omega^{(1,2)}, \Omega^{(1,3)}, \Omega^{(2,2)}$ (cp. [12]). By means of eq. (91) the first three Ω integrals can be expressed in terms of $\Omega^{(1,1)}$ only.

Integrating the I integrals over a Maxwellian distribution function for the neutrals α they can be related to the Ω integrals by

$$\langle I^{(l,2n)} \rangle_\alpha = 8 \left(\frac{a_{\alpha\beta}}{a_\beta} \right)^{2n} \Omega^{(l,n)}; \quad n = 0, 1... \tag{92}$$

So the I integrals in the Monte Carlo description correspond to the Ω integrals in the hydrodynamic approach. The integrals of different order in the second variable are related one to another by eqs. (80), (91), respectively, which reduce the number of fits needed in both approaches to the lowest order one ($n = 0$).

4 Monte Carlo Procedure [1]

Usually, Monte Carlo methods for neutral gas transport in plasmas are developed from intuition. Rigorous Monte Carlo procedures to describe inelastic processes in plasmas are well known (e.g. [23] and references therein), therefore we restrict ourselves here to a description of the elastic interactions. In order to illustrate this, we write the collision integral in the linear Boltzmann equation (for the single particle distribution function f) for hydrogen neutral particles in a hydrogen plasma background in the following form:

$$\begin{aligned} \left(\frac{\partial f}{\partial t} \right)_{Coll} = & \int\int\int W(\mathrm{v}', \mathrm{v}_1' \rightarrow \mathrm{v}, \mathrm{v}_1) f(\mathrm{v}') f(\mathrm{v}_1') d\mathrm{v}_1 d\mathrm{v}' d\mathrm{v}_1' \\ & - \int\int\int W(\mathrm{v}, \mathrm{v}_1 \rightarrow \mathrm{v}', \mathrm{v}_1') f(\mathrm{v}) f(\mathrm{v}_1) d\mathrm{v}_1 d\mathrm{v}' d\mathrm{v}_1' \end{aligned} \tag{93}$$

which can readily be generalized to dissimilar masses (e.g. the $H^+ + H_2$ collision mentioned above). Here $W$is a transition probability for post-collision states v (for the neutrals) and v_1 (for the ions), given pre-collision states v' and v_1'. Implicit in this form is the assumption of a finite cross section, which in our case is ensured by introducing a maximum impact parameter as discussed above. The transition probability is given by

$$W(\mathrm{v}, \mathrm{v}_1 \rightarrow \mathrm{v}', \mathrm{v}_1') = \sigma(\mid \mathrm{v} - \mathrm{v}_1 \mid, \theta) \cdot \delta_3 \left(\frac{\mathrm{v} + \mathrm{v}_1 - \mathrm{v}' - \mathrm{v}_1'}{2} \right) \cdot \delta_1 \left(\frac{(\mathrm{v} - \mathrm{v}_1)^2 - (\mathrm{v}' - \mathrm{v}_1')^2}{2} \right) \tag{94}$$

where σ denotes the differential cross section, θ is the observable scattering angle in the centre of mass system. The delta functions express conservation of momentum and energy,

[1] Written by D. Reiter, cf. [24].

respectively. The second integral in eq.(7) yields the term $[n_i \cdot \langle \sigma(v_{rel}) \cdot v_{rel} \rangle / v] \cdot v \cdot f(v)$, wherein the first factor is just the macroscopic cross section $\Sigma(v)$ (the inverse mean free path). Including this term in the Monte Carlo procedure is simply done by enhancing the total macroscopic cross-section accordingly.

Because we are only concerned with the fate of the neutrals, and not the ions, we can formally express the first integral as

$$\int C(\mathbf{v}' \rightarrow \mathbf{v}) \cdot \Sigma(v') \cdot v' f(\mathbf{v}') d\mathbf{v}' \tag{95}$$

where the kernel C now reads, after some rearrangement:

$$C(\mathbf{v}' \rightarrow \mathbf{v}) = \int \int \frac{W(\mathbf{v}', \mathbf{v}_1' \rightarrow \mathbf{v}, \mathbf{v}_1)}{n_i \cdot \langle \sigma \cdot v_{rel} \rangle (v')} f(\mathbf{v}_1') d\mathbf{v}_1' d\mathbf{v}_1. \tag{96}$$

In order to incorporate this kernel C into the Monte Carlo procedure, random vectors $\mathbf{v}$, given $\mathbf{v}'$, have to be generated, once an elastic collision process is identified by a random selection between all processes contributing to the total cross-section. This requires random sampling from a multidimensional distribution involving the differential cross-section (as e.g. in ref. [1]). To avoid this, we rewrite Cas:

$$C(\mathbf{v}' \rightarrow \mathbf{v}) = \int \int \left[\frac{\sigma(v_{rel}) \cdot v_{rel} \cdot f(\mathbf{v}_1')}{n_i \langle \sigma \cdot v_{rel} \rangle (v')} \right] \cdot [2\pi b(v_{rel})] \cdot \left[\hat{\delta}_3(...) \cdot \hat{\delta}_1(...) \right] \cdot \cdot d\mathbf{v}_1' db d\epsilon \tag{97}$$

According to the standard Monte Carlo method, sampling the post-collision state $\mathbf{v}$ now proceeds as follows: First sample $\mathbf{v}_1'$ from the first factor in eq.(15), then find b according to the second factor (conditional on $\mathbf{v}_1'$) and ϵ from a uniform distribution, and finally compute $\mathbf{v}$ from the deterministic delta distributions (given b, ϵ and $\mid \mathbf{v}' - \mathbf{v}_1' \mid$ and the effective potential field $V_{eff}(r)$ eq. (1). Thus we see that the Monte Carlo simulation of the elastic processes as described above and as implemented into the EIRENE code is entirely equivalent to solving the linear Boltzmann equation. Up to this point we have described how to generate the pathes of a stochasic process corresponding to the linear Boltzmann equation. In order to optain macroscopic quantities from such random walks, (generally referred to as "responses" in neutron transport applications), standard Monte Carlo estimation techniques can be applied. They involve various different types of maxwellian averaged cross-sections, ie. collision rate coefficients weighted by the particle, momentum or energy exchange rate per collision [25] (section 3).

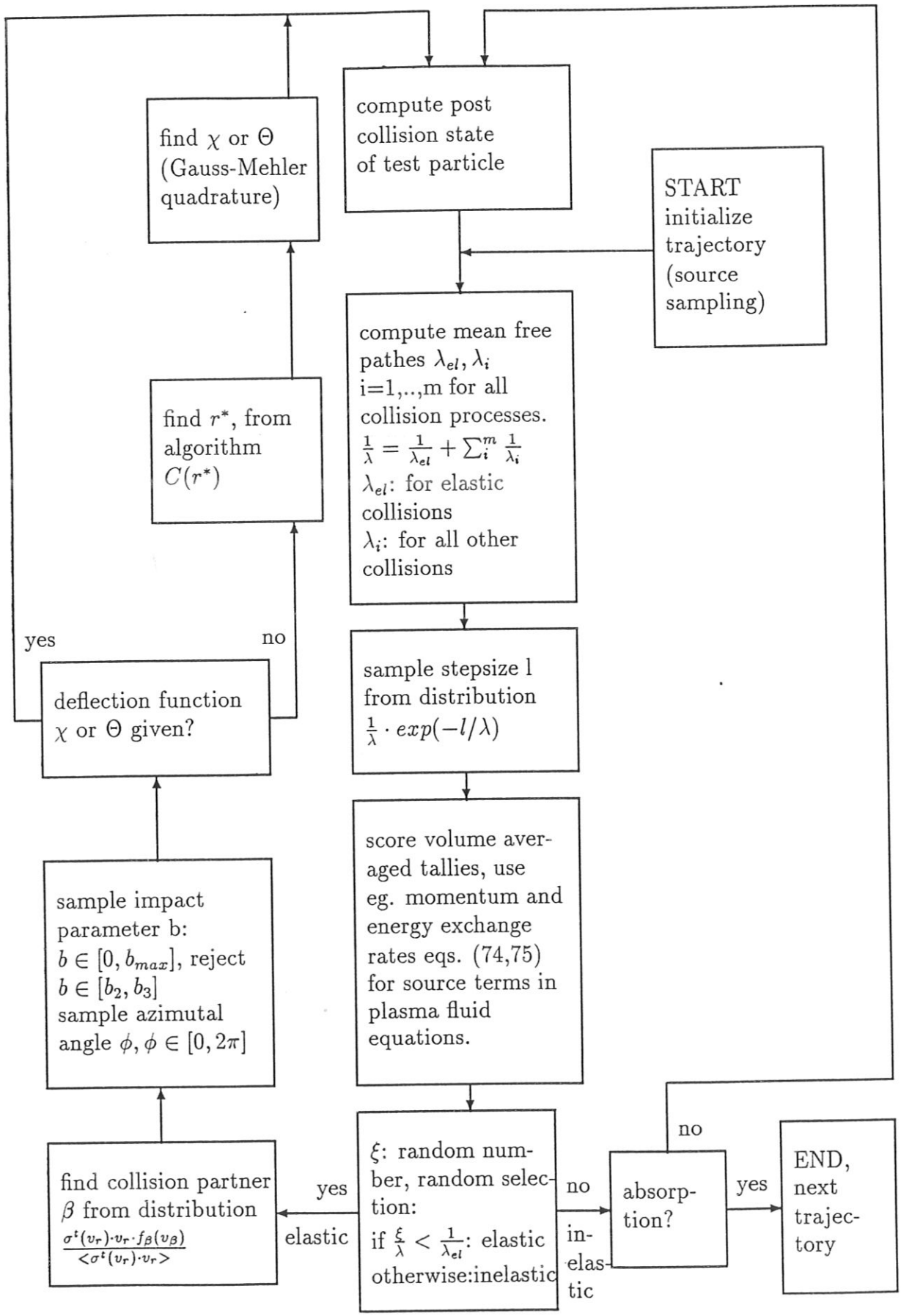
START
initialize
trajectory
(source
sampling)
compute post
collision state
of test particle
compute mean free
pathes λ_{el}, λ_i
i=1,..,m for all
collision processes.
$\frac{1}{\lambda} = \frac{1}{\lambda_{el}} + \sum_i^m \frac{1}{\lambda_i}$
λ_{el}: for elastic
collisions
λ_i: for all other
collisions
sample stepsize l
from distribution
$\frac{1}{\lambda} \cdot exp(-l/\lambda)$
score volume aver-
aged tallies, use
eg. momentum and
energy exchange
rates eqs. (74,75)
for source terms in
plasma fluid
equations.
ξ: random num-
ber, random selec-
tion:
if $\frac{\xi}{\lambda} < \frac{1}{\lambda_{el}}$: elastic
otherwise:inelastic
no
in-
elas-
tic
absorp-
tion?
yes
no
END,
next
trajec-
tory
yes
elastic
find collision partner
β from distribution
$\frac{\sigma^t(v_r) \cdot v_r \cdot f_\beta(v_\beta)}{<\sigma^t(v_r) \cdot v_r>}$
sample impact
parameter b:
$b \in [0, b_{max}]$, reject
$b \in [b_2, b_3]$
sample azimutal
angle $\phi, \phi \in [0, 2\pi]$
yes
no
deflection function
χ or Θ given?
find r^*, from
algorithm
$C(r^*)$
find χ or Θ
(Gauss-Mehler
quadrature)

5 Data Fits for Cross Sections

5.1 Outline of Procedure

Each collision process is decribed by the vector $\vec{R}$ which is compared to eq. (39) redefined by adding the second characteristic energy E_{r0} (41):

$$\vec{R} := \begin{cases} (0) & \text{for} \quad E_{r0} = 0 \\ (\epsilon, g_1, g_2, r_m, r_0, r_w, r_c, b_c, E_{rc}, E_{r0}) & \text{for} \quad E_{r0} > 0 \end{cases} \tag{98}$$

ϵ, g_1, g_2, r_m – parameters (29) of the Morse potential (28)

r_0 – eq. (31)

r_w – eq. (33)

Critical parameters (section 2.2.2):

r_c – numerically calculated

b_c – eq. (38)

E_{rc} – eq. (37)

As maximal collision parameter we use: $b_{max} = 25$.

All cross sections are calculated in the energy range

$$0.01eV \leq E_r \leq 100eV.$$

and fitted according to:

$$ln\ \sigma^{t,d,v}(E_r) \simeq \sum_{n=0}^{8} a_n^{t,d,v} (\ln E_r)^n, \qquad E_{rmin} \leq E_r \leq E_{rmax}. \tag{99}$$

E_{rmin}, E_{rmax} are given. For the total cross section and Case II (R2 - R4) these limit values are given by the characteristic energies E_{rc}, E_{r0}. This shows the meaning of these quantities: The total cross section of Case II is approximated by a least square fit in the energy range between E_{rc}, E_{r0}; outside this range it is only an asymptotic quantity (63).

Diffusion and viscosity cross sections $\sigma^{d,v}$ are represented analogously according to (99) and (63). The energy limits are the computation limits.

The asymptotic parameters a_0, a_1, a_2 are additionally labeled by either "l" ("left", i.e. $E_r \to 0$) or "r" ("right", i.e. $E_r \to \infty$).

In order to be consistent with [13] *we go over to the laboratory ion energy*

$$E_{lab} := \frac{m_i}{2} v_r^2 \equiv \frac{m_i}{m_r} E_r. \tag{100}$$

We use the above mentioned fits, replacing there the relative energy E_r by the laboratory ion energy E_{lab}.

The following *dimensions* are used:

$E_{r(lab)}, V$ in eV,

$\sigma^{t,d,v}$ in cm^2,

r, b in $a_0 = 0.52917 \mathring{A}$.

5.2 R1: $H^+ + H$

(Repulsive) Potential (Case I) [7]:

$$V(r) = \epsilon \left([S(r) - 1]^{-1} \left[r^{-1} - \left(1 + r^{-1}\right) e^{-2r} - (1 + r) e^{r} \right] + r^{-1} \right), \tag{101}$$

$$S(r) = \left(1 + r + r^2/3\right) \, e^{-r}, \; \epsilon = 27.211 eV, \tag{102}$$

$$\vec{R} = (0). \tag{103}$$

The deflection function χ is represented in Fig. 5. The matrix $A(m, n)$ is represented in Tab. 1 The two-parameter fit is according to eq. (22). (There we use exceptionally the relative energy E_r instead of the ion laboratory energy E_{lab}.) Cross Sections s. Fig. 6, fitting parameters s. Tab. 2.

	Er-Index: 0	1	2
b-Index:			
0	1.776566650789D-04	1.855322980624D-03	2.814879435626D-03
1	5.800163476447D-01	4.025727537412D-01	2.350494282005D-01
2	8.961720867515D-04	2.717940166261D-02	8.133177076638D-02
3	-5.378363832594D-03	-3.679620344642D-02	-9.416378439238D-02
4	1.403086334034D-05	7.716290911417D-03	2.604212472132D-02
5	1.263297186698D-04	-1.067207481809D-03	-3.876325025095D-03
6	-2.395080677610D-05	1.062049115863D-04	3.668225256930D-04
7	1.987085392037D-06	-6.034790121757D-06	-2.080164719113D-05
8	-6.093049227396D-08	1.381514509566D-07	5.201314001636D-07
	Er-Index: 3	4	5
b-Index:			
0	-3.664907417572D-03	-1.063987732945D-02	-4.211662874743D-03
1	1.666138990907D-01	1.911893550209D-01	1.293931033356D-01
2	3.714506245192D-02	-1.397148070239D-01	-1.807805463274D-01
3	-9.872736783319D-02	3.409146026316D-03	7.169447310606D-02
4	3.516381498679D-02	1.353207184504D-02	-9.614318042249D-03
5	-5.562242214128D-03	-3.318847140116D-03	-1.702969355132D-04
6	4.622506110672D-04	3.163789332944D-04	1.510270667181D-04
7	-2.022300842732D-05	-1.250896502233D-05	-1.255843447284D-05
8	3.796451629808D-07	1.392648739108D-07	3.282528647163D-07
	Er-Index: 6	7	8
b-Index:			
0	5.260472693069D-03	4.717588716645D-03	1.037581141596D-03
1	6.293258269033D-03	-2.813415544944D-02	-8.090313155856D-03
2	-4.799935529825D-02	2.078852667665D-02	8.629078009560D-03
3	3.119154873654D-02	-5.388469488718D-03	-3.624349532837D-03
4	-6.011121508833D-03	1.443119485342D-03	9.293586951192D-04
5	-4.366350033421D-05	-5.145545678476D-04	-1.823754390621D-04
6	1.366859407965D-04	1.006166346060D-04	2.488598774731D-05
7	-1.475015885534D-05	-8.825780695868D-06	-1.875590567703D-06
8	4.883487802579D-07	2.824671792873D-07	5.653464120248D-08

Table 1. Matrix A(m,n)

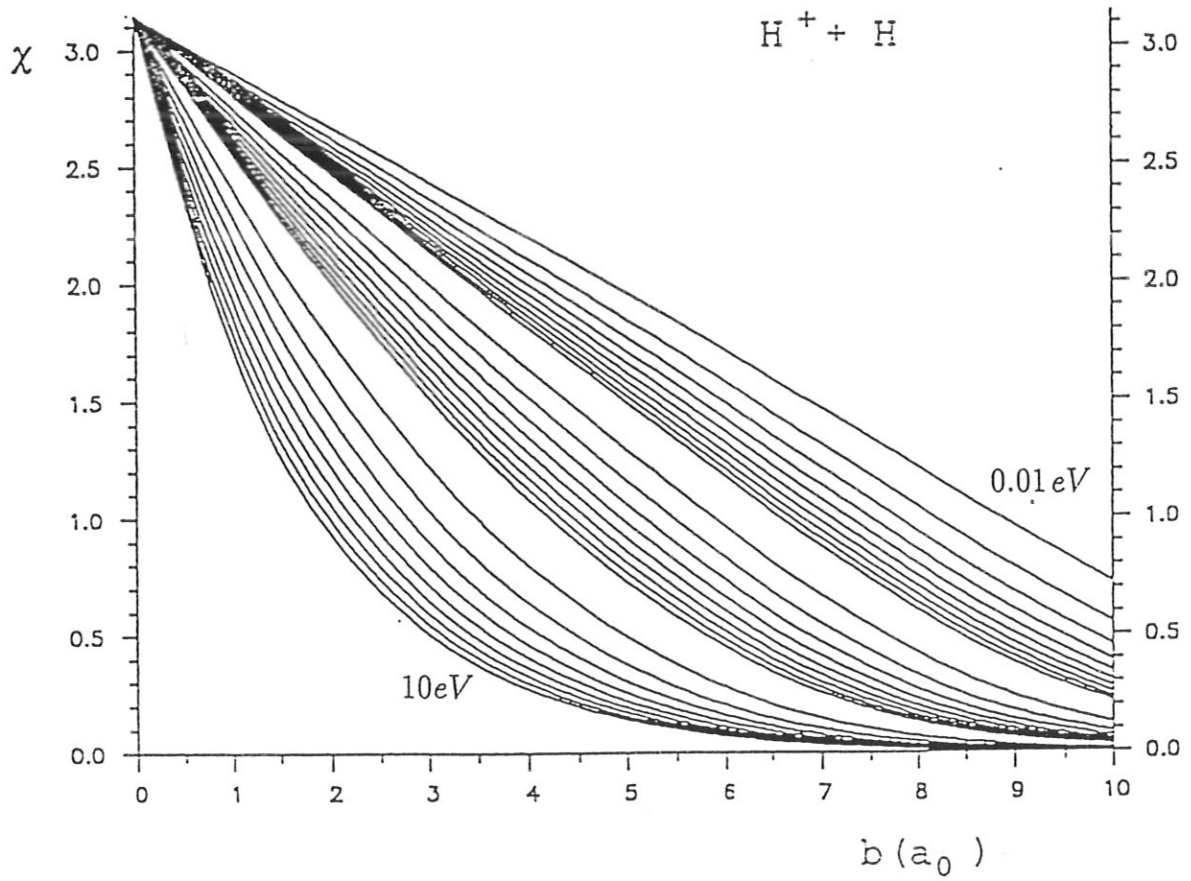

Figure 5: Deflection function $\chi(b, E_r)$ as function of the collision parameter b for relative energies $E_r = 0.01 - 10eV$.

R1 $H^+ + H$

SIGMA-TOTAL(ELAB)

ELABMIN=ELABMAX=1.8206 eV

a0	0.000000000000D+00	a1	0.000000000000D+00	a2	0.000000000000D+00
a3	0.000000000000D+00	a4	0.000000000000D+00	a5	0.000000000000D+00
a6	0.000000000000D+00	a7	0.000000000000D+00	a8	0.000000000000D+00
al0	-3.253031352541D+01	al1	-2.559032645641D-01	al2	-1.449996483552D-02
ar0	-3.262937357400D+01	ar1	-8.719626183599D-02	ar2	-7.346647926269D-02

SIGMA-DIFFUSION

ELABMIN=0.02 eV, ELABMAX=200 eV

a0	-3.349115100108D+01	a1	-4.047040620920D-01	a2	-4.340959073105D-02
a3	-5.224890973622D-03	a4	-1.019115858754D-04	a5	-3.314157761518D-06
a6	-4.336259011986D-05	a7	-1.781020734395D-06	a8	1.220393550627D-06
al0	-3.320677627738D+01	al1	-2.205942040112D-01	al2	0.000000000000D+00
ar0	-2.753878563969D+01	ar1	-2.000000000000D+00	ar2	0.000000000000D+00

SIGMA-VISCOSITY

ELABMIN=0.02 eV, ELABMAX=200 eV

a0	-3.353420922048D+01	a1	-3.522409780724D-01	a2	-3.587214262651D-02
a3	-4.282561006823D-03	a4	-3.230618998917D-04	a5	-4.343173698940D-05
a6	-1.753965583282D-05	a7	-4.580920664987D-07	a8	3.738689325195D-07
al0	-3.330015157525D+01	al1	-1.992625366488D-01	al2	0.000000000000D+00
ar0	-2.709329427260D+01	ar1	-2.000000000000D+00	ar2	0.000000000000D+00

Table 2: Fitting parameters for cross sections for R1 $H^+ + H$.

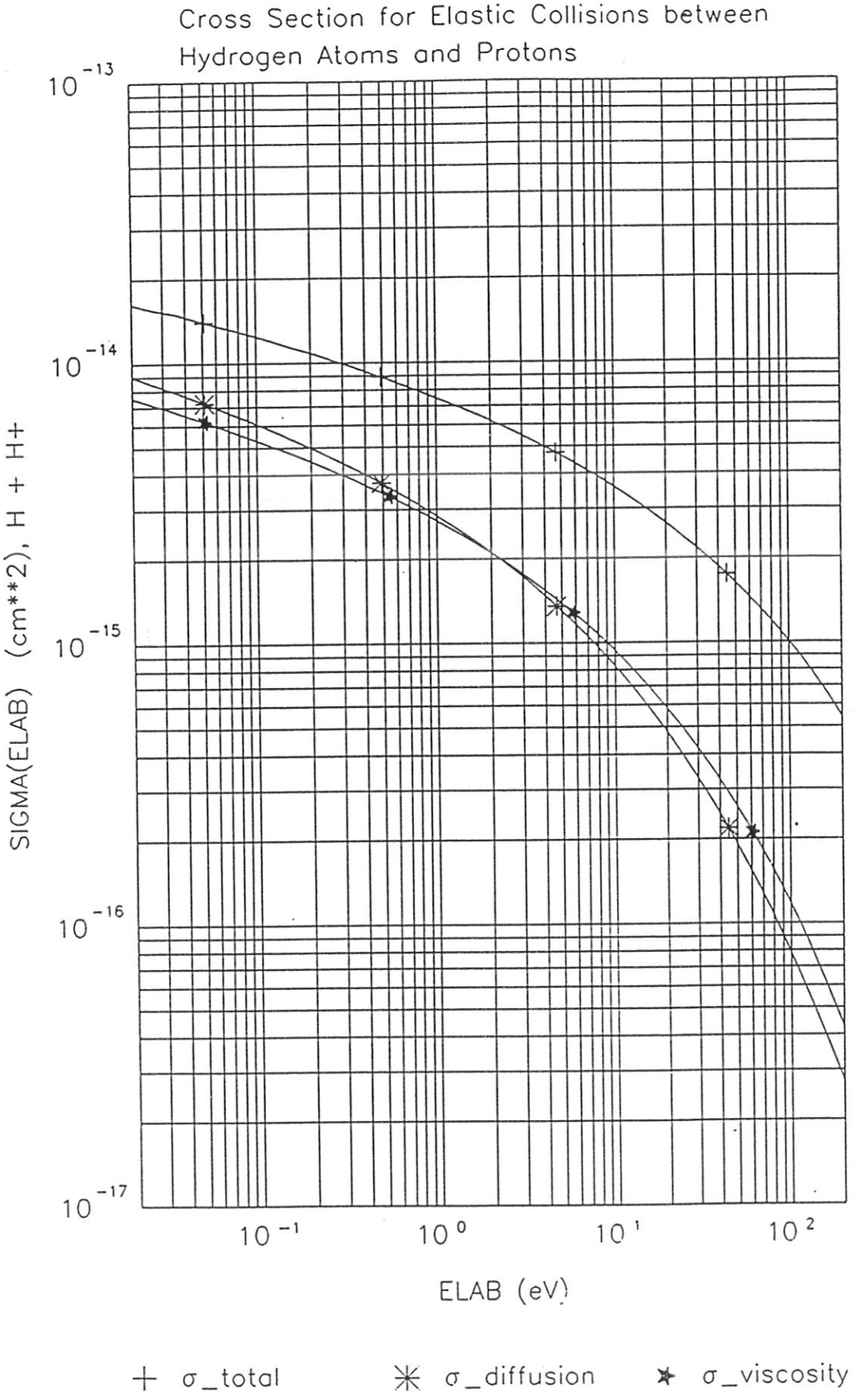

Figure 6: Cross sections as function of the ion energy E_{lab} for R1 $H^+ + H$.

5.3 R2: $H^+ + He$

S. ref. [29].

$$\vec{R} = (2.0, 2.2, 0.85, 1.4556, 0.9970, 1.9952, 2.8833, 4.5099, 0.4065, 23.555) \quad (101)$$

(The characteristic ion lab energies are: $E_{labc} = 0.5081, E_{lab0} = 29.4434$.)

SIGMA-TOTAL(ELAB)

ELABMIN=ELABC=0.5081 eV, ELABMAX=ELAB0=29.4431 eV

a0	-3.357907136508D+01	a1	-9.811659406594D-02	a2	3.798308269292D-01
a3	-1.259671949006D+00	a4	-4.473947519984D-02	a5	1.565182597363D+00
a6	-1.203733922915D+00	a7	3.525830383820D-01	a8	-3.668922671043D-02
al0	-3.355838377904D+01	al1	-2.845473342853D-01	al2	-1.351427675077D-02
ar0	-3.706830076698D+01	ar1	4.204258692619D-01	ar2	-9.648359210100D-02

SIGMA-DIFFUSION

ELABMIN=0.0125 eV, ELABMAX=125 eV

a0	-3.425585328953D+01	a1	-8.999762959781D-01	a2	-3.434858124811D-01
a3	1.549750110754D-02	a4	3.963555202866D-02	a5	3.343570605088D-04
a6	-2.207534449376D-03	a7	-3.378852519380D-05	a8	4.224511209820D-05
al0	-3.390101844960D+01	al1	-2.111706771112D-01	al2	0.000000000000D+00
ar0	-3.034765152080D+01	ar1	-2.000000000000D+00	ar2	0.000000000000D+00

SIGMA-VISCOSITY

ELABMIN=0.0125 eV, ELABMAX=125 eV

a0	-3.443725345071D+01	a1	-4.337427858507D-01	a2	-2.896488696126D-01
a3	-6.451669335555D-02	a4	2.950009865269D-02	a5	5.752283385868D-03
a6	-1.589840628629D-03	a7	-1.502468439244D-04	a8	3.151161681447D-05
al0	-3.432276031579D+01	al1	-2.111706771112D-01	al2	0.000000000000D+00
ar0	-2.978907423990D+01	ar1	-2.000000000000D+00	ar2	0.000000000000D+00

Table 3: Fitting parameters for cross sections for R2 $H^+ + He$.

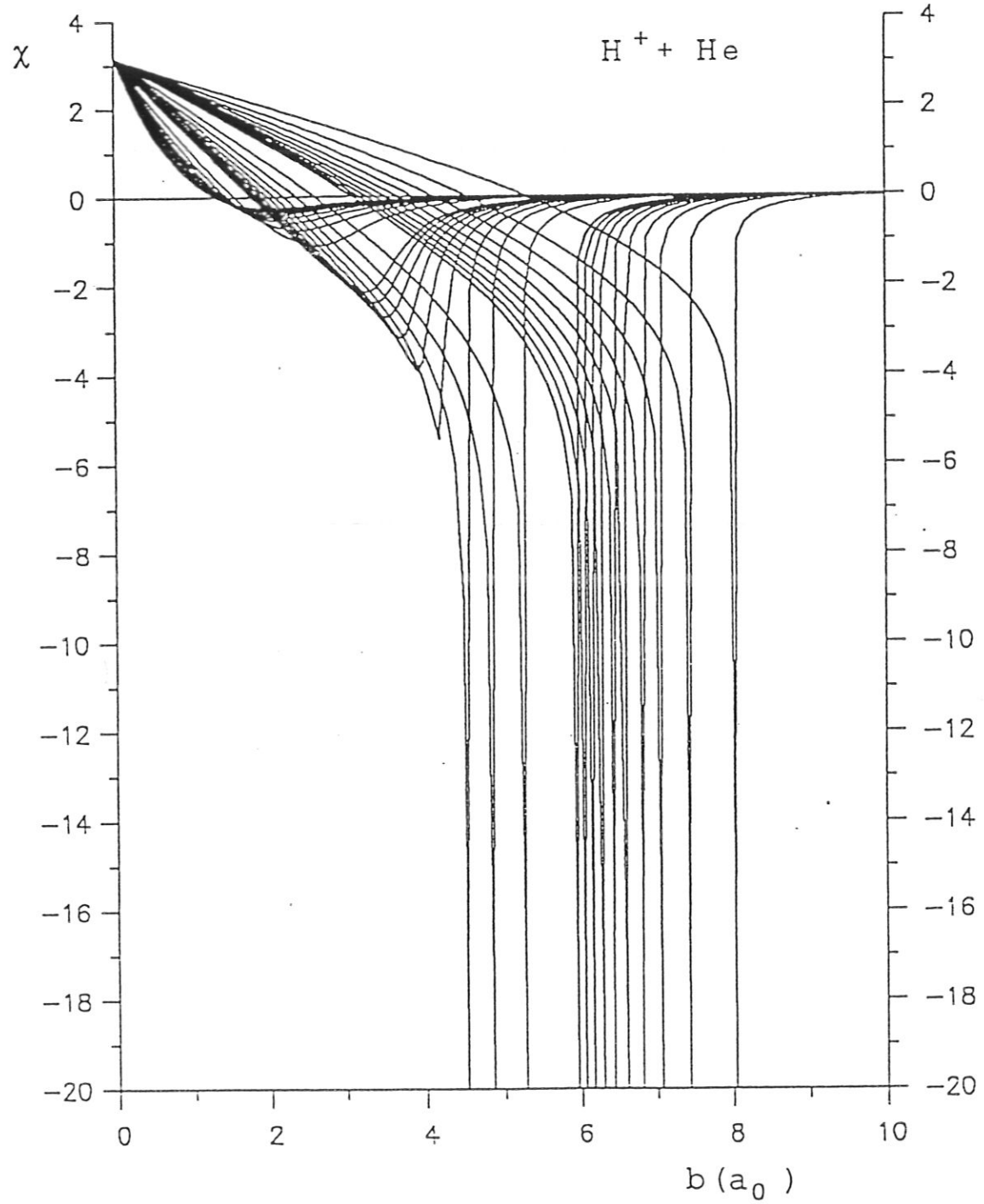

Figure 7: Deflection function $\chi(b, E_r)$ as function of the collision parameter b for relative energies $E_r = 0.01 - 10eV$.

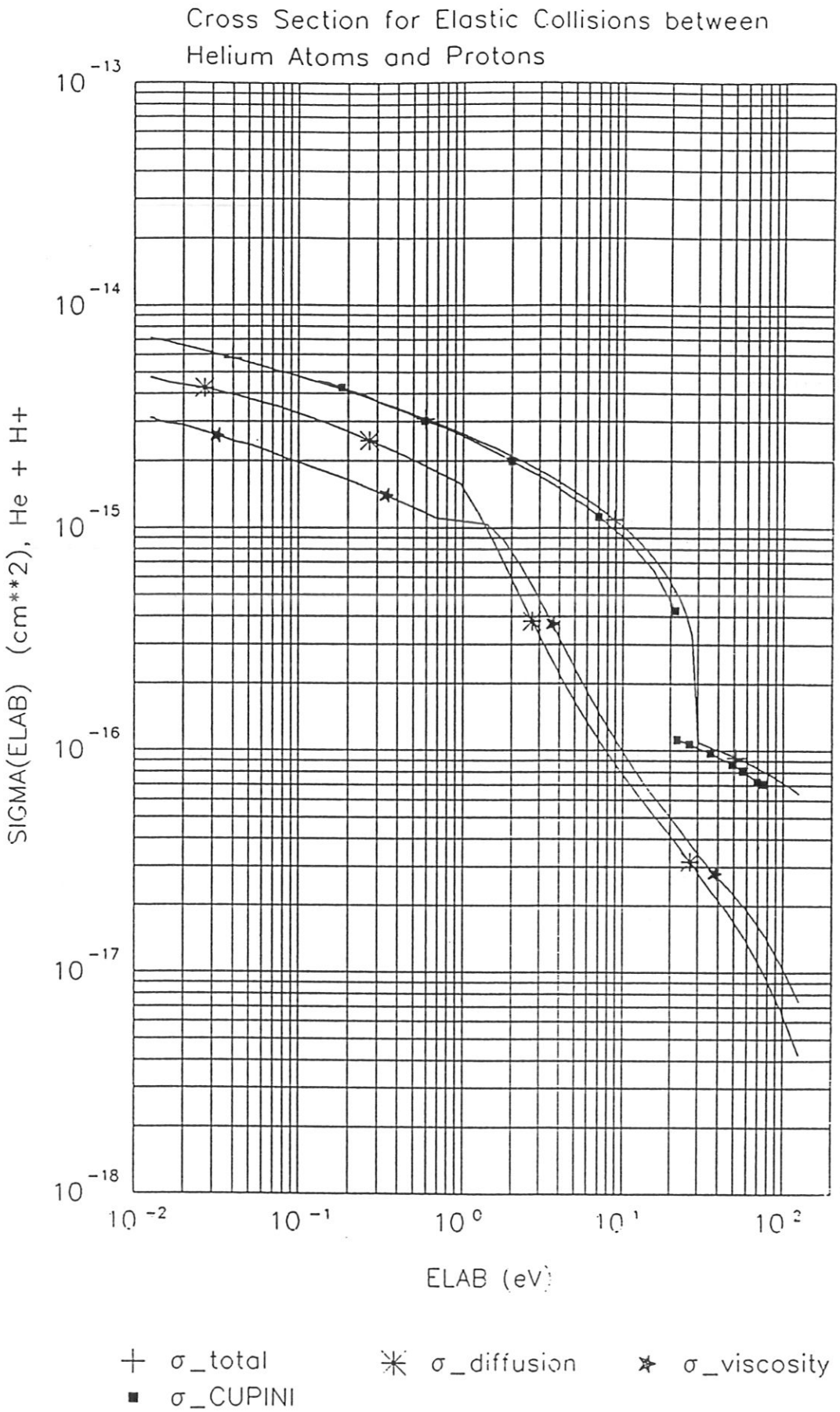

Figure 8: Cross sections as function of the ion energy E_{lab} for R2 $H^+ + He$. The result of Cupini et al. [7] for $c_{max} = 0.99$ is also displayed.

5.4 R3: $H^+ + H_2$

S. ref. [17].

$$\vec{R} = (2.7, 3.0, 1.0, 2.8355, 2.1804, 3.4907, 4.1736, 6.0591, 1.0399, 41.211) \quad (105)$$

($E_{labc} = 1.5598, E_{lab0} = 61.8164$)

SIGMA-TOTAL(ELAB)

ELABMIN=ELABC=1.5598 eV, ELABMAX=ELAB0=61.8164 eV

a0	-3.452141819446D+01	a1	1.092015526305D+01	a2	-2.732690257819D+01
a3	3.466297654768D+01	a4	-2.524607958646D+01	a5	1.092376446349D+01
a6	-2.770065796605D+00	a7	3.796353200921D-01	a8	-2.168988142310D-02
al0	-3.275286840950D+01	al1	-2.351764912137D-01	al2	-1.045602118569D-02
ar0	-3.537275807146D+01	ar1	2.144573517210D-01	ar2	-4.643079956637D-02

SIGMA-DIFFUSION

ELABMIN=0.015 eV, ELABMAX=150 eV

a0	-3.318680874597D+01	a1	-3.580417289312D-01	a2	-2.274382376951D-01
a3	-5.005702120342D-02	a4	2.369248748869D-02	a5	5.013459267775D-03
a6	-1.357018742589D-03	a7	-1.393776090855D-04	a8	3.029808591929D-05
al0	3.839304000000D-15	al1	-1.726918000000D-01	al2	0.000000000000D+00
ar0	2.568502600000D-12	ar1	0.000000000000D+00	ar2	0.000000000000D+00

SIGMA-VISCOSITY

ELABMIN=0.015 eV, ELABMAX=150 eV

a0	-3.362402037774D+01	a1	-2.337285826242D-01	a2	-5.404526201247D-02
a3	-4.473235272373D-02	a4	-4.691524784882D-03	a5	3.121568334037D-03
a6	4.229065229431D-04	a7	-6.739555319843D-05	a8	-7.756198335533D-06
al0	3.053906071449D-15	al1	-1.726917299089D-01	al2	0.000000000000D+00
ar0	2.833830531873D-12	ar1	0.000000000000D+00	ar2	0.000000000000D+00

Table 4: Fitting parameters for cross sections for R3 $H^+ + H_2$.

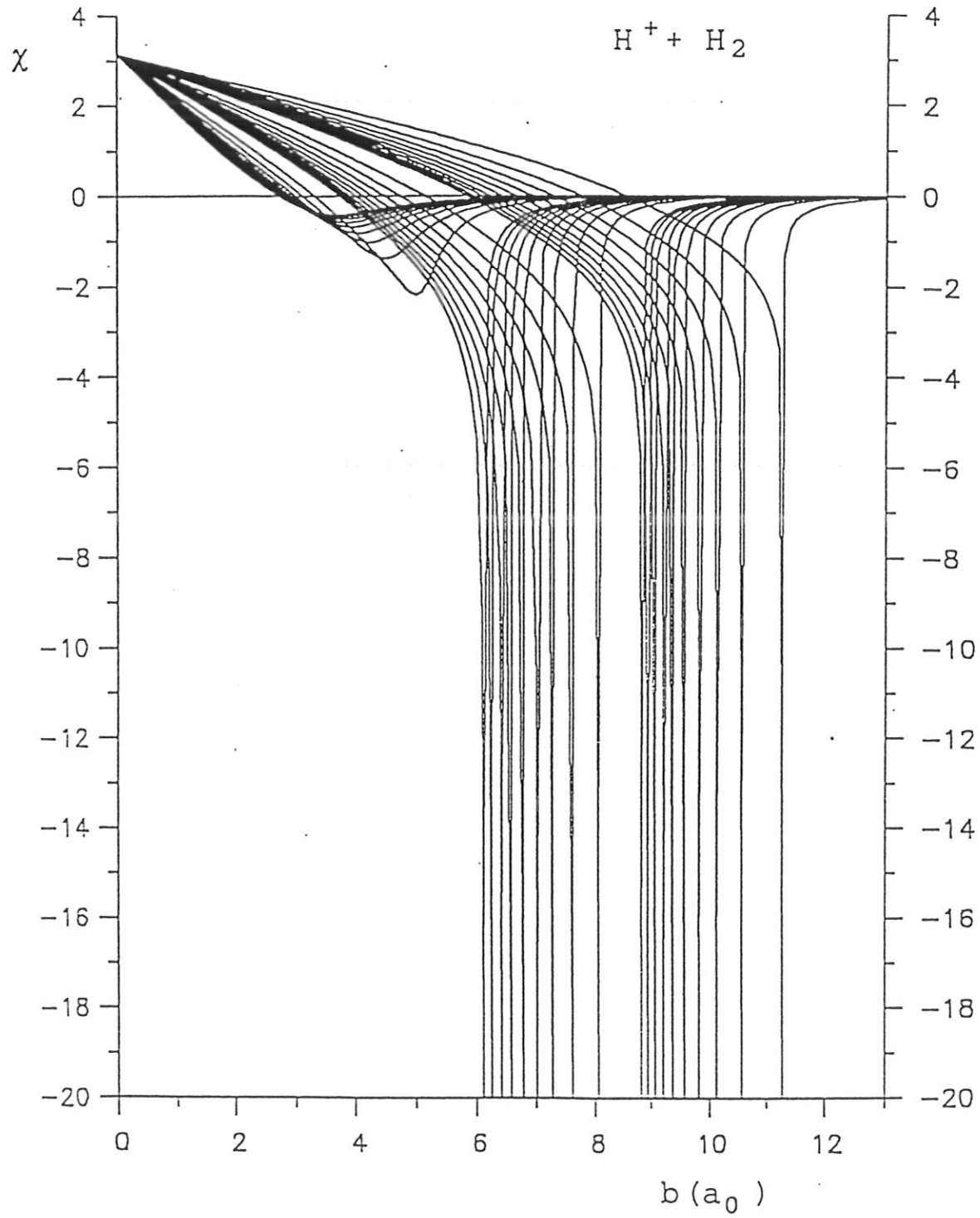

Figure 9: Deflection function $\chi(b, E_r)$ as function of the collision parameter b for relative energies $E_r = 0.01 - 10eV$.

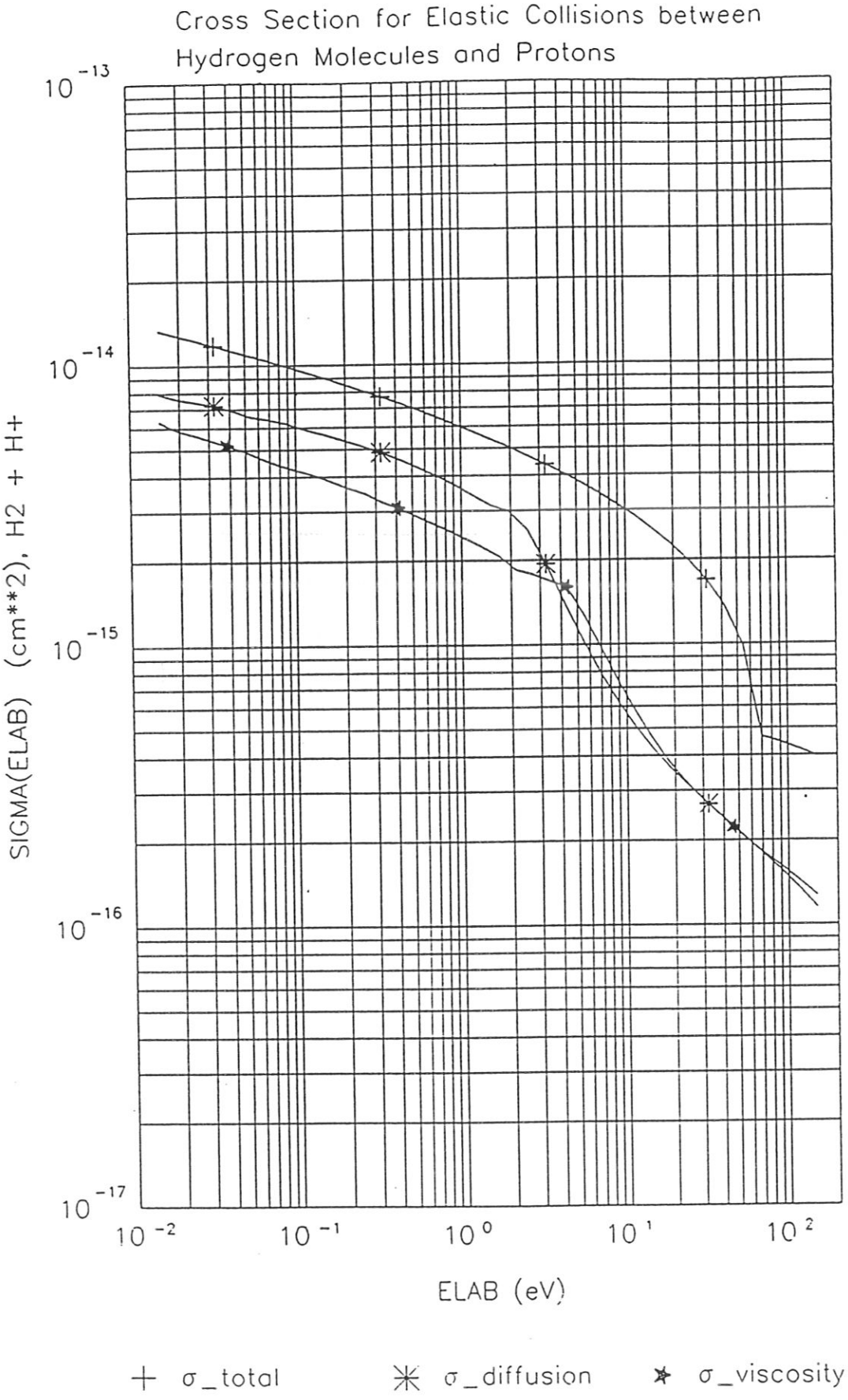

Figure 10: Cross sections as function of the ion energy E_{lab} for R3 $H^+ + H_2$.

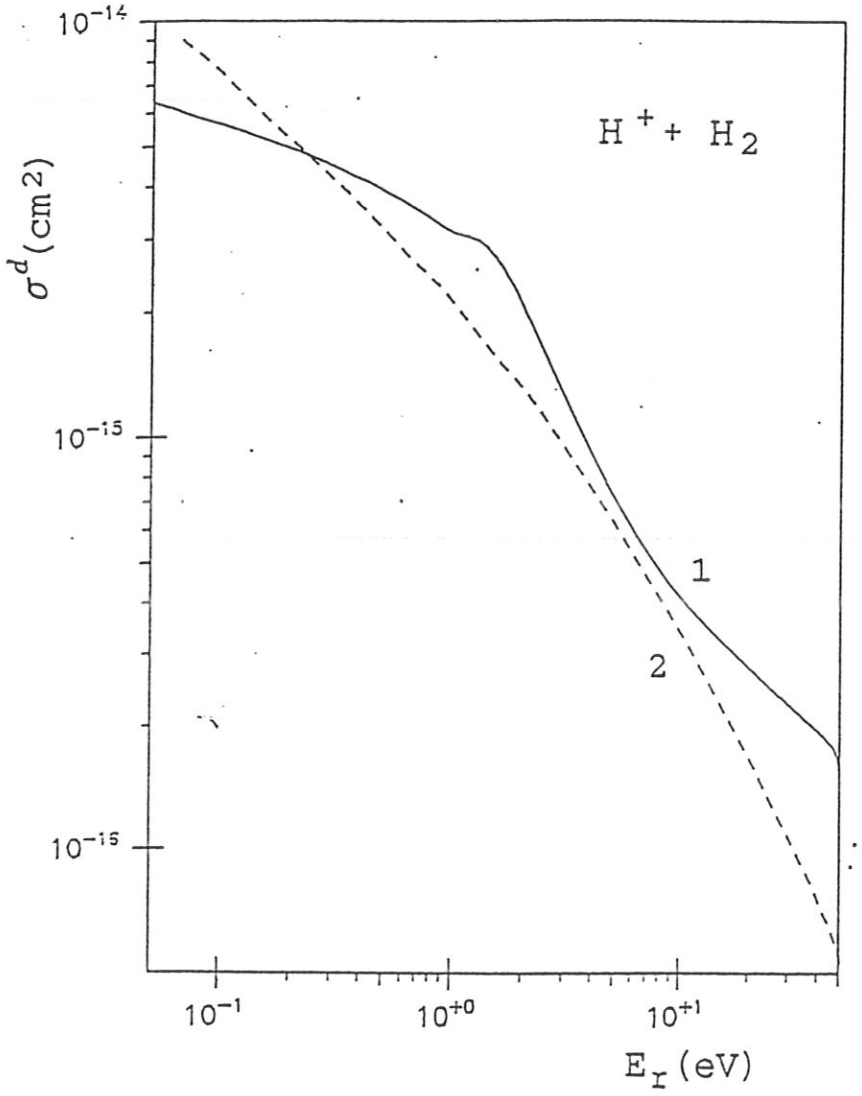

Figure 11: Comparison of diffusion cross section calculations for $H^+ - H_2$ collisions; 1 - this paper, 2 - [22].

Our results for the transport cross section are compared with latest calculations of [22] in Fig. 11. The agreement is rather satisfactory, especially in the energy range of interest $0.1 - 50eV$.

5.5 R4: $He^+ + He$

S. ref. [29].

$$\vec{R} = (2.55, 2.35, 0.9, 1.9842, 1.3990, 2.6345, 3.5986, 5.5410, 0.6061, 32.305) \quad (106)$$

($E_{labc} = 1.2122, E_{lab0} = 64.6090$)

SIGMA-TOTAL(ELAB)

ELABMIN=ELABC=1.2122 eV, ELABMAX=ELAB0=64.6090 eV

a0	-3.336949020454D+01	a1	4.374909804779D+00	a2	-1.517973301721D+01
a3	2.345459194687D+01	a4	-1.969436659467D+01	a5	9.472303986781D+00
a6	-2.604153028956D+00	a7	3.801132783280D-01	a8	-2.282922057203D-02
al0	-3.291071330248D+01	al1	-2.416669402887D-01	al2	-9.821377921757D-03
ar0	-3.664691925424D+01	ar1	4.752719886448D-01	ar2	-8.280792916138D-02

SIGMA-DIFFUSION

ELABMIN=0.02 eV, ELABMAX=200 eV

a0	-3.332091557452D+01	a1	-3.823354679977D-01	a2	-2.666453887008D-01
a3	-8.177418933677D-02	a4	2.593188019755D-02	a5	8.320863897668D-03
a6	-1.649825718076D-03	a7	-2.491587647454D-04	a8	4.351897658362D-05
al0	4.524094200000D-15	al1	-1.115060000000D-01	al2	0.000000000000D+00
ar0	7.673020700000D-13	ar1	0.000000000000D+00	ar2	0.000000000000D+00

SIGMA-VISCOSITY

ELABMIN=0.02 eV, ELABMAX=200 eV

a0	-3.379346231200D+01	a1	-1.740525006979D-01	a2	-8.091712353563D-02
a3	-8.223847315134D-02	a4	-1.443276051210D-03	a5	6.530393601967D-03
a6	-5.593294441844D-05	a7	-1.742244159818D-04	a8	1.068285383642D-05
al0	3.261848864837D-15	al1	-1.115060177785D-01	al2	0.000000000000D+00
ar0	1.120563328874D-12	ar1	0.000000000000D+00	ar2	0.000000000000D+00

Table 4: Fitting parameters for cross sections for R3 $H^+ + H_2$.

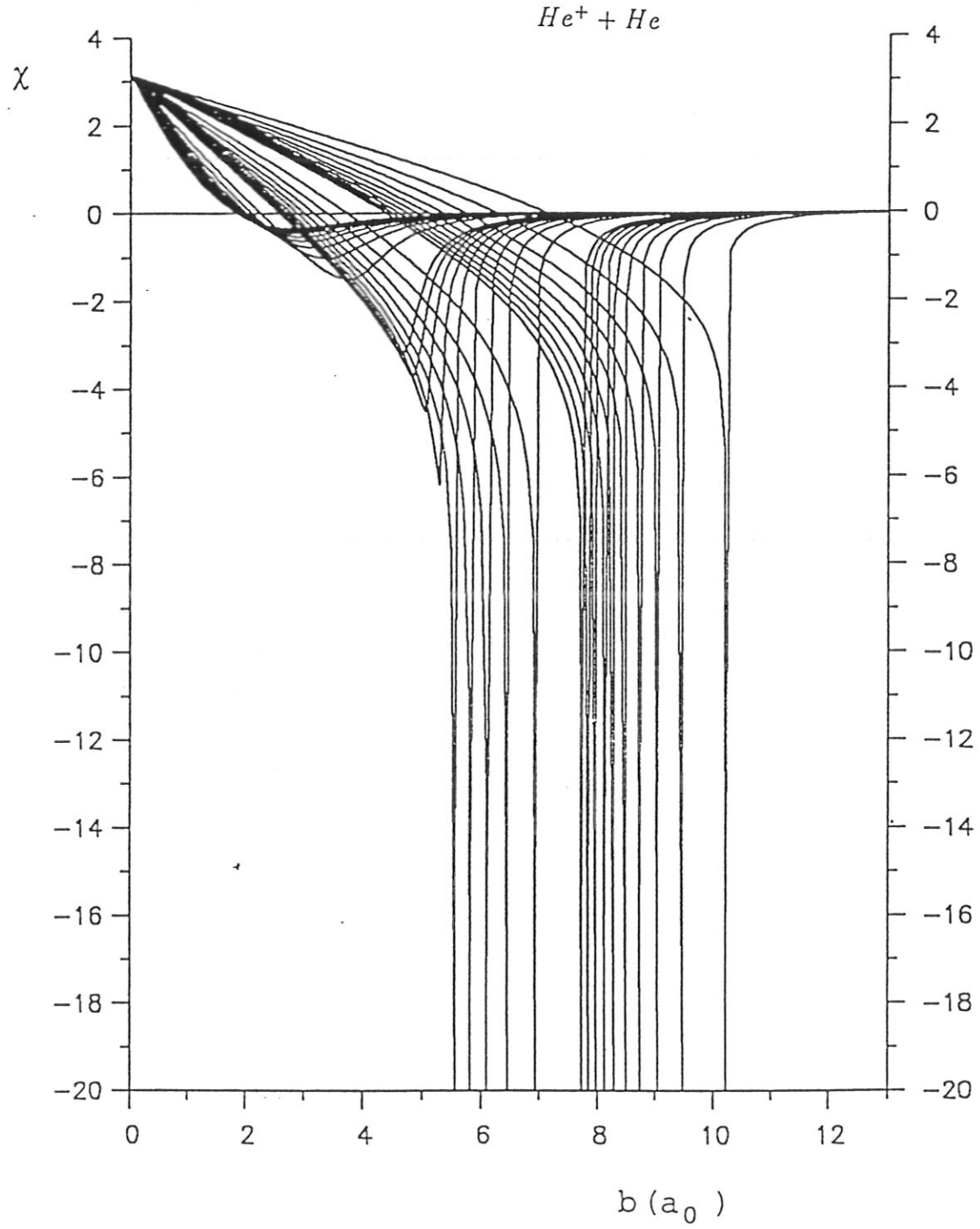

Figure 12: Deflection function $\chi(b, E_r)$ as function of the collision parameter b for relative energies $E_r = 0.01 - 10eV$.

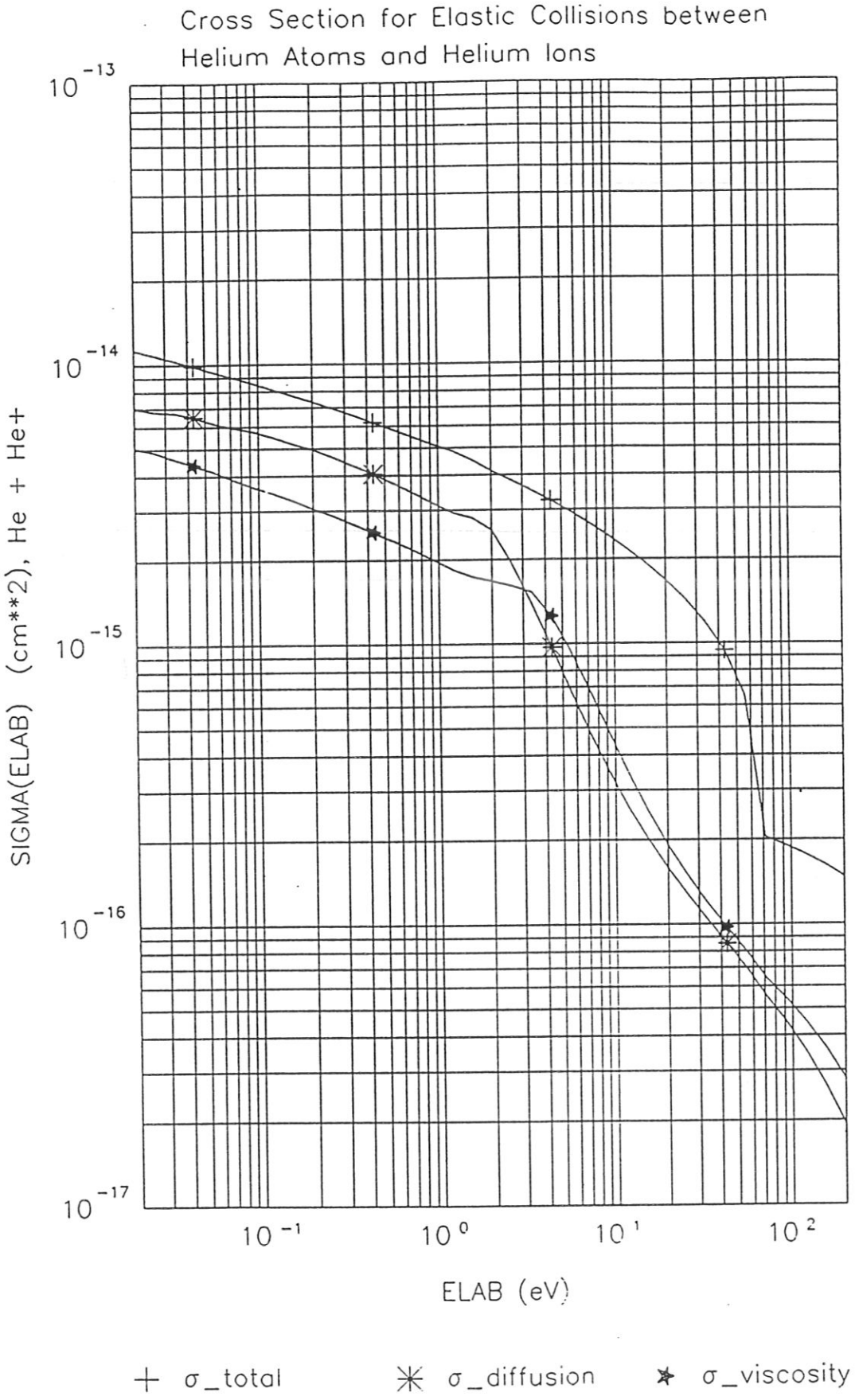

Figure 13: Cross sections as function of the ion energy E_{lab} for R4 $He^+ + He$.

5.6 Isotopes

"H" stands also for "D" and "T". For the isotopes we use the wellknown rule "that the relevant cross sections are independent of the isotope of hydrogen when the velocity in the center of mass system is the same" [11]. Let e.g. the following quantities be given:

$$\chi(b, E_r),\ \sigma^{t,d,v}(E_r),\ \langle v_r \sigma^t \rangle_\beta(E_\alpha, T_\beta),\ \langle v_r \sigma^t \rangle_{\beta\alpha}(T_{\alpha\beta}) \tag{104}$$

($E_\alpha := \frac{m_\alpha}{2} v_\alpha^2$) then the the simple scaling relations follows for the isotopes (denoted by "I"):

$$\chi^I(b, E_r) = \chi\left(b, \frac{m_r}{m_r^I} E_r\right), \tag{105}$$

$$\sigma^{t,d,v,I}(E_r) = \sigma^{t,d,v}(\frac{m_r}{m_r^I} E_r), \tag{106}$$

$$\langle v_r \sigma^t \rangle_\beta^I(E_\alpha, T_\beta) = \langle v_r \sigma^t \rangle_\beta \left(\frac{m_\alpha}{m_r^I} E_\alpha, \frac{m_r}{m_r^I} T_\beta\right), \tag{107}$$

$$\langle v_r \sigma^t \rangle_{\beta\alpha}^I(T_{\alpha\beta}) = \langle v_r \sigma^t \rangle_{\beta\alpha} \left(\frac{m_r}{m_r^I} T_{\alpha\beta}\right). \tag{108}$$

6 Data Fits for Collision Rates

6.1 Rates for the Monte Carlo Description

The collision rates for the Monte Carlo description (section 3.2) are functions of the two independent variables E_α (neutral beam energy in eV) and T_β (ion temperature in eV) and can be expressed in terms of the $I^{(l,r)}$ integrals which are represented by a two-parameter fit:

$$I^{(l,r)} \simeq \sum_{m=0}^{8} \sum_{n=0}^{8} A^{(l,r)}(m,n)\ (\ln E_\alpha)^m\ (\ln T_\beta)^m. \tag{109}$$

$I^{(0,0)}$, $I^{(1,0)}$, $I^{(1,1)}$:
R1 - Figs. 14, 15, 16, Tabs. 5, 6, 7
R2 - Figs. 17, 18, 19, Tabs. 8, 9, 10
R3 - Figs. 21, 21, 22, Tabs. 11, 12, 13
R4 - Figs. 23, 24, 25, Tabs. 14, 15, 16

R_{pd} - Figs. 26, 27, 28, 29 (R1 - R4)
R_{Ed} - Figs. 30, 31, 32, 33 (R1 - R4)

E-Index:	0	1	2
T-Index:			
0	-1.823472394862D+01	1.043929094352D-01	3.385021298310D-02
1	1.218869427323D-01	-8.071776515805D-02	-6.163024588310D-03
2	2.183144859635D-02	6.947238019788D-03	-1.029753867911D-02
3	-8.144414285471D-03	7.950619428888D-03	1.480212482573D-03
4	-2.414158185489D-03	-1.610515523206D-03	1.147576632073D-03
5	4.042335482230D-04	-3.333068266837D-04	-2.109287055048D-04
6	6.684610364551D-05	1.395481729149D-04	-3.872093410396D-05
7	-1.814826813629D-05	-1.589238118662D-05	1.137141330233D-05
8	1.049993252610D-06	6.124957529757D-07	-6.966443729323D-07

E-Index:	3	4	5
T-Index:			
0	-2.048059867515D-03	-4.577324303045D-03	5.174052650323D-05
1	8.404776509987D-03	5.448141329729D-04	-6.017991251450D-04
2	-1.660137737426D-03	1.687354957150D-03	1.123876140912D-05
3	-1.907814505083D-03	2.558232467687D-05	1.587671168547D-04
4	5.801892116713D-04	-2.945348864215D-04	-2.556467005779D-05
5	8.053144974289D-05	2.875034864587D-05	-9.746625582656D-06
6	-5.043290334814D-05	1.493675458929D-05	3.216371174204D-06
7	6.798870422148D-06	-3.269371275613D-06	-3.202325463122D-07
8	-3.006730549005D-07	1.854263211106D-07	1.033863743276D-08

E-Index:	6	7	8
T-Index:			
0	2.673201510283D-04	-4.451268371503D-05	2.199498285047D-06
1	3.536937592691D-05	9.054714466075D-06	-8.596768109209D-07
2	-1.224423097417D-04	2.126181472934D-05	-1.100195177512D-06
3	-2.858120151811D-05	1.112919746718D-06	4.374805864224D-08
4	2.747846551451D-05	-4.380086290415D-06	2.202510674285D-07
5	-6.360748557750D-07	3.783870577323D-07	-2.732689440408D-08
6	-1.738436960565D-06	2.363371059212D-07	-1.072861195261D-08
7	3.156490387804D-07	-5.006550452098D-08	2.526895478569D-09
8	-1.655735806555D-08	2.801053970232D-09	-1.467609659450D-10

Max. rel. Error: 0.5284 % Mean rel. Error: 0.0853 %

Table 5: R1 H+ + H I-0,0: <sigma*vrel>(Ti,Ebeam) (cm**3/s)

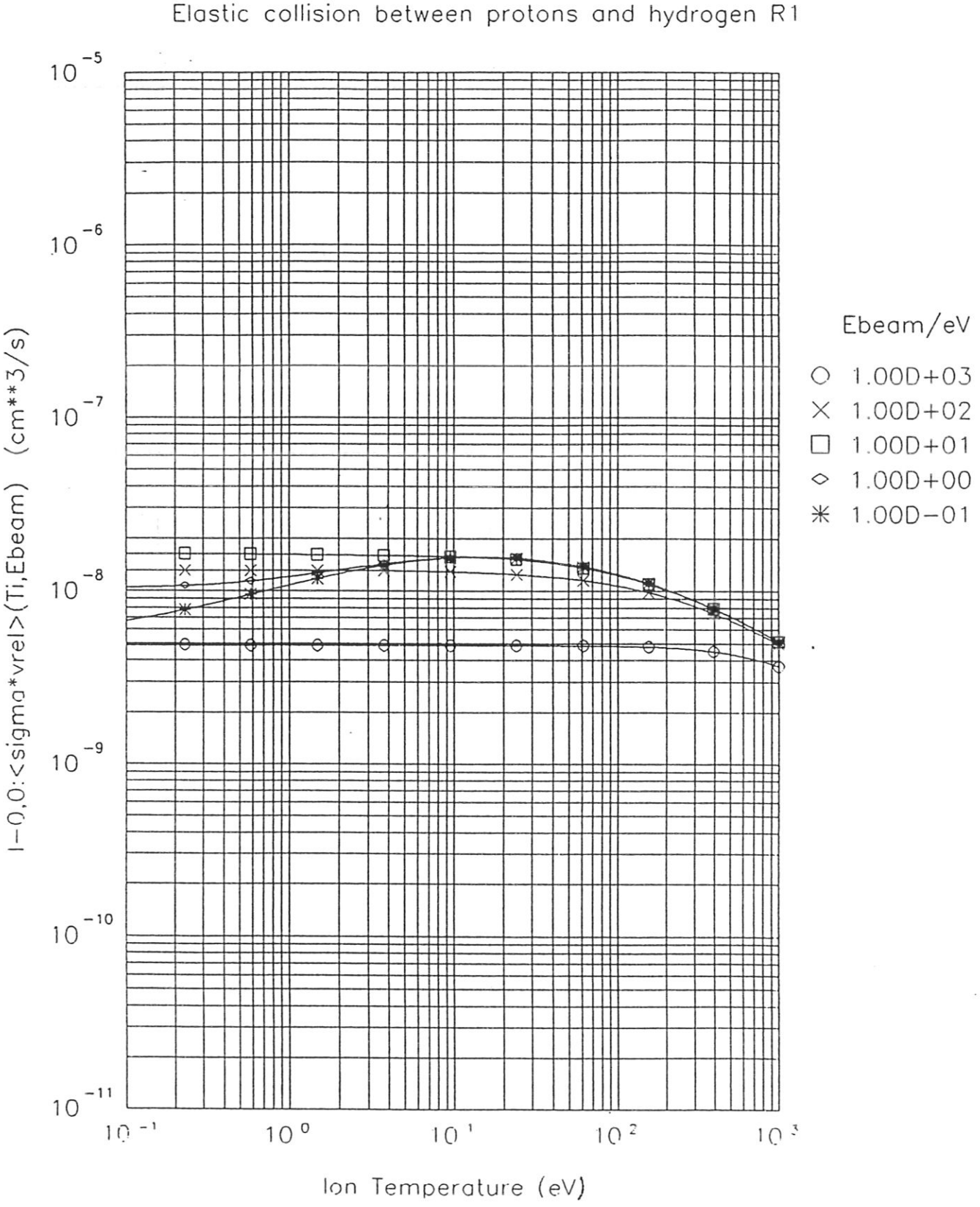

Figure 14: R1 $I^{(0,0)}$

E-Index:	0	1	2
T-Index:			
0	-1.934778779385D+01	2.193162842747D-02	-5.787610534513D-04
1	8.400121290584D-04	-5.025758478606D-02	9.405606314808D-03
2	-1.072570686950D-02	1.258217951174D-02	-7.629292880371D-03
3	-7.329656452946D-03	1.017355462044D-02	-2.212101744320D-03
4	-1.548110966373D-03	-4.141816249813D-03	1.623377903131D-03
5	8.780715214347D-05	-5.483013774324D-04	1.371503461028D-04
6	6.351915617491D-05	4.711920962053D-04	-1.702351291260D-04
7	-1.071915622348D-05	-7.653900655552D-05	2.828377077442D-05
8	5.468789447600D-07	3.989227802803D-06	-1.457895095025D-06

E-Index:	3	4	5
T-Index:			
0	-9.555854995025D-03	-3.071069026823D-03	5.668304238739D-04
1	1.213464571187D-02	-3.615417883123D-03	-8.289738887452D-04
2	-3.222678509228D-03	2.181349883244D-03	1.491076548317D-04
3	-4.530314087059D-03	1.707627243838D-03	3.285319171515D-04
4	1.894095127078D-03	-8.173359548467D-04	-1.268607651578D-04
5	2.806873100807D-04	-1.147859100868D-04	-2.036026302326D-05
6	-2.386998803904D-04	9.947217842552D-05	1.676927171418D-05
7	3.936468195914D-05	-1.609704117822D-05	-2.801579443731D-06
8	-2.077060263537D-06	8.298532548793D-07	1.504259503231D-07

E-Index:	6	7	8
T-Index:			
0	1.023499873278D-04	-4.375997865613D-05	3.554762032992D-06
1	4.794896057762D-04	-7.011568552117D-05	3.413857855011D-06
2	-2.352460376261D-04	4.210499686989D-05	-2.314387560956D-06
3	-2.365796504952D-04	3.759133611684D-05	-1.934588738006D-06
4	1.083092577128D-04	-1.817871861306D-05	9.758474990215D-07
5	1.584828965214D-05	-2.554030249359D-06	1.314431146313D-07
6	-1.358046593907D-05	2.254690862488D-06	-1.202340694084D-07
7	2.216781743757D-06	-3.678764178035D-07	1.970465840287D-08
8	-1.154459633382D-07	1.906633038081D-08	-1.021379321893D-09

Max. rel. Error: 2.5240 % Mean rel. Error: 0.4077 %

Table 6: R1 H+ + H I-1,0:<sigmad*vrel>(Ti,Ebeam) (cm**3/s)

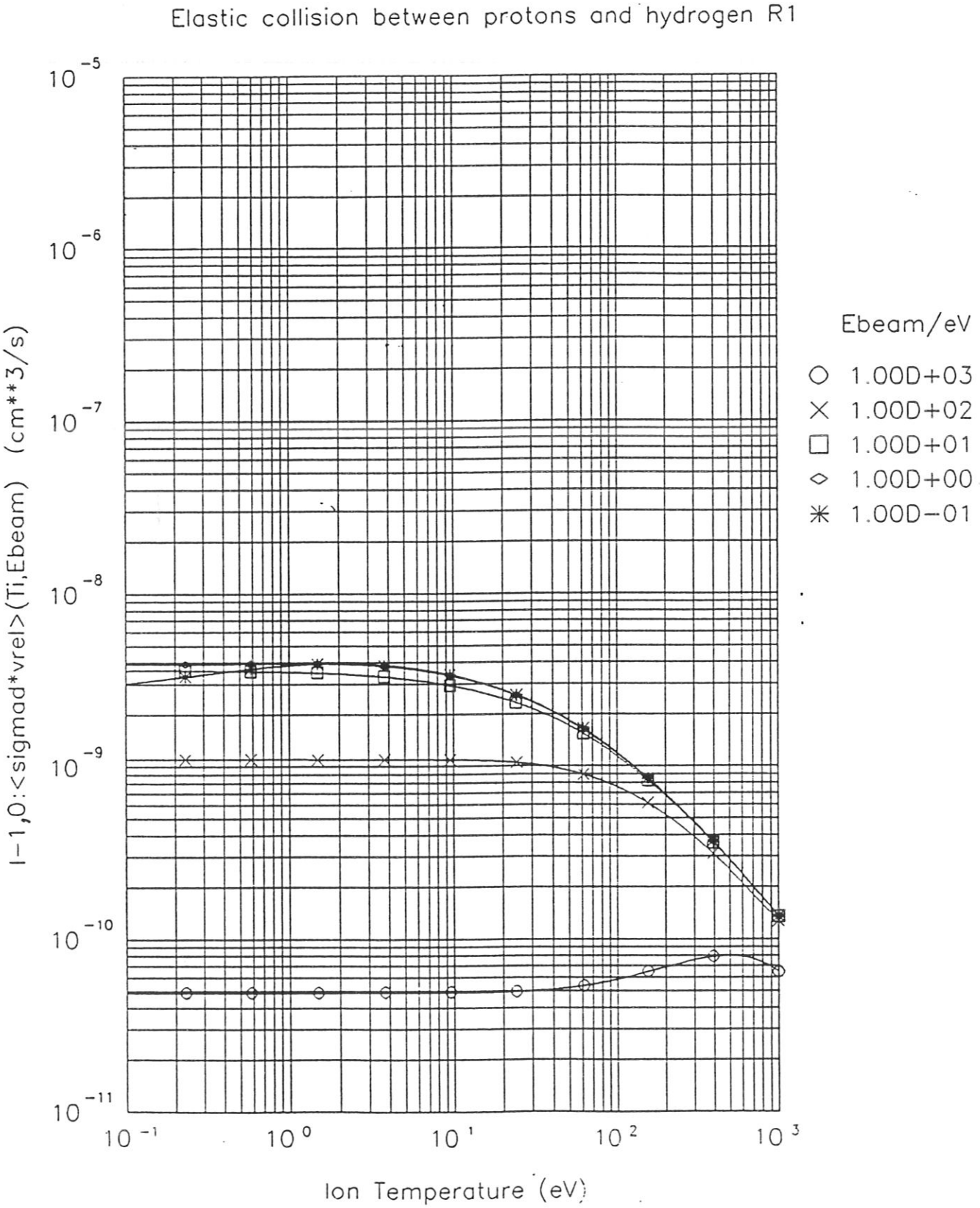

Figure 15: R1 $I^{(1,0)}$

E-Index:	0	1	2
T-Index:			
0	-1.893280308383D+01	1.809332485148D-01	1.037805412246D-01
1	-1.813705745114D-01	-2.429682065885D-01	3.669799030821D-02
2	9.573973280768D-02	-3.973236921355D-02	-2.207157450405D-02
3	5.847919043287D-03	8.646421713245D-03	-6.531680606595D-03
4	-4.821566918646D-03	6.981254569951D-03	2.271774294591D-03
5	-4.638780826729D-04	-5.798221624203D-04	3.495724706466D-04
6	2.209068836223D-04	-5.767720758207D-04	-1.428771763633D-04
7	-1.895897158953D-05	1.247954124608D-04	1.057955472741D-05
8	4.297598261156D-07	-7.279964818905D-06	-4.506748043711D-08

E-Index:	3	4	5
T-Index:			
0	-2.206664404116D-02	-4.112631526425D-03	1.331149639804D-03
1	8.922888262508D-03	-2.238872561608D-03	1.291726428852D-04
2	1.194590008826D-02	3.419600901668D-04	-1.077456946411D-03
3	1.098216188335D-03	2.011921632250D-04	-2.654423894351D-04
4	-3.240963831081D-03	3.223959313737D-04	3.237721432584D-04
5	6.174626810400D-05	-3.211981605184D-05	3.870111863120D-06
6	3.173447589758D-04	-4.853140104261D-05	-3.258534557599D-05
7	-6.460070103047D-05	1.209270360903D-05	6.305362305960D-06
8	3.751536468437D-06	-7.904476779972D-07	-3.576070642518D-07

E-Index:	6	7	8
T-Index:			
0	-6.879199183529D-05	-2.425931906907D-05	2.666077961877D-06
1	-7.278298736045D-05	1.927298683908D-05	-1.316844084907D-06
2	2.328248055432D-04	-2.009304248550D-05	6.267336072663D-07
3	9.936290403211D-05	-1.526644351318D-05	8.226433714787D-07
4	-1.080370300365D-04	1.292049390518D-05	-5.536714827713D-07
5	-2.182907372321D-06	5.733100495282D-07	-4.117187369787D-08
6	1.278264277649D-05	-1.680525966610D-06	7.746785072481D-08
7	-2.600477805112D-06	3.409251954936D-07	-1.545589066661D-08
8	1.543811101222D-07	-2.042813606586D-08	9.258970196457D-10

Max. rel. Error: 2.4038 % Mean rel. Error: 0.4386 %

Table 7: R1 H+ + H I-1,1:<vr*sigmad*vrel>(Ti,Ebeam) (cm**3/s)

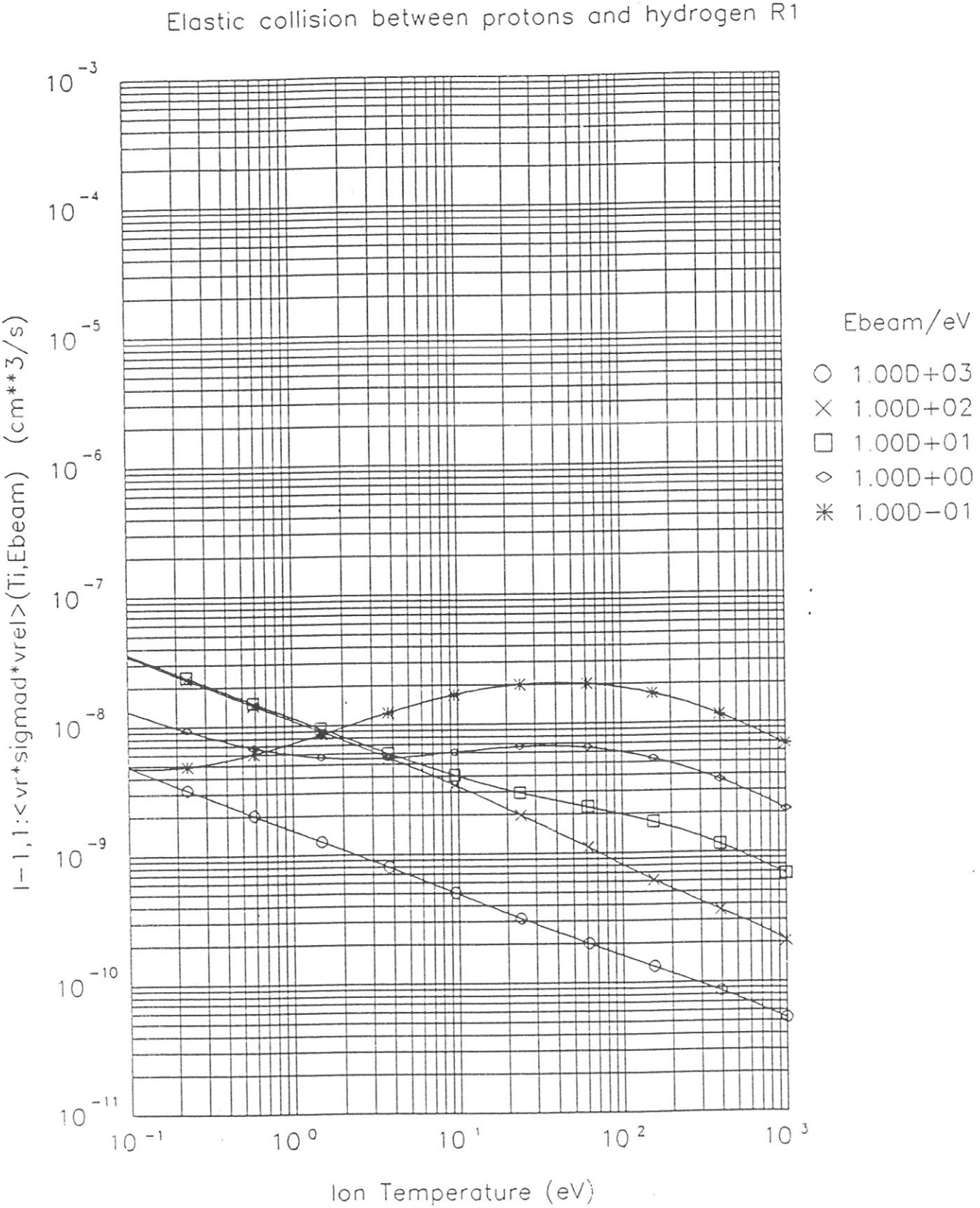

Figure 16: R1 $I^{(1,1)}$

E-Index:	0	1	2
T-Index:			
0	-1.934393021918D+01	6.563446707236D-02	-1.132533853318D-01
1	1.301350106064D-01	-4.071555273225D-02	2.016906859537D-02
2	1.828664127573D-02	1.460635793653D-02	6.745665311224D-03
3	-1.572566883649D-02	-3.953675178715D-03	1.747850519967D-03
4	-1.651243630315D-02	-2.847284094044D-04	-1.016420463987D-03
5	1.536731193440D-03	5.204625005620D-04	-1.110404741405D-04
6	1.407936221176D-03	-1.273303544933D-04	7.874267771795D-05
7	-3.024575206489D-04	1.258652128299D-05	-9.943699290077D-06
8	1.717075379788D-05	-4.489657191575D-07	3.942435517534D-07

E-Index:	3	4	5
T-Index:			
0	-2.108203840264D-02	5.126981927132D-02	-3.332060792240D-03
1	4.145056754712D-03	-1.207683748654D-02	9.777916409735D-04
2	-2.343836845279D-03	-2.643817205066D-03	4.122233549648D-04
3	1.316616725294D-03	-3.328603688720D-04	-1.025202074732D-04
4	2.115185323595D-04	3.305924890461D-04	-4.422649148500D-05
5	-2.096646478748D-04	4.907753719257D-05	1.750257851569D-05
6	3.694523090258D-05	-3.137559296212D-05	-2.054573401396D-06
7	-2.076330117601D-06	3.934064976552D-06	7.117080375326D-08
8	5.837947019108D-09	-1.543181228289D-07	1.142825149606D-09

E-Index:	6	7	8
T-Index:			
0	-5.396242466413D-03	1.236276138019D-03	-7.628885182442D-05
1	1.273531852240D-03	-3.057392495993D-04	1.949879233267D-05
2	2.238463116916D-04	-5.822708605029D-05	3.713522343609D-06
3	3.644852940119D-05	-2.948705115200D-06	2.772902778994D-08
4	-2.296832307757D-05	5.703124977270D-06	-3.560603032570D-07
5	-7.404629231556D-06	8.730873892378D-07	-3.238131969596D-08
6	3.004305767140D-06	-4.823864866020D-07	2.370653749977D-08
7	-3.116821151336D-07	4.985170981511D-08	-2.366645009836D-09
8	9.670471248063D-09	-1.366953072466D-09	5.308492125136D-11

Max. rel. Error: 43.0372 % Mean rel. Error: 3.6615 %

Table 8: R2 H+ + He I-0,0:<sigma*vrel>(Ti,Ebeam) (cm**3/s)

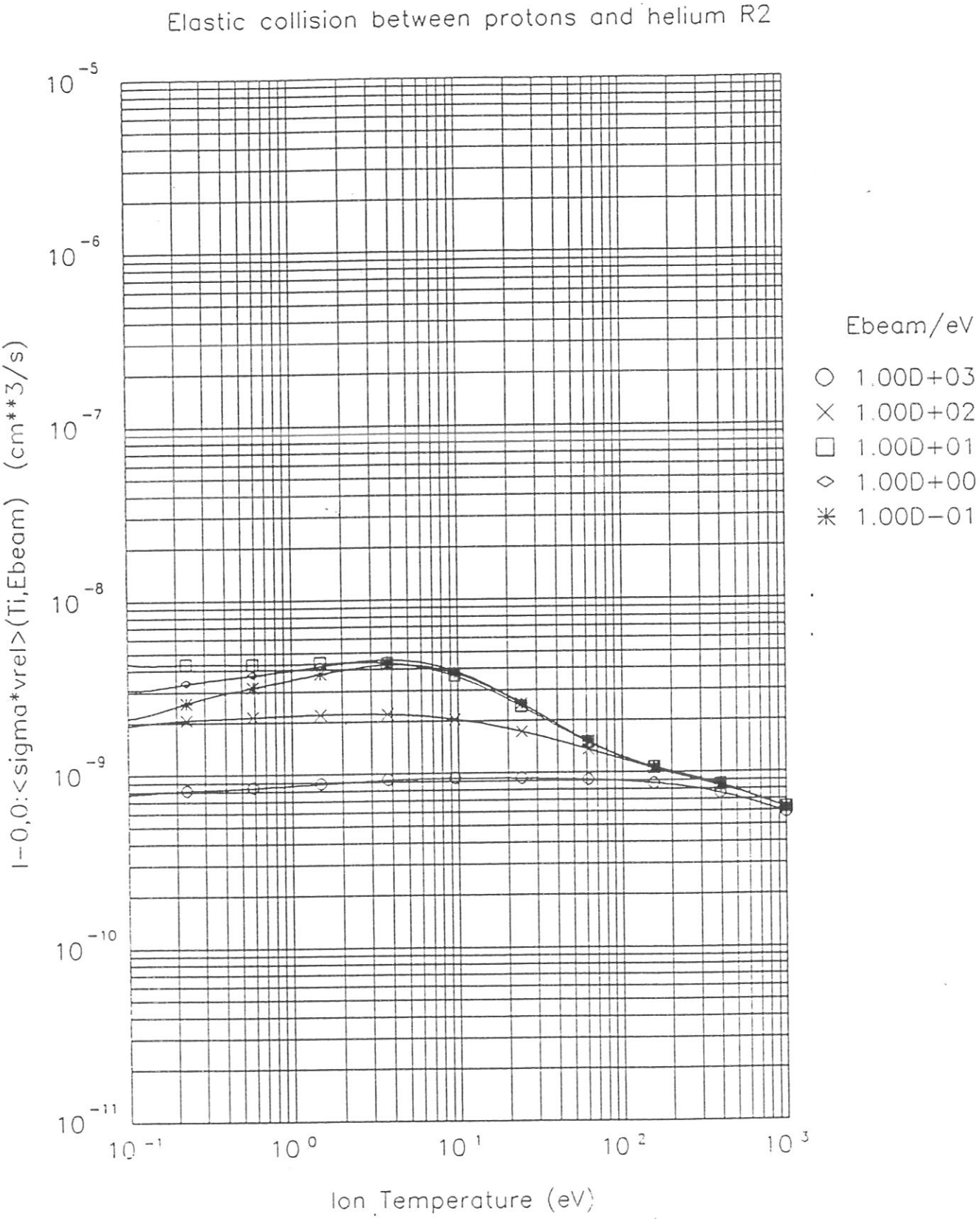

Figure 17: R2 $I^{(0,0)}$

E-Index:	0	1	2
T-Index:			
0	-2.038078616420D+01	-4.993496998398D-02	2.460551521383D-02
1	-3.301657139332D-01	-3.084287321372D-02	1.554461839749D-02
2	-1.250516030333D-01	3.495799299565D-02	-1.424614705786D-02
3	6.328424290736D-03	-3.821208294684D-03	-1.623627120526D-03
4	1.127524699096D-02	-2.410962290755D-03	1.757598241612D-03
5	-1.287708708939D-03	4.847023005705D-04	9.455808977270D-05
6	-6.368309748535D-04	4.413818051866D-05	-1.552922023412D-04
7	1.421859797928D-04	-1.659744792044D-05	2.551798508100D-05
8	-8.055939868827D-06	1.038460845033D-06	-1.289836231544D-06

E-Index:	3	4	5
T-Index:			
0	-1.517017165274D-02	-2.397648448576D-02	3.029365163804D-03
1	3.040700264374D-02	-2.593835985009D-03	-3.146176415388D-03
2	-9.657174093701D-03	7.433666067399D-03	4.191585645845D-04
3	-2.321909525809D-03	7.614727149051D-04	2.681001889717D-04
4	1.188908537635D-03	-1.115315269461D-03	-4.859218322237D-05
5	3.089582619996D-05	7.699187722499D-06	-8.863762072239D-06
6	-6.629197652130D-05	8.154996921696D-05	1.796356820001D-06
7	9.800954064911D-06	-1.473582389149D-05	6.040382986474D-08
8	-4.465334549154D-07	7.821310450330D-07	-1.548297648690D-08

E-Index:	6	7	8
T-Index:			
0	2.120043324652D-03	-5.206063712236D-04	3.229462400161D-05
1	6.652125688558D-04	-2.834612166641D-05	-1.127219264426D-06
2	-8.556829101842D-04	1.582340533265D-04	-8.789744795492D-06
3	-1.226460004470D-04	1.517380199975D-05	-6.070841562603D-07
4	1.341954089088D-04	-2.572769659598D-05	1.459166812937D-06
5	-8.619326544178D-07	6.166331772717D-07	-5.093661426041D-08
6	-9.360612397745D-06	1.830066731050D-06	-1.043424396036D-07
7	1.676084936402D-06	-3.453407619810D-07	2.029350887316D-08
8	-8.843599781403D-08	1.879251002731D-08	-1.123059892608D-09

Max. rel. Error: 4.5211 % Mean rel. Error: 1.0118 %

Table 9: R2 H+ + H I-1,0:<sigmad*vrel>(Ti,Ebeam) (cm**3/s)

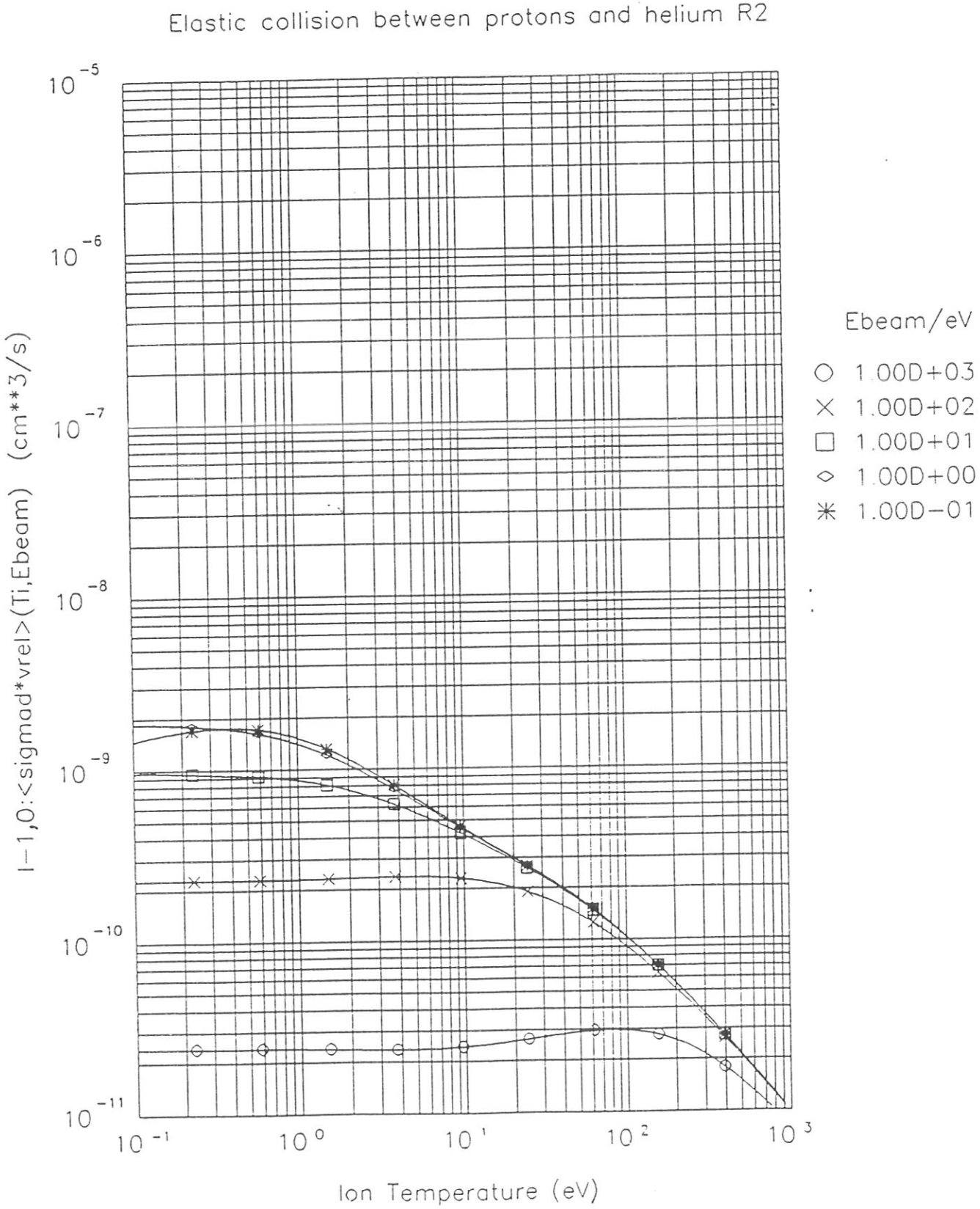

Figure 18: R2 $I^{(1,0)}$

E-Index:	0	1	2
T-Index:			
0	-2.004262674664D+01	-2.648788466793D-01	1.064561889610D-01
1	-1.797764352869D-01	-2.589808822195D-01	-2.877014349235D-02
2	1.737174089599D-02	8.451574686690D-02	-2.935292568884D-02
3	-5.858089549375D-03	1.300116465449D-02	9.529310584181D-03
4	4.388729900726D-03	-1.056813465073D-02	2.159091590529D-03
5	-4.504574356457D-05	2.276319679821D-04	-8.858013316042D-04
6	-4.476770214249D-04	6.274874468379D-04	-1.058851113237D-05
7	8.341320590920D-05	-1.152282812127D-04	2.416987285310D-05
8	-4.390962355387D-06	6.178247531671D-06	-1.856948074661D-06

E-Index:	3	4	5
T-Index:			
0	-4.738221512682D-03	-1.901339515018D-02	2.343037793374D-03
1	3.650521345152D-02	3.453680140262D-03	-3.282325570479D-03
2	-1.891965944862D-02	7.358231901363D-03	1.147601395752D-03
3	-3.671491036801D-03	-1.222846070981D-03	4.129698568122D-04
4	3.308490461853D-03	-9.985060699640D-04	-2.436577400879D-04
5	-9.078613592366D-05	1.963992719243D-04	-3.960007005625D-06
6	-2.145126223323D-04	4.375988559671D-05	1.763349019291D-05
7	4.102795185965D-05	-1.327072526267D-05	-3.079164153708D-06
8	-2.262313786878D-06	8.562456646479D-07	1.623733246626D-07

E-Index:	6	7	8
T-Index:			
0	1.535354337471D-03	-3.866801577896D-04	2.439791534963D-05
1	2.010776605309D-04	5.225211354986D-05	-5.112713443335D-06
2	-8.223456065458D-04	1.243832224007D-04	-6.129991458811D-06
3	2.187254434187D-05	-1.403000390400D-05	9.871340103785D-07
4	1.336318399731D-04	-1.877384276977D-05	8.784316542217D-07
5	-1.631297718648D-05	3.130542032283D-06	-1.720444423354D-07
6	-7.282426495611D-06	9.082225071317D-07	-3.861661099382D-08
7	1.774399156600D-06	-2.521618280322D-07	1.180298559372D-08
8	-1.078832469048D-07	1.597831941309D-08	-7.678677547486D-10

Max. rel. Error: 4.1291 % Mean rel. Error: 0.7842 %

Table 10: R2 H+ + He I-1,1:<vr*sigmad*vrel>(Ti,Ebeam) (cm**3/s)

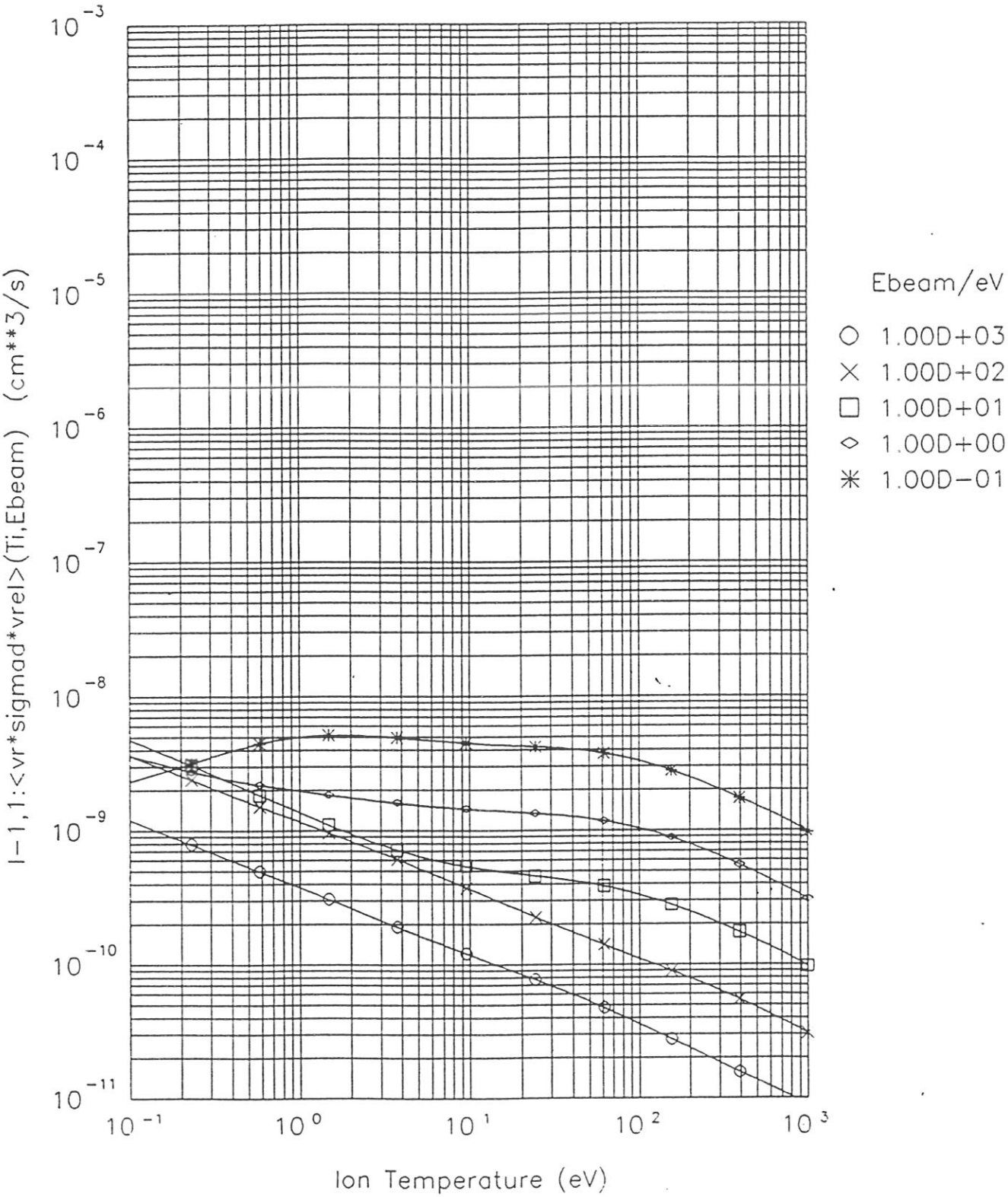

Figure 19: R2 $I^{(1,1)}$

E-Index:	0	1	2
T-Index:			
0	-1.849409655754D+01	1.283419330269D-01	-9.298076119636D-02
1	2.081196490227D-01	-9.595770725433D-02	4.590705202119D-03
2	2.269143436656D-02	1.280835259137D-02	8.136623918103D-03
3	-1.773337829348D-02	8.439634080507D-03	1.676970175345D-03
4	-3.401294776240D-03	-2.696330270142D-03	-6.940218497937D-04
5	7.343036400267D-04	-2.038654949880D-04	-6.593949718670D-05
6	2.652476273846D-05	1.927604876128D-04	1.809419316709D-05
7	6.337331418786D-06	-2.897453013352D-05	1.426825700338D-06
8	-1.578591104791D-06	1.406208601823D-06	-2.508973082776D-07

E-Index:	3	4	5
T-Index:			
0	-2.537075343502D-02	4.761917937356D-02	-2.553053848041D-03
1	1.867292112155D-02	-9.369885267014D-03	-8.401790822053D-04
2	-4.767913695117D-03	-2.290960318722D-03	7.788867997223D-04
3	-1.606852983370D-03	5.325916848483D-05	1.224912824963D-04
4	1.111251759459D-03	-1.558450822527D-05	-1.220029473342D-04
5	-7.986437587006D-05	3.876946204606D-05	9.247368834482D-06
6	-5.107081868448D-05	4.879840170679D-06	4.871705406541D-06
7	1.083969091569D-05	-2.902641341133D-06	-1.004649260515D-06
8	-6.187460034531D-07	2.283013287947D-07	5.553630018999D-08

E-Index:	6	7	8
T-Index:			
0	-5.037914229016D-03	1.138466433594D-03	-7.014258440180D-05
1	1.262887221191D-03	-2.416533313825D-04	1.404526178368D-05
2	8.757785677951D-05	-4.129953020508D-05	2.994931683705D-06
3	-3.199601152587D-05	3.558766184985D-06	-1.610597401676D-07
4	2.893643028282D-05	-2.458585462832D-06	6.646447259350D-08
5	-6.022503903813D-06	8.928998880663D-07	-4.229893426780D-08
6	-1.828423548214D-06	2.625630760445D-07	-1.381327118590D-08
7	5.782666407450D-07	-9.315692860387D-08	5.028993633703D-09
8	-3.933252554179D-08	6.613689510186D-09	-3.620889707449D-10

Max. rel. Error: 24.2419 % Mean rel. Error: 3.5613 %

Table 11: R3 H+ + H2 I-0,0:<sigma*vrel>(Ti,Ebeam) (cm**3/s)

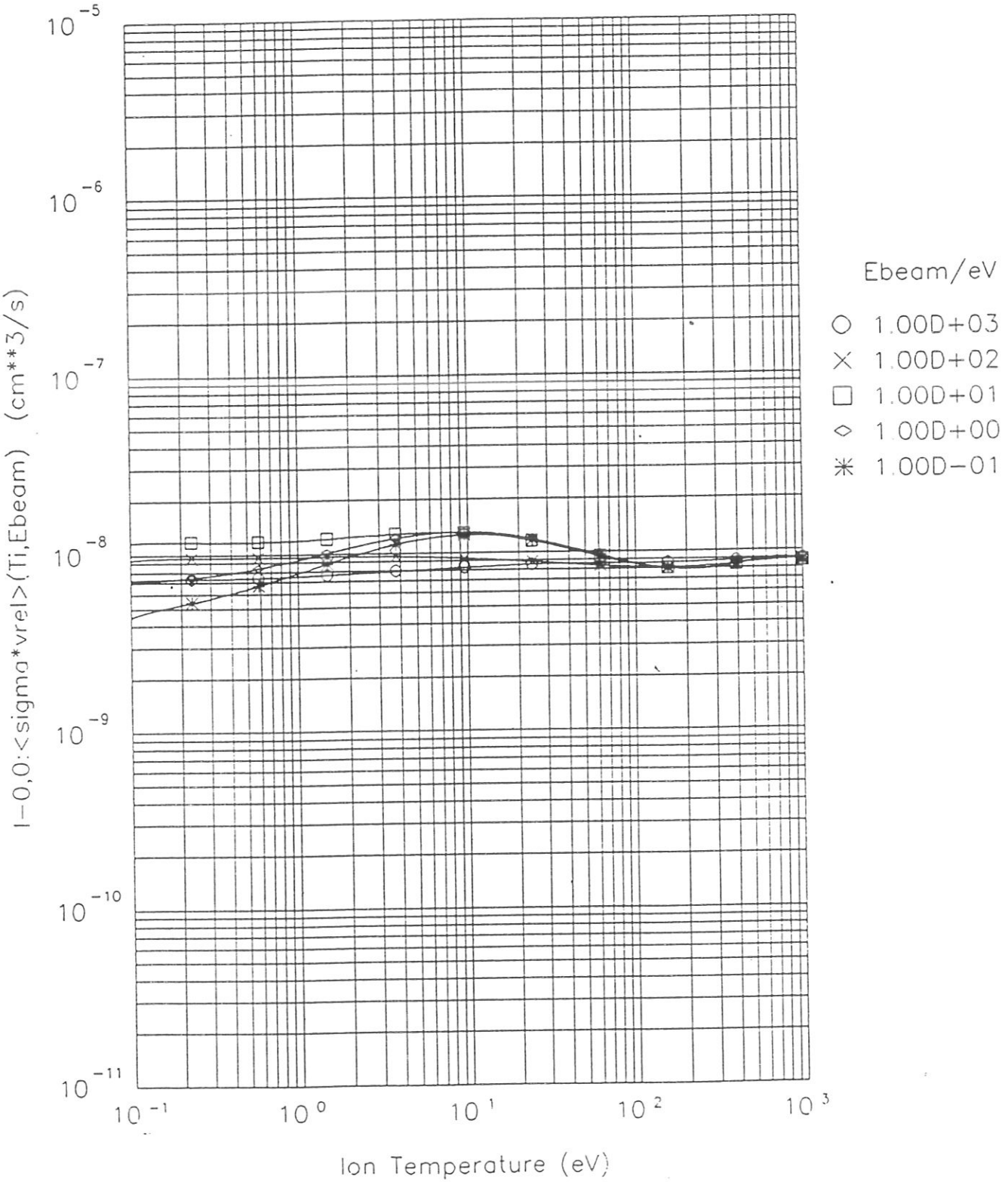

Figure 20: R3 $I^{(0,0)}$

E-Index:	0	1	2
T-Index:			
0	-1.919275366997D+01	-1.865238346305D-02	4.682617815803D-02
1	-5.947780482087D-02	-5.971382726967D-02	5.854568958623D-03
2	-9.004077564531D-02	3.225709371997D-02	-6.402554946956D-03
3	-1.870459871354D-02	-1.438038218134D-03	2.190778358004D-03
4	1.491376597764D-02	-1.614133948666D-03	-1.009422051586D-03
5	9.563126960467D-04	3.707880488168D-04	-7.731975035804D-05
6	-1.330077285945D-03	-5.353962725785D-05	1.351235395106D-04
7	2.020583687196D-04	6.849923024482D-06	-2.550615695507D-05
8	-9.277851726161D-06	-4.082429350941D-07	1.441579661485D-06

E-Index:	3	4	5
T-Index:			
0	-8.932266130300D-03	-2.903882752834D-02	3.477806471368D-03
1	1.637194804434D-02	-3.291459604645D-04	-1.492225099738D-03
2	-1.308998760658D-03	2.367849536658D-03	-2.633913429665D-04
3	-2.828299306442D-04	-4.686890203582D-07	4.818941917867D-05
4	-5.326505552258D-04	1.673303613736D-04	6.564947466483D-05
5	2.493241008729D-05	-2.434562819338D-05	-5.585591947606D-06
6	6.595946297185D-05	-2.509630806820D-05	-5.474903148493D-06
7	-1.420945572125D-05	6.290869308799D-06	1.207885423899D-06
8	8.431661832790D-07	-4.002257378192D-07	-7.135379893415D-08

E-Index:	6	7	8
T-Index:			
0	2.790218940150D-03	-6.908438427090D-04	4.338681573230D-05
1	1.443370523034D-04	2.409850106077D-05	-2.849926680503D-06
2	-1.712112384677D-04	4.233619961041D-05	-2.665571098691D-06
3	-1.902274102571D-05	2.446426035585D-06	-9.693955463859D-08
4	-2.847616427622D-05	3.578927723952D-06	-1.517016799547D-07
5	4.669438326556D-06	-7.601170248698D-07	3.823110747713D-08
6	3.257943960303D-06	-4.775908920414D-07	2.342435491722D-08
7	-8.361574596535D-07	1.290522448864D-07	-6.505820743915D-09
8	5.318078186713D-08	-8.385721089159D-09	4.277930018700D-10

Max. rel. Error: 5.2866 % Mean rel. Error: 1.2591 %

Table 12: R3 H+ + H2 I-0,1:<sigmad*vrel>(Ti,Ebeam) (cm**3/s)

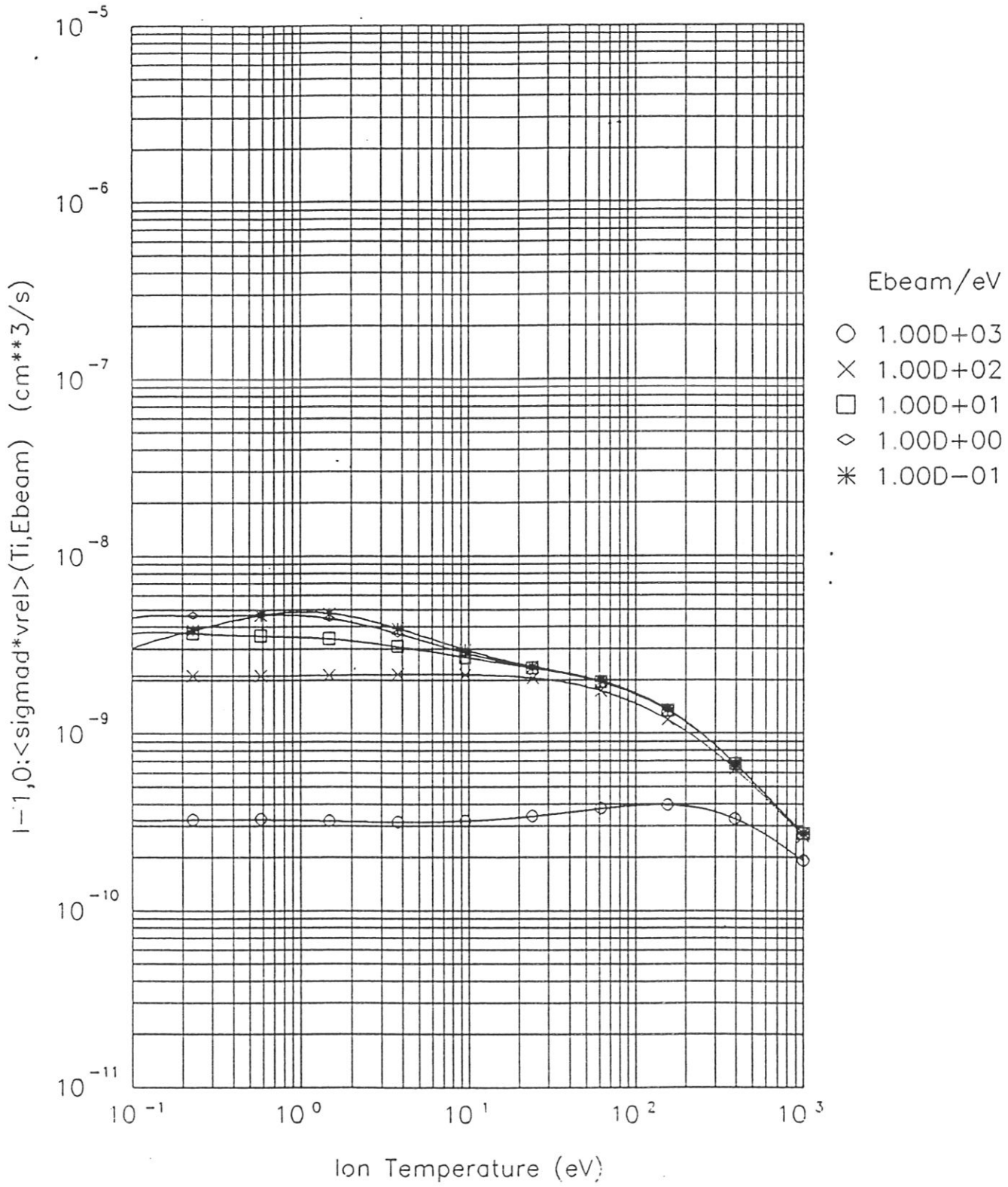

Figure 21: R3 $I^{(1,0)}$

E-Index:	0	1	2
T-Index:			
0	-1.885898159191D+01	-4.688742905730D-02	1.582000037005D-01
1	-1.142551728176D-01	-3.215442885845D-01	1.200002792532D-02
2	5.269447194063D-02	3.599963694446D-02	-3.743328945056D-02
3	-5.859028934034D-03	2.937916336270D-02	-1.635042388527D-03
4	4.963643933604D-03	-6.526710593352D-03	4.446380490362D-03
5	6.273092424172D-04	-1.687023563665D-03	-1.546192352476D-04
6	-6.668683746445D-04	7.486594274767D-04	-2.809911360537D-04
7	9.698091658029D-05	-9.393125909791D-05	5.290146271669D-05
8	-4.119108753583D-06	4.034865399708D-06	-2.851860740278D-06

E-Index:	3	4	5
T-Index:			
0	-4.742405501071D-03	-3.108751699462D-02	3.176766890632D-03
1	3.765795665438D-02	-2.352463912513D-03	-2.649501890791D-03
2	-4.608950153007D-03	6.497109332889D-03	-1.491179263739D-04
3	-8.449447888792D-03	1.839512419771D-03	6.213043072631D-04
4	1.833331856490D-03	-1.225797593418D-03	-7.486796463097D-05
5	6.475870274156D-04	-1.102956384497D-04	-5.565277982267D-05
6	-2.837797987792D-04	1.242725396467D-04	1.853928286841D-05
7	3.727608212769D-05	-2.033930573360D-05	-2.132867354414D-06
8	-1.688838198945D-06	1.045631687925D-06	8.675038559898D-08

E-Index:	6	7	8
T-Index:			
0	2.825016549631D-03	-6.817991936508D-04	4.244138278321D-05
1	4.562732456525D-04	-6.170529795689D-06	-1.752440295665D-06
2	-4.912030915473D-04	9.501442890057D-05	-5.283202586212D-06
3	-2.814162490200D-04	3.749919921800D-05	-1.708722663175D-06
4	1.194502891300D-04	-2.047826139669D-05	1.077170260238D-06
5	2.202273223120D-05	-2.809057152922D-06	1.247331052428D-07
6	-1.516681298686D-05	2.419606326774D-06	-1.235024924784D-07
7	2.317594651850D-06	-3.893258058753D-07	2.044727340968D-08
8	-1.156976062895D-07	2.005593649245D-08	-1.072246817479D-09

Max. rel. Error: 5.3290 % Mean rel. Error: 1.2016 %

Table 13: R3 H+ + H2 I-1,1:<vr*sigmad*vrel>(Ti,Ebeam) (cm**3/s)

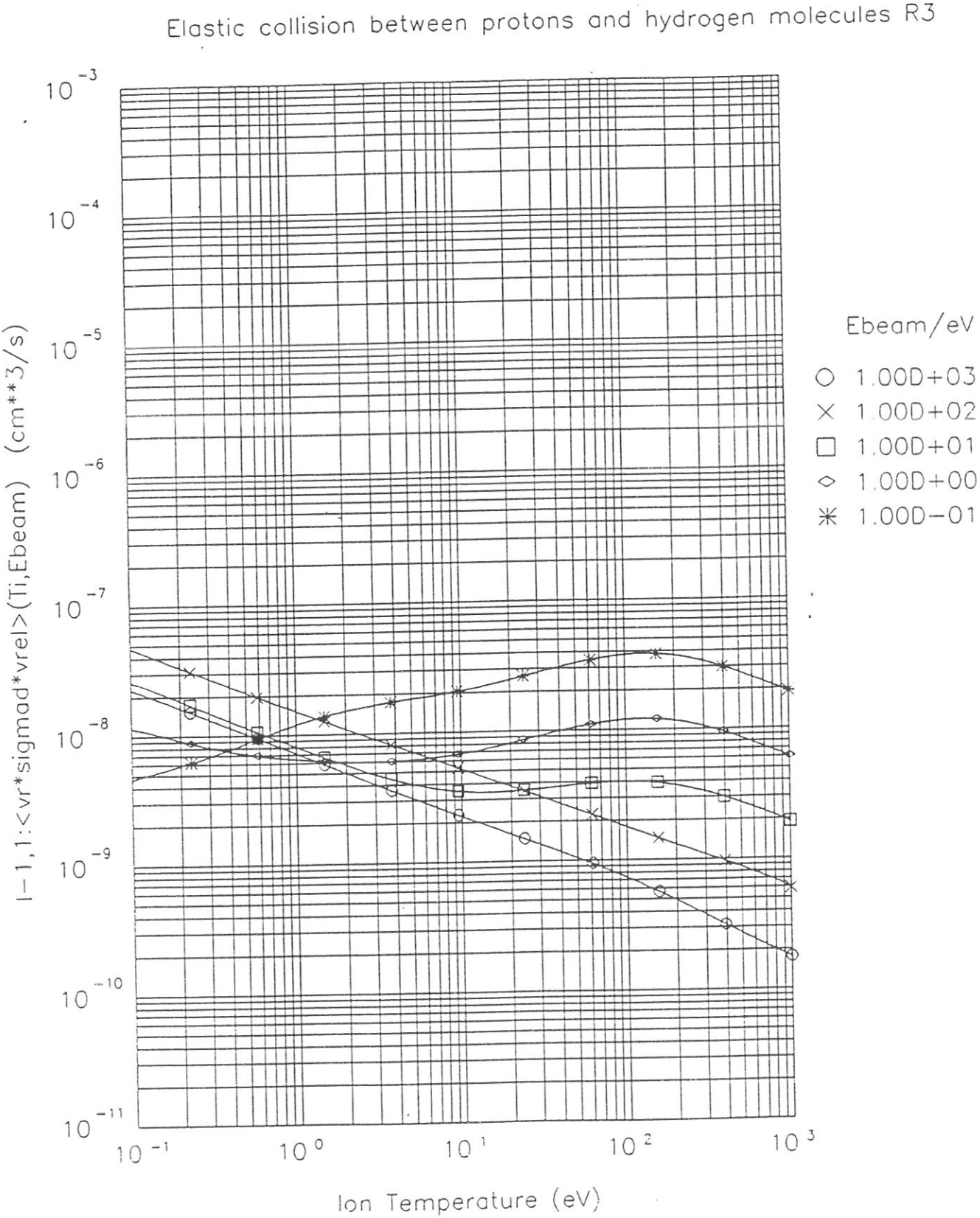

Figure 22: R3 $I^{(1,1)}$

E-Index:	0	1	2
T-Index:			
0	-1.932287393135D+01	-6.254173654177D-02	7.946623543420D-02
1	7.420452433663D-02	-1.124812231885D-02	-2.699799758379D-02
2	4.578246117879D-02	5.807748349427D-03	-6.767337797049D-03
3	9.376519610500D-03	3.743869063612D-03	1.935668442071D-03
4	-1.232363387636D-02	-1.100675144650D-03	3.439916049619D-04
5	-1.307054294818D-03	-8.910211076373D-05	-1.851109052007D-04
6	1.118562583548D-03	5.617956521495D-05	4.722943119535D-05
7	-1.434031268233D-04	-6.365356860650D-06	-7.103013883339D-06
8	5.358989072610D-06	2.334269507353D-07	4.090109024266D-07

E-Index:	3	4	5
T-Index:			
0	8.838505558116D-02	-2.793201134092D-02	-9.954061526499D-03
1	-1.884565424365D-02	1.123857510199D-02	1.596841699378D-03
2	-2.495042935023D-03	1.439511185350D-04	2.861967025267D-04
3	-2.047050990056D-03	-1.947991019023D-04	2.018359028340D-04
4	7.434976678383D-04	-4.730384293613D-05	-6.250784297096D-05
5	1.117168152610D-04	3.115251093953D-05	-1.325389437604D-05
6	-5.881739628460D-05	-1.308533305864D-05	6.051250040246D-06
7	6.666955388827D-06	2.380955160803D-06	-7.094040977952D-07
8	-2.367498282831D-07	-1.427503775556D-07	2.786934787376D-08

E-Index:	6	7	8
T-Index:			
0	3.764403463819D-03	-3.408466490224D-04	6.412518246520D-06
1	-1.389644457539D-03	2.161107270253D-04	-1.049187773127D-05
2	-4.171591875990D-06	-1.196874977368D-05	1.094079145119D-06
3	-1.598805546650D-05	-2.311078550298D-06	2.483893468689D-07
4	1.280702702425D-05	-7.877322455546D-07	9.482501133602D-09
5	-2.131389375108D-07	3.650222503579D-07	-2.688165319879D-08
6	1.603031094261D-07	-1.683294115673D-07	1.140269704662D-08
7	-1.056486811884D-07	3.540020523528D-08	-2.124298972987D-09
8	9.141132772747D-09	-2.324505150923D-09	1.328831955405D-10

Max. rel. Error: 45.6817 % Mean rel. Error: 5.1917 %

Table 14: R4 He+ + He I-0,0:<sigma*vrel>(Ti,Ebeam) (cm**3/s)

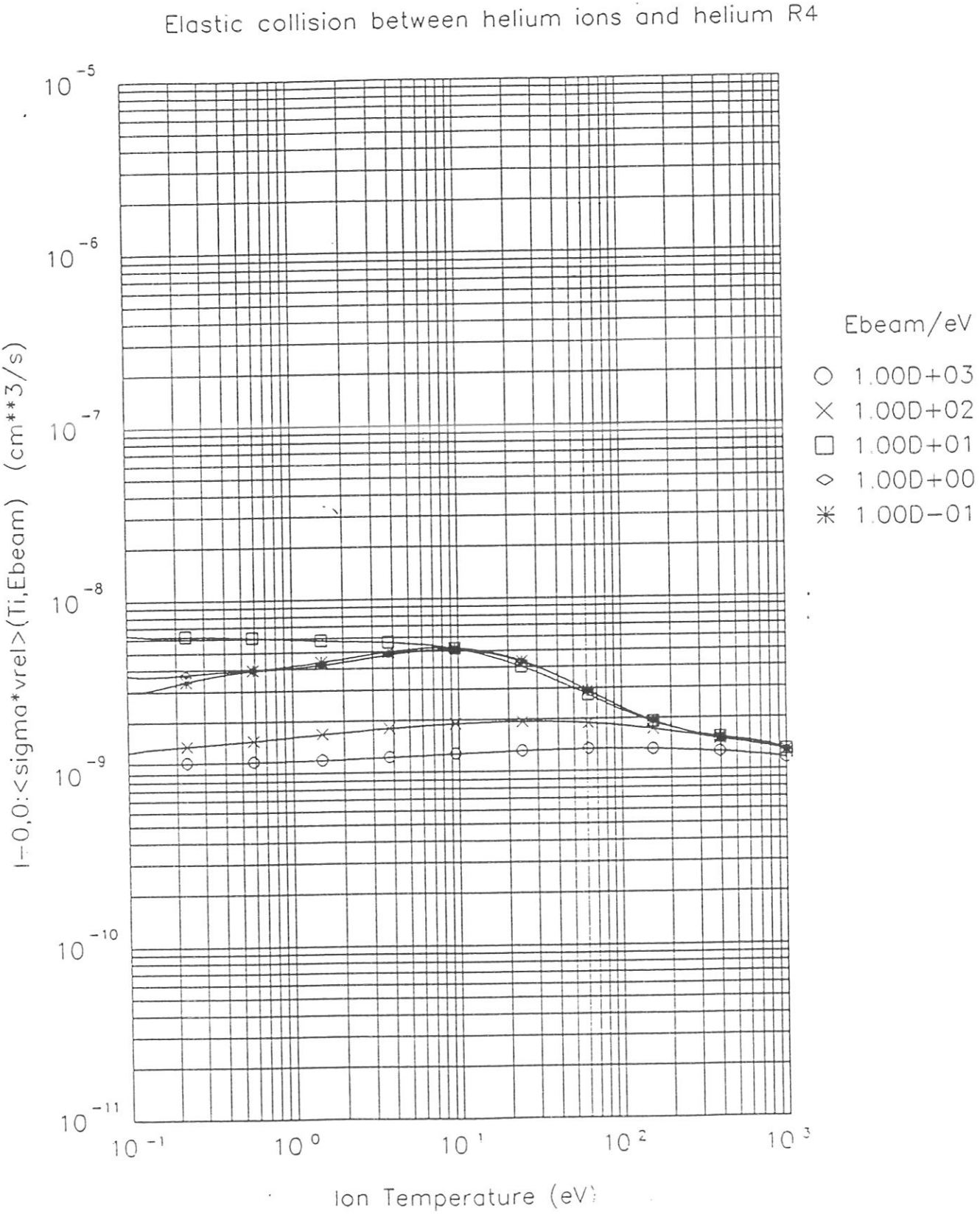

Figure 23: R4 $I^{(0,0)}$

E-Index:	0	1	2
T-Index:			
0	-2.005856706409D+01	-2.416298567134D-02	-1.290643907647D-01
1	-1.723033466633D-01	-2.876974997211D-02	6.358697996829D-02
2	-8.480540790141D-02	2.121102722373D-02	1.060648053441D-03
3	-1.583772608067D-02	2.831738365425D-04	3.604228124024D-04
4	7.141918601934D-03	-2.712847139884D-03	-1.390046088713D-03
5	1.050415524504D-03	3.514199969505D-04	-1.430457735837D-04
6	-5.609743409859D-04	1.114910501595D-04	1.776137463792D-04
7	5.528775780351D-05	-2.849479698839D-05	-2.957402039735D-05
8	-1.298487796038D-06	1.744141312203D-06	1.511018855995D-06

E-Index:	3	4	5
T-Index:			
0	-7.609374902789D-02	2.051842775759D-02	6.700343984959D-03
1	1.484173774740D-02	-1.259800535085D-02	-3.314345389346D-04
2	7.437796246116D-03	-1.933320600619D-03	-8.197110013265D-04
3	5.722003993817D-04	1.577284882295D-04	-1.165904265498D-04
4	-7.836120750894D-04	5.279763008829D-04	7.329216329788D-05
5	-8.871424676206D-05	1.610771935311D-06	9.934442032629D-06
6	6.401396318081D-05	-5.184619145829D-05	-4.985193070868D-06
7	-7.539210289621D-06	9.524059409052D-06	4.297672500003D-07
8	2.529392826633D-07	-5.084304524420D-07	-5.932611004947D-09

E-Index:	6	7	8
T-Index:			
0	-2.466827019035D-03	2.195450363238D-04	-4.275624910534D-06
1	9.943338501590D-04	-1.676144873446D-04	8.508217370560D-06
2	3.610884437671D-04	-4.659019201525D-05	2.019277552554D-06
3	1.134360853468D-05	9.293505569914D-07	-1.249357290876D-07
4	-6.844730630933D-05	1.119496625366D-05	-5.759041144367D-07
5	-1.298801064099D-06	-4.988842872544D-08	9.924160039487D-09
6	6.074150104979D-06	-1.029965177536D-06	5.399132209393D-08
7	-1.048375199655D-06	1.905679254148D-07	-1.033208843896D-08
8	5.357991449124D-08	-1.021819231976D-08	5.659599344410D-10

Max. rel. Error: 4.6006 % Mean rel. Error: 1.4030 %

Table 15: R4 He+ + He I-1,0:<sigmad*vrel>(Ti,Ebeam) (cm**3/s)

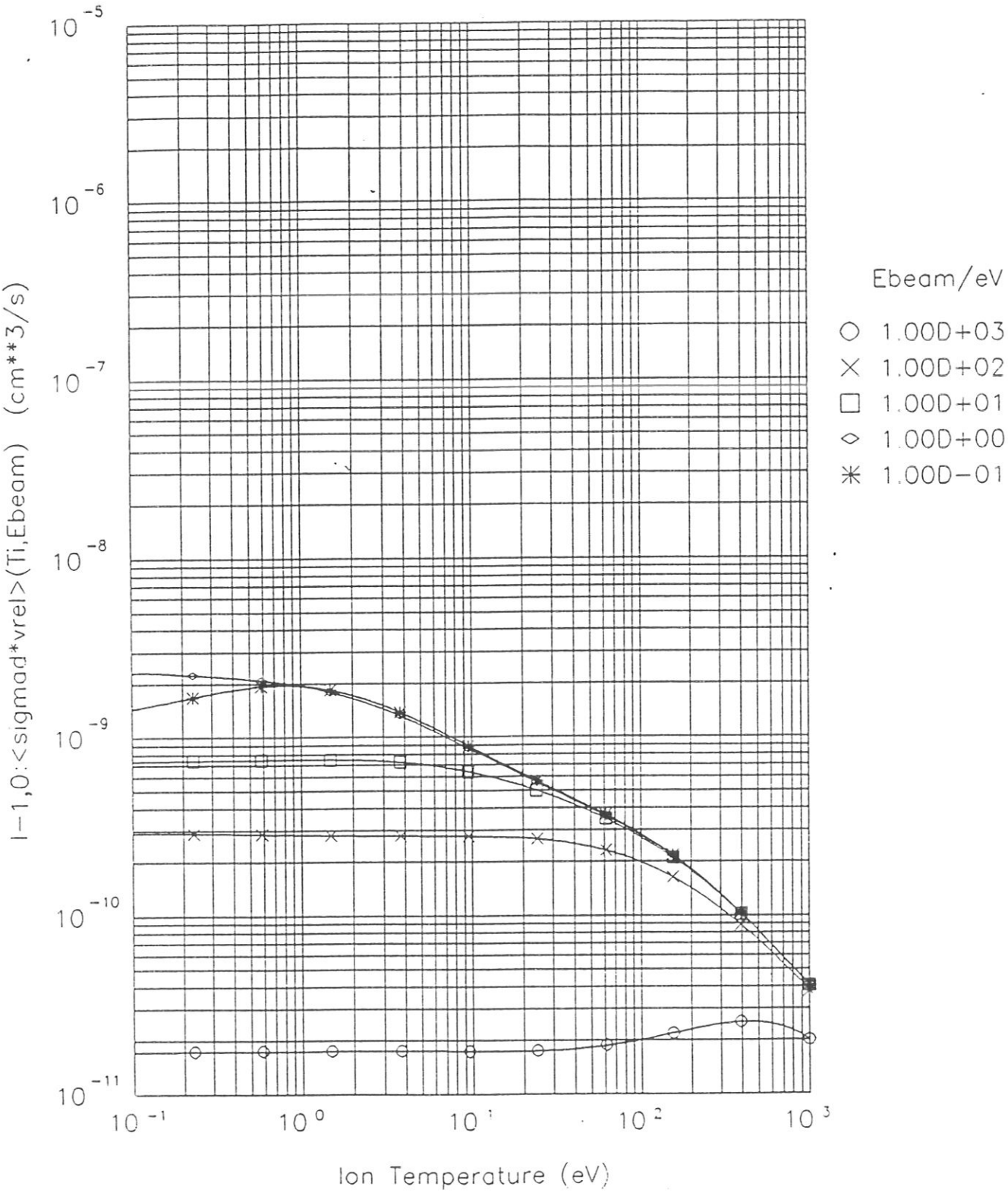

Figure 24: R4 $I^{(1,0)}$

E-Index:	0	1	2
T-Index:			
0	-1.971841089063D+01	8.328765891080D-02	-1.558343694814D-02
1	-4.021129107175D-01	-2.609736943206D-01	9.369633467927D-02
2	4.312686516296D-02	-2.138581379431D-02	-2.482925441555D-02
3	1.131603337384D-02	1.708943095018D-02	-9.669574079521D-03
4	-6.372279656275D-04	3.450989688689D-03	3.184862321732D-03
5	-4.197496216945D-04	-1.262006156495D-03	4.585825771369D-04
6	7.546872796026D-05	-1.355206530675D-04	-2.568705325515D-04
7	-1.404336436508D-05	5.894573516008D-05	3.150657122684D-05
8	1.145393186470D-06	-4.036098852278D-06	-1.245916015334D-06

E-Index:	3	4	5
T-Index:			
0	-7.188457180471D-02	1.700074938281D-02	6.003940077275D-03
1	2.894601328535D-02	-1.437496876274D-02	-1.045514358604D-03
2	1.296618463705D-02	9.376854211214D-04	-1.265992229210D-03
3	-3.011807860079D-03	1.779968374464D-03	6.322638402017D-05
4	-1.871916988104D-03	-2.204394122651D-04	1.988822588653D-04
5	3.595112707997D-04	-1.285009061291D-04	-1.961633516217D-05
6	8.787448883177D-05	3.320568895670D-05	-1.208420235447D-05
7	-2.507555005698D-05	-2.280086851128D-06	2.688408341473D-06
8	1.567816078760D-06	1.474230539862D-08	-1.559378727675D-07

E-Index:	6	7	8
T-Index:			
0	-2.192070799975D-03	1.960877020940D-04	-3.835692931077D-06
1	1.111722282165D-03	-1.651931882424D-04	7.727138359170D-06
2	1.937830444880D-04	-5.622220551477D-06	-3.940184224074D-07
3	-1.271755094339D-04	2.037772536199D-05	-1.002903796084D-06
4	-2.252300950102D-05	-6.752170751509D-07	1.483686590519D-07
5	1.243641416480D-05	-1.683451044181D-06	7.373587051673D-08
6	-2.172726597347D-07	3.374797313219D-07	-2.527501107844D-08
7	-3.006255833068D-07	-1.619043934512D-08	2.715431242193D-09
8	2.549917411141D-08	-3.891395046704D-10	-9.433802280274D-11

Max. rel. Error: 4.3483 % Mean rel. Error: 1.1783 %

Table 16: R4 He+ + He I-1,1:<vr*sigmad*vrel>(Ti,Ebeam) (cm**3/s)

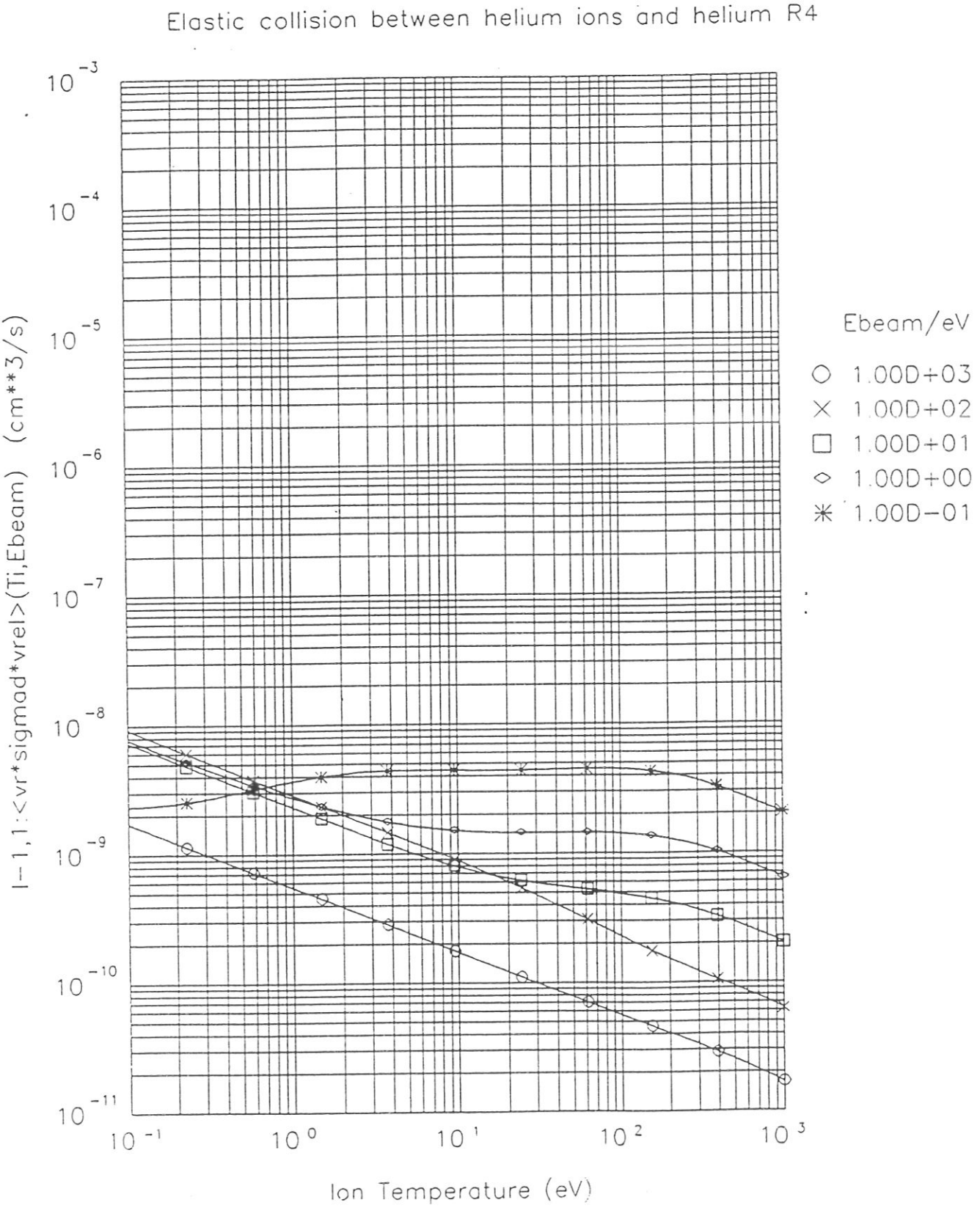

Figure 25: R4 $I^{(1,1)}$

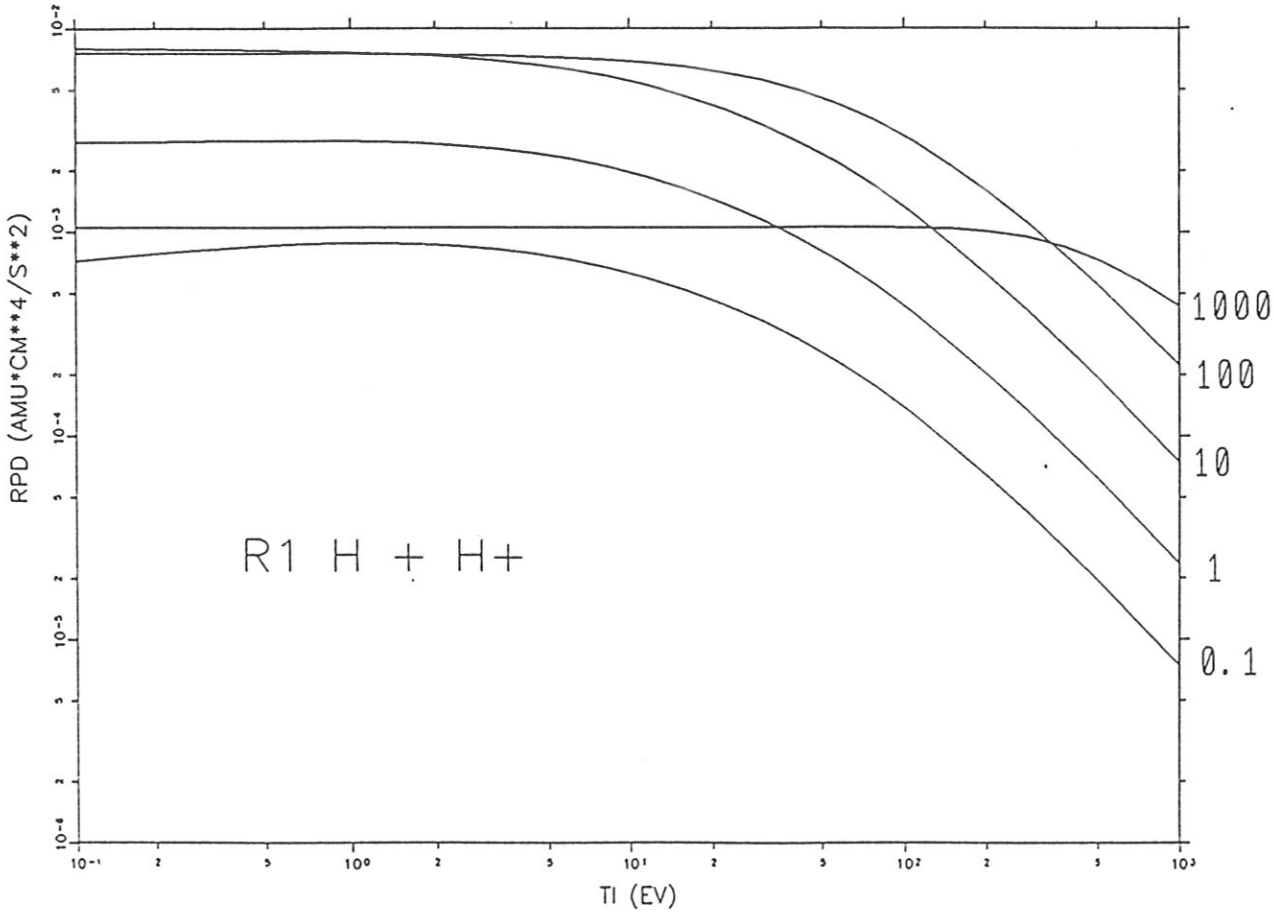

Figure 26: R1 R_{pd} as a function of T_i with the neutral beam energy $E_\alpha(eV)$ as parameter.

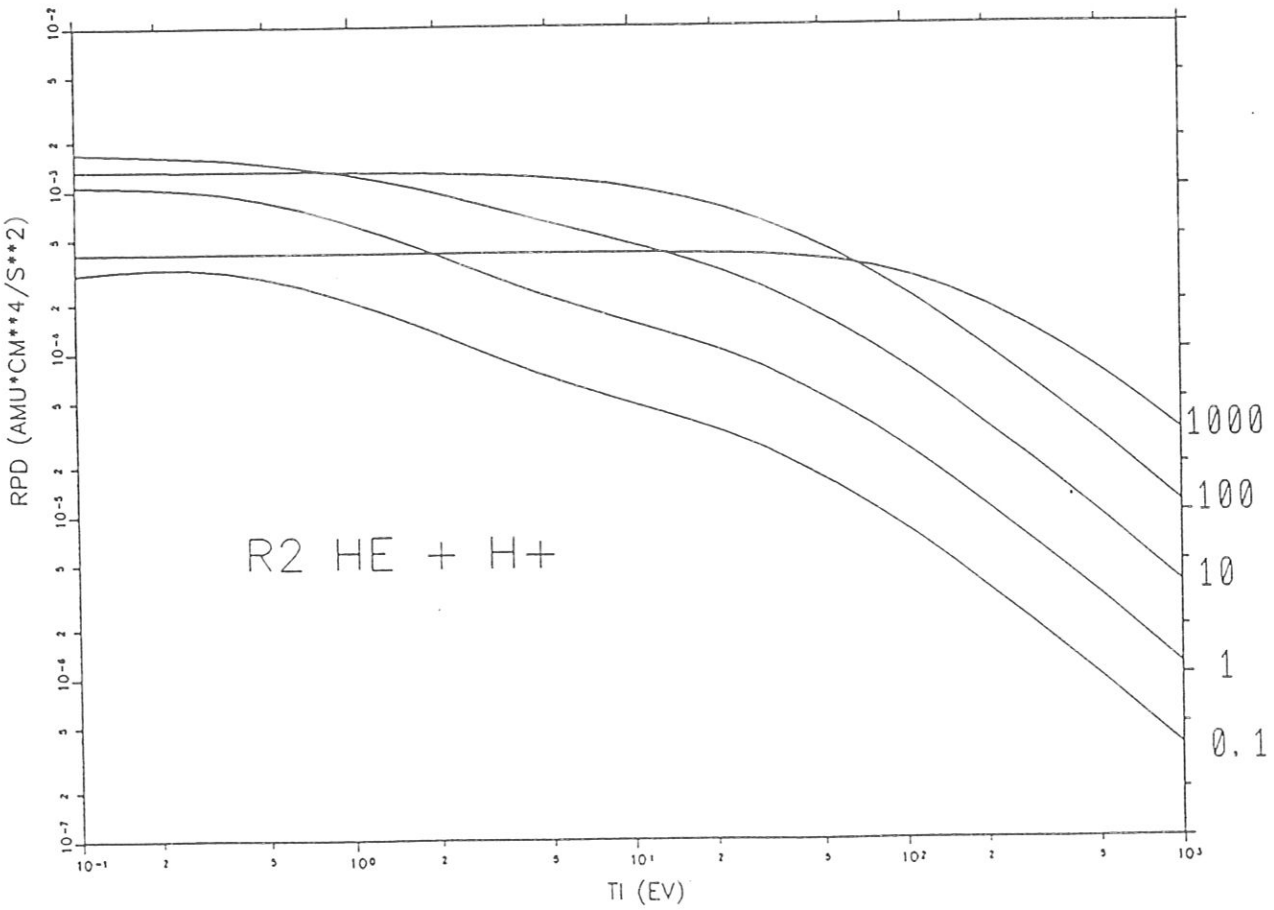

Figure 27: R2 R_{pd} as a function of T_i with the neutral beam energy $E_\alpha(eV)$ as parameter.

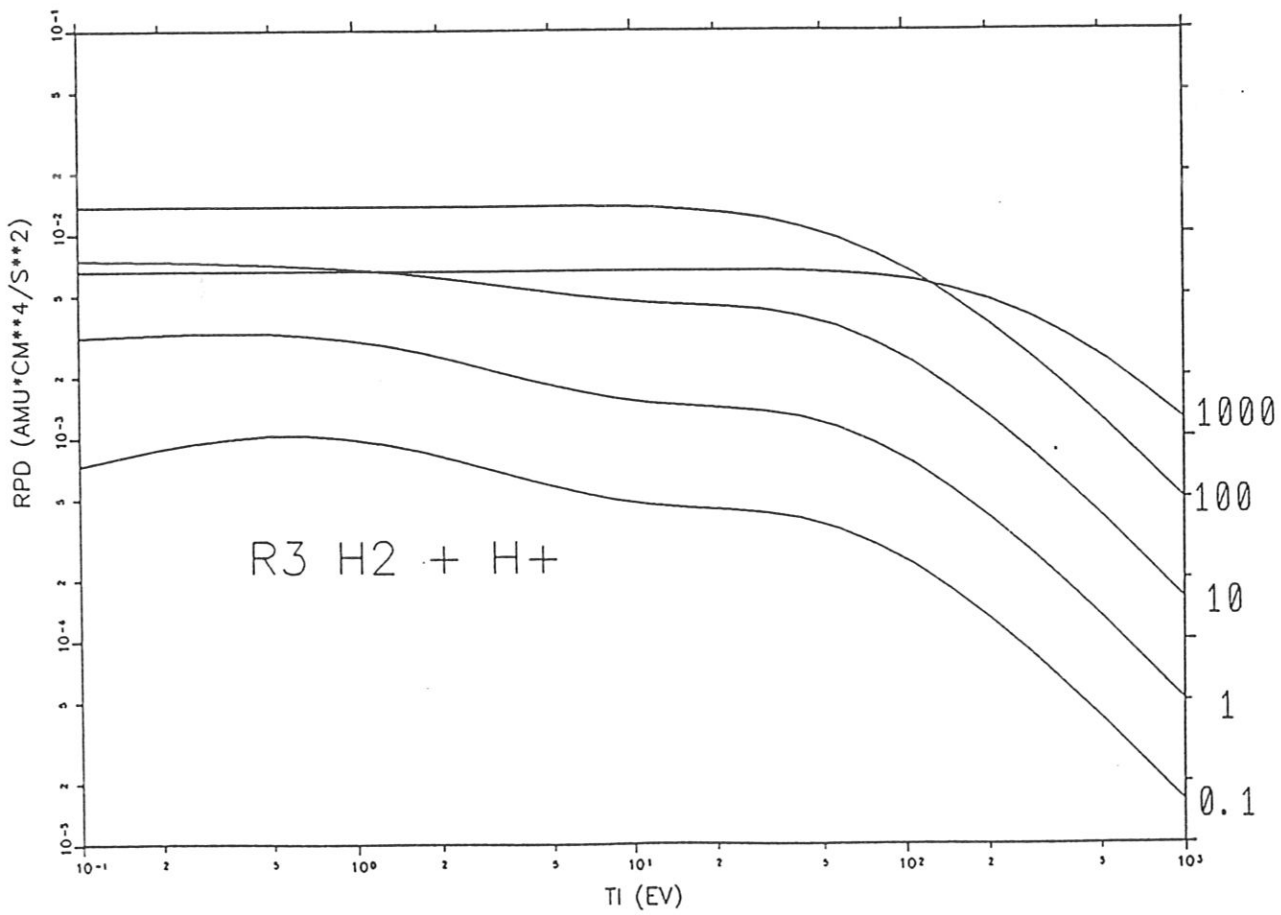

Figure 28: R3 R_{pd} as a function of T_i with the neutral beam energy $E_\alpha(eV)$ as parameter.

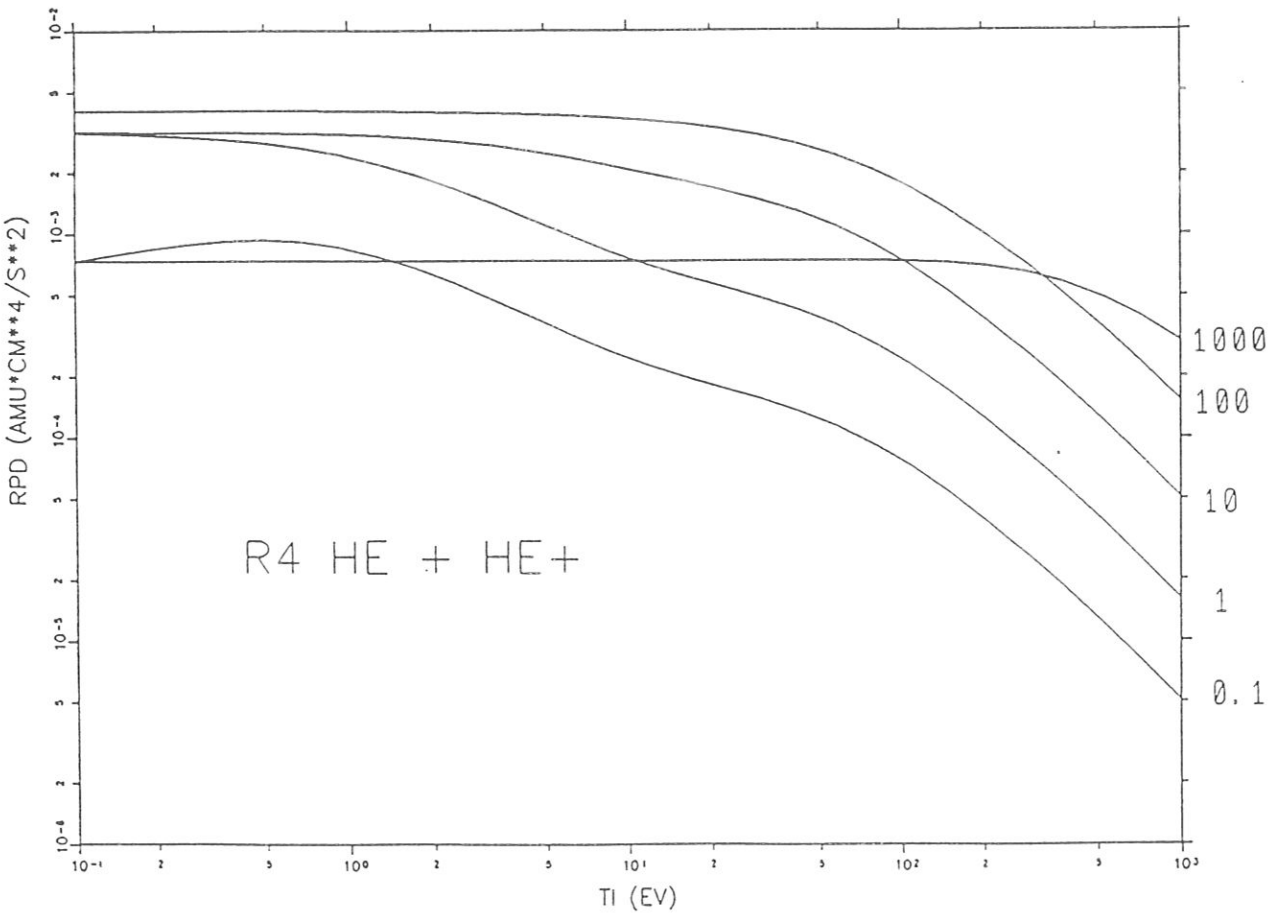

Figure 29: R4 R_{pd} as a function of T_i with the neutral beam energy $E_\alpha(eV)$ as parameter.

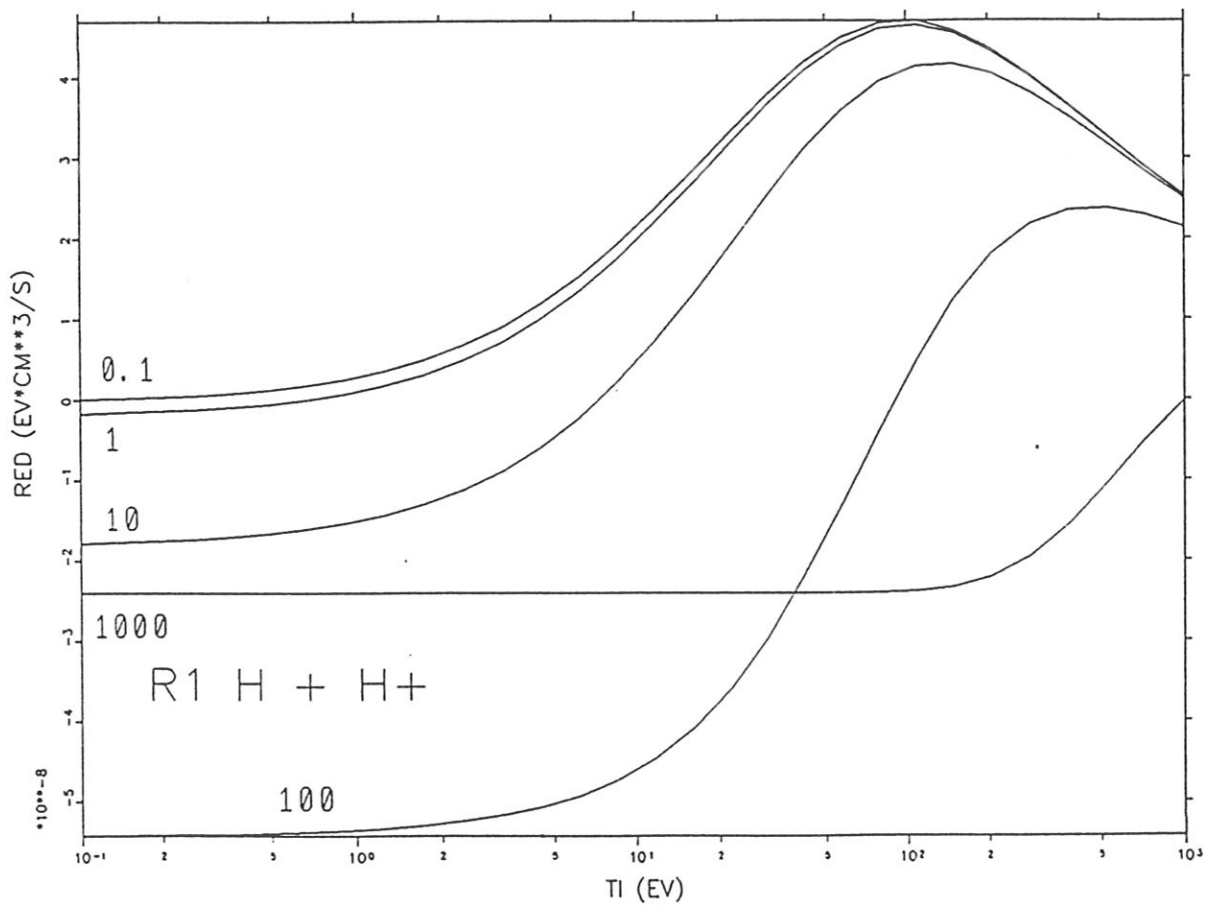

Figure 30: R1 R_{Ed} as a function of T_i with the neutral beam energy $E_\alpha(eV)$ as parameter.

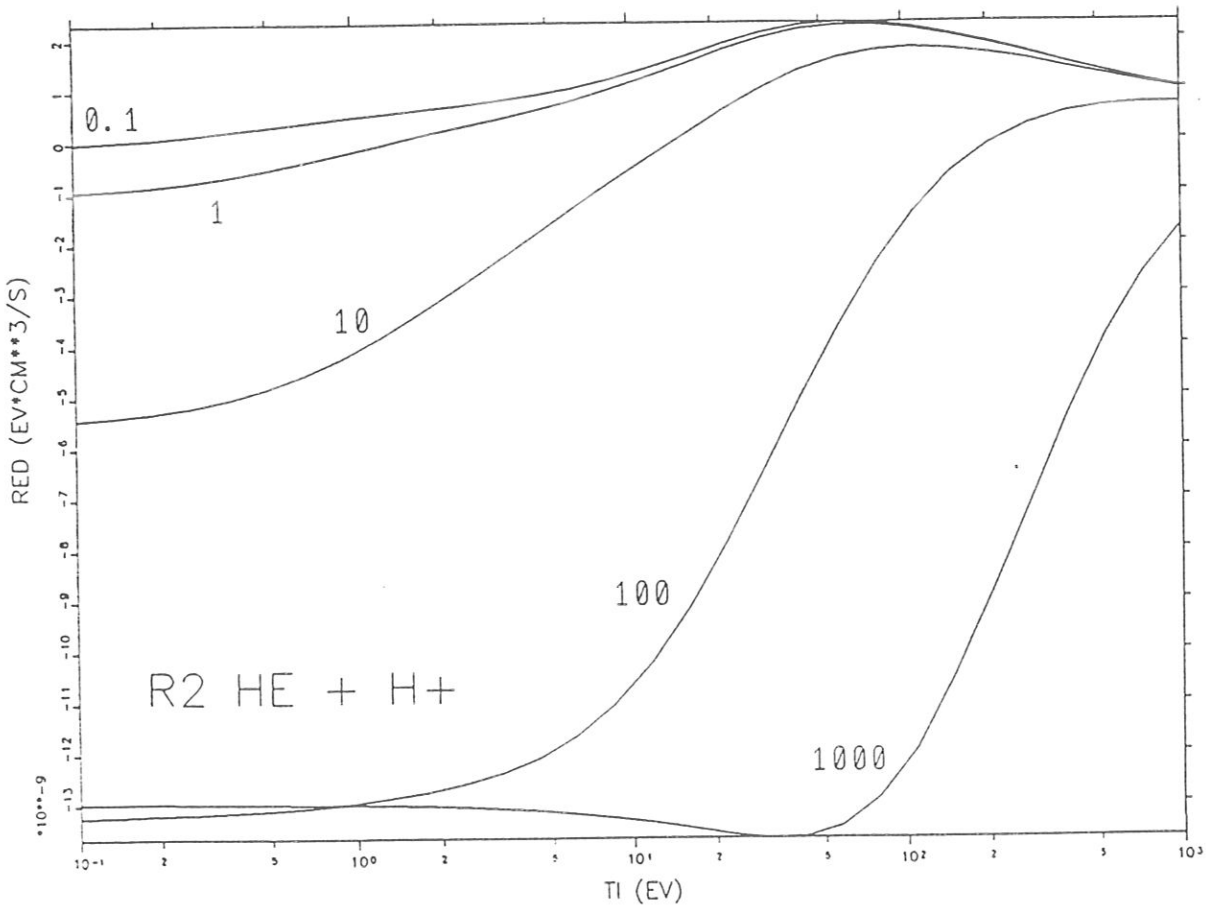

Figure 31: R2 R_{Ed} as a function of T_i with parameter neutral beam energy $E_\alpha(eV)$.

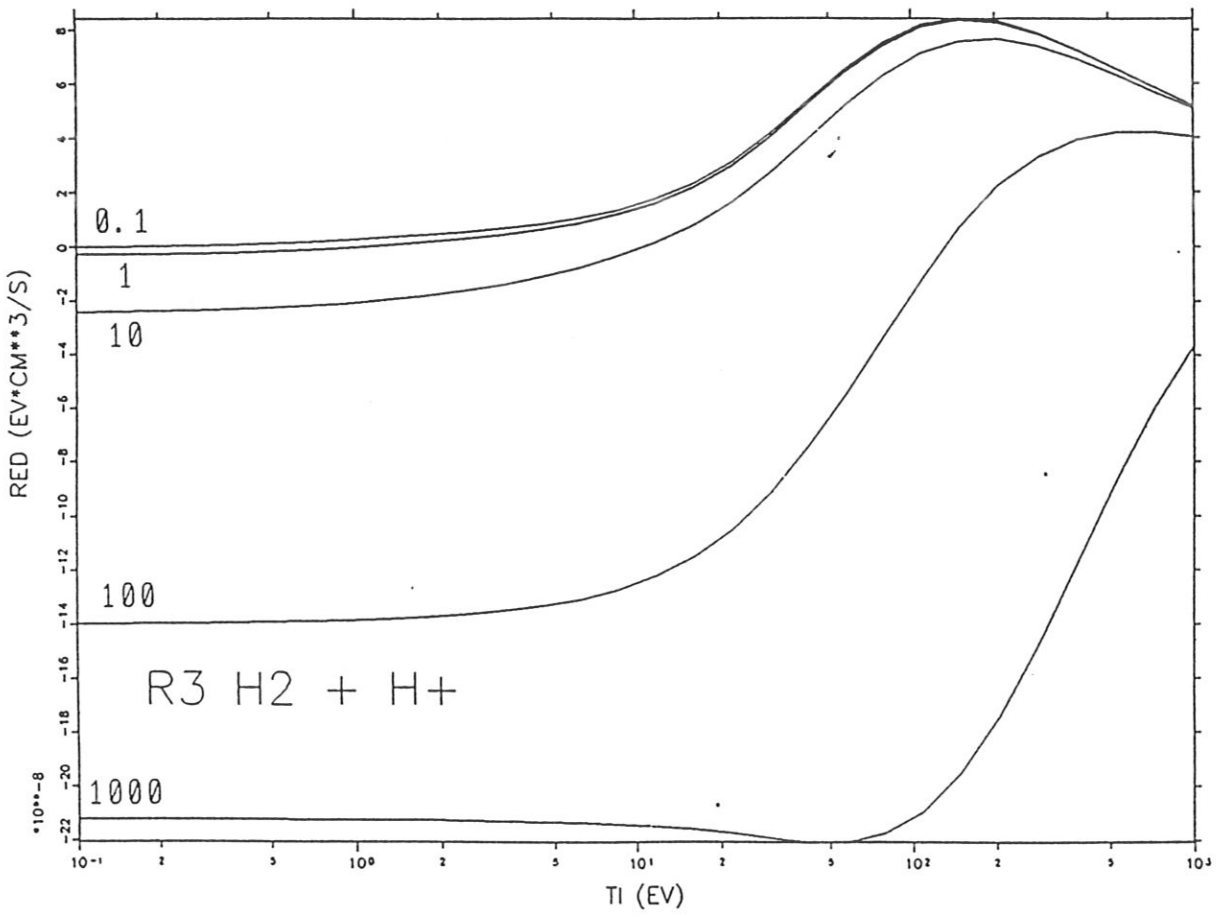

Figure 32: R3 R_{Ed} as a function of T_i with the neutral beam energy $E_\alpha(eV)$ as parameter.

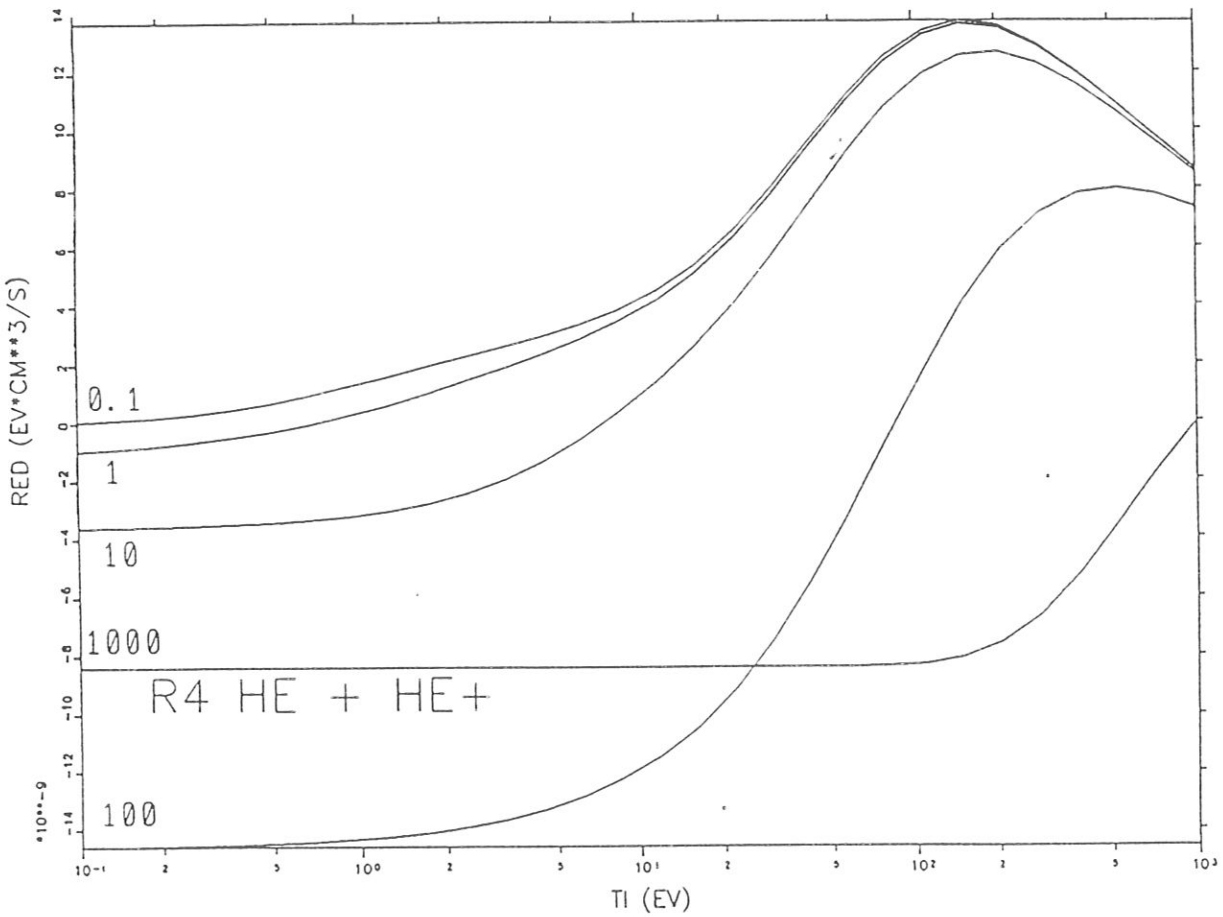

Figure 33: R4 R_{Ed} as a function of T_i with the neutral beam energy $E_\alpha(eV)$ as parameter.

6.2 Rates for Hydrodynamic Description

The collision rates for the hydrodynamic description (section 3.3) are functions of the effective temperature $T_{\alpha,\beta}$ (in eV) and are represented by a one-parameter fit (for $R \equiv 8\Omega^{(0,0)}$ and the $\Omega^{(l,r)}$ integrals), e.g.:

$$\ln\ \Omega^{(l,n)}(T_{\alpha,\beta}) \simeq \sum_{n=0}^{8} a_n^{(l,r)}\ (\ln T_{\alpha,\beta})^n. \tag{113}$$

$R, \Omega^{(1,1)}, \Omega^{(1,2)}, \Omega^{(1,3)}, \Omega^{(2,2)}$:

Figs. 34 (R1), 35 (R2), 36 (R3), 37 (R4)

Fits for R: Tab 17

Fits for $\Omega^{(1,1)}$: Tab 18

Fits for $\Omega^{(2,2)}$: Tab 19

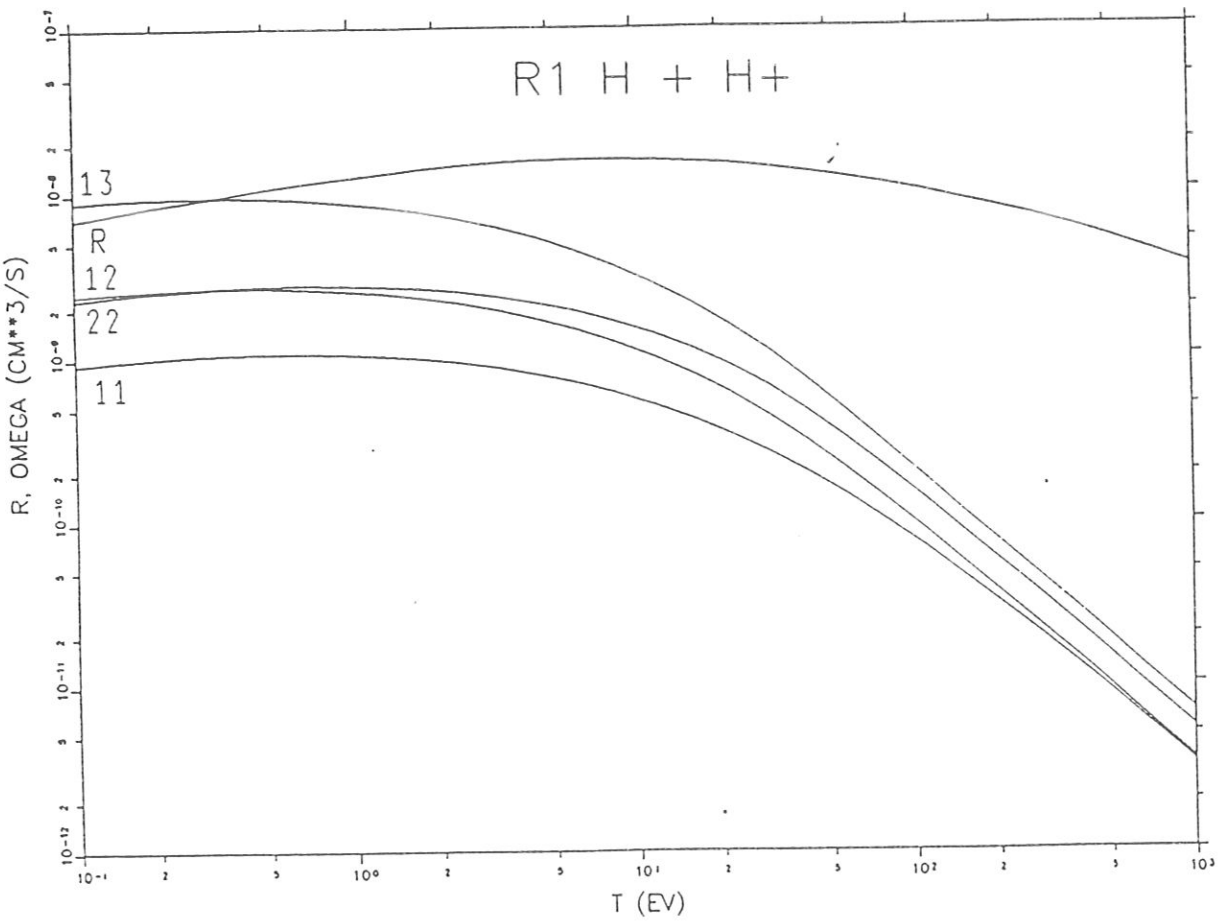

Figure 34: R1 H+ + H $R, \Omega^{(1,1)}, \Omega^{(1,2)}, \Omega^{(1,3)}, \Omega^{(2,2)}$ as a function of the effective temperature $T \equiv T_{\alpha,\beta}$

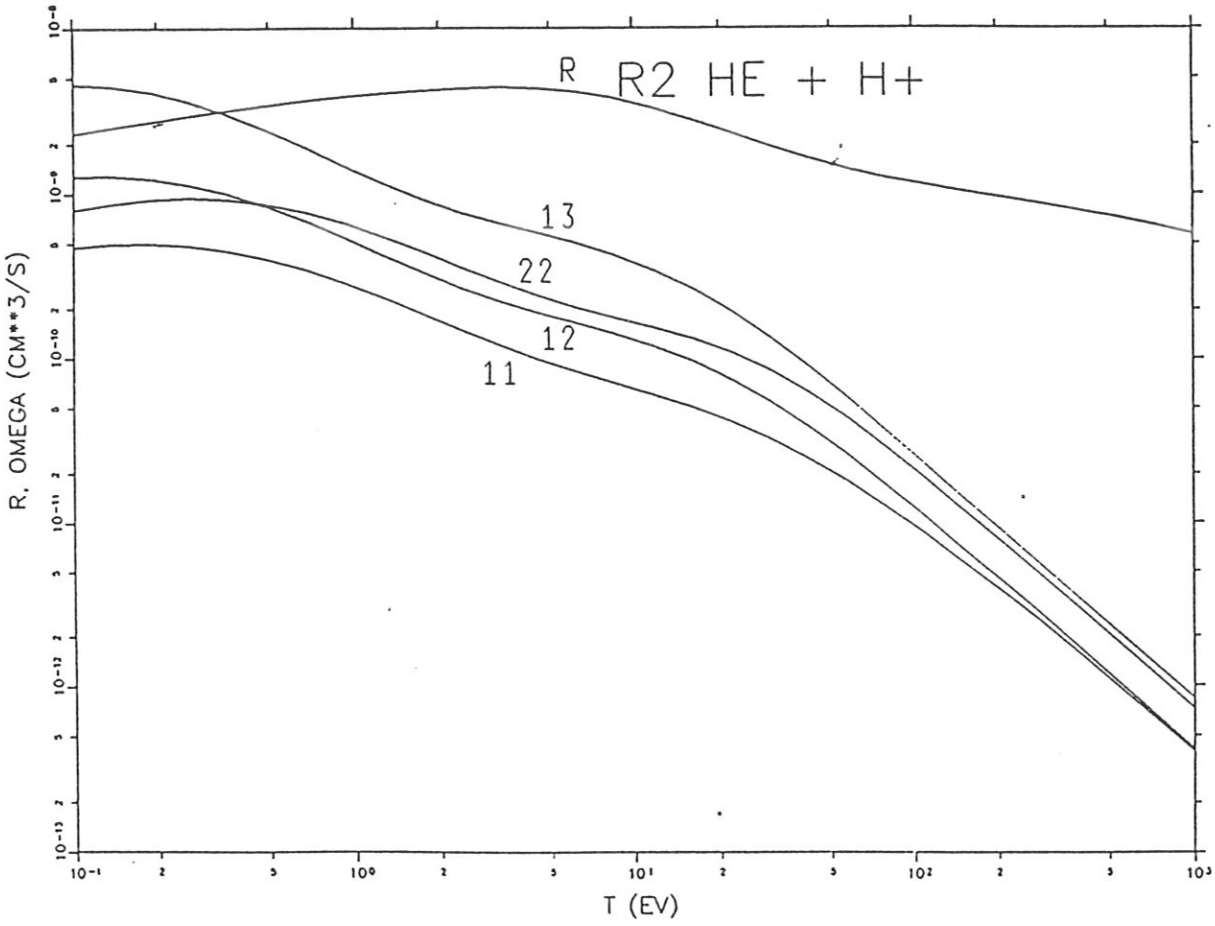

Figure 35: R2 H+ + He $R, \Omega^{(1,1)}, \Omega^{(1,2)}, \Omega^{(1,3)}, \Omega^{(2,2)}$ as a function of the effective temperature $T \equiv T_{\alpha,\beta}$

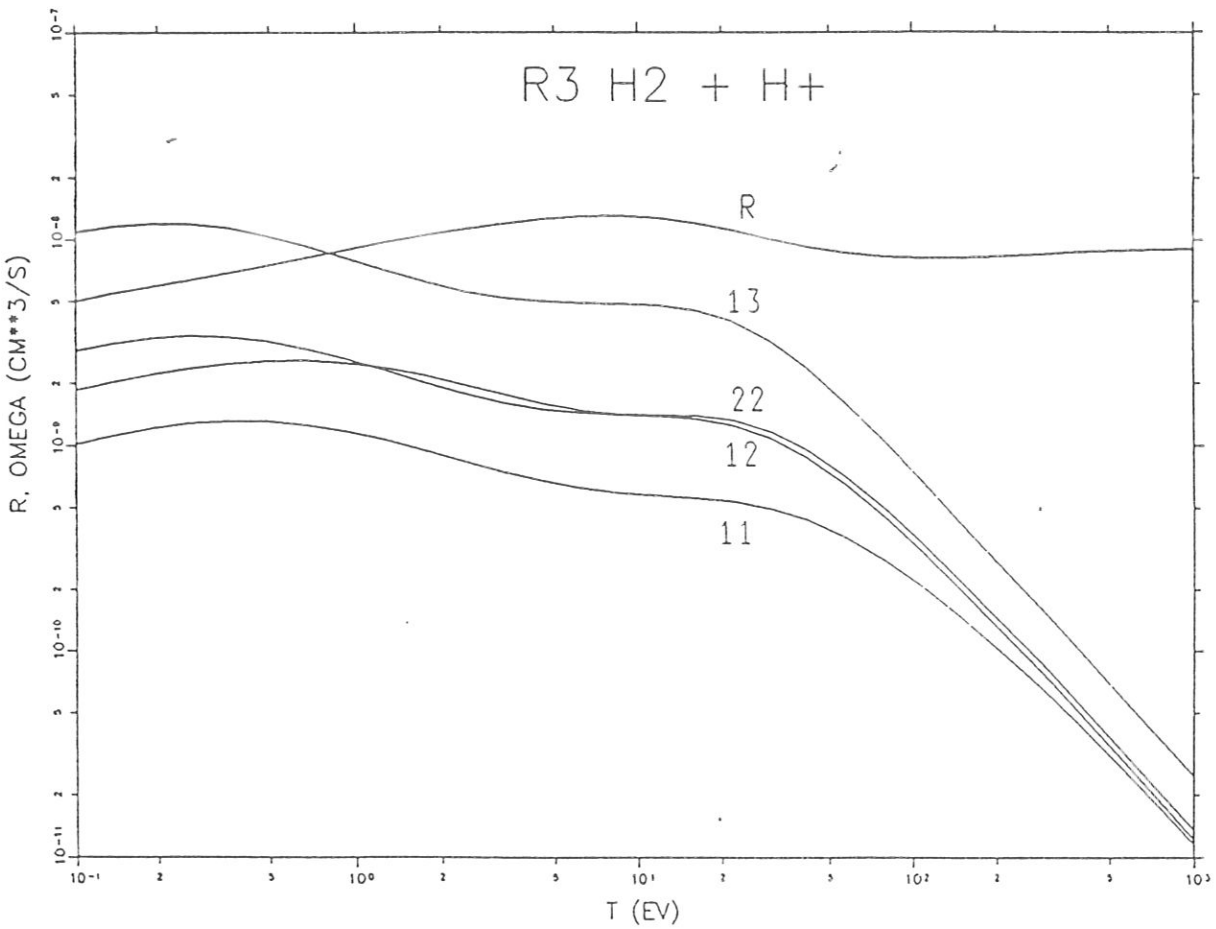

Figure 36: R3 H+ + H2 $R, \Omega^{(1,1)}, \Omega^{(1,2)}, \Omega^{(1,3)}, \Omega^{(2,2)}$ as a function of the effective temperature $T \equiv T_{\alpha,\beta}$

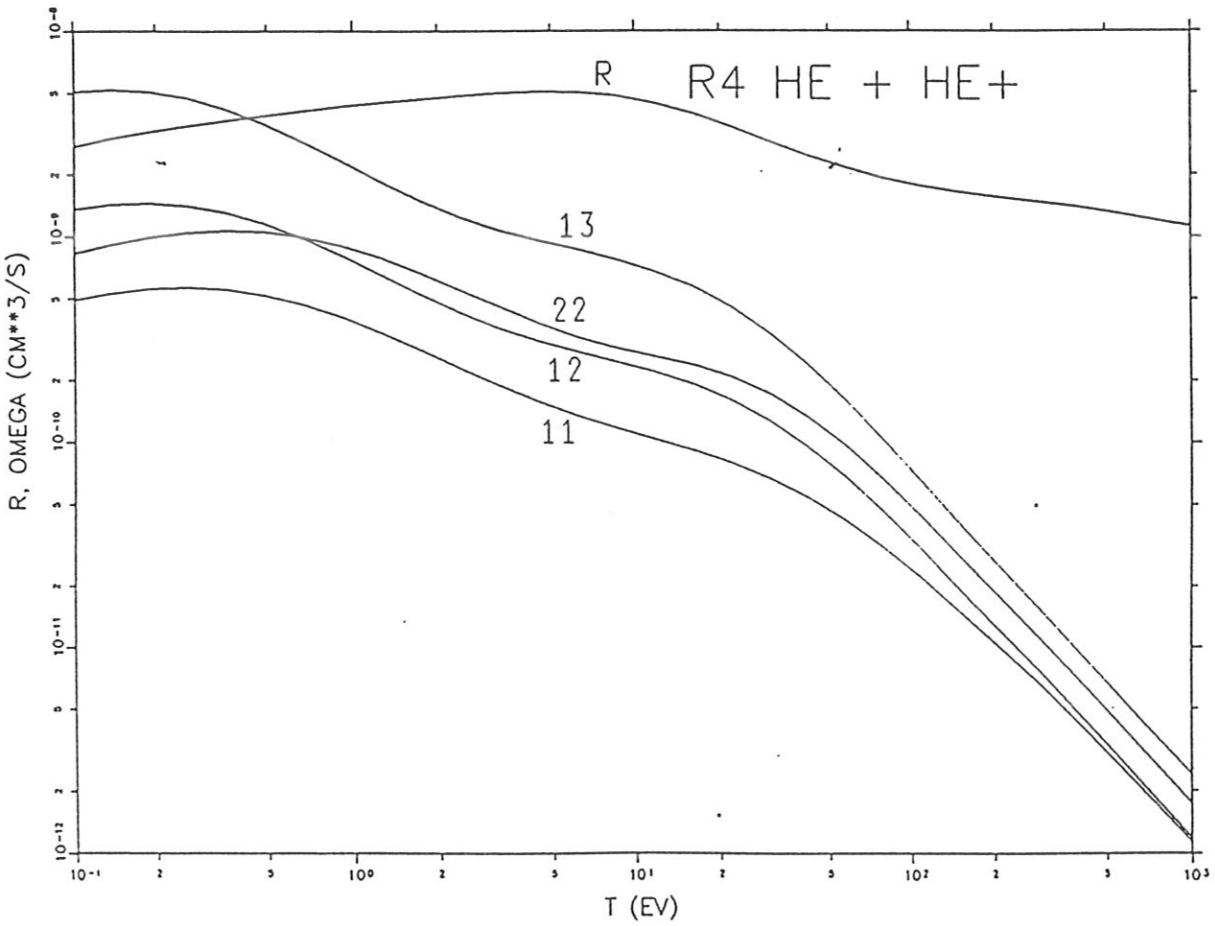

Figure 37: R4 He+ + He $R, \Omega^{(1,1)}, \Omega^{(1,2)}, \Omega^{(1,3)}, \Omega^{(2,2)}$ as a function of the effective temperature $T \equiv T_{\alpha,\beta}$

R(T) (cm**3/s) R1 H + H+

a0 -1.820301019850D+01	a1 2.129097882981D-01	a2 -3.319721546062D-02
a3 -9.219441585651D-03	a4 5.351258558196D-04	a5 3.784499807334D-04
a6 -1.021209574651D-04	a7 1.044107275669D-05	a8 -3.937241365267D-07

R(T) (cm**3/s) R2 H + He

a0 -1.937488793273D+01	a1 1.759108971539D-01	a2 -1.693965011113D-02
a3 -2.164290342772D-02	a4 -1.394395875351D-02	a5 2.443778636181D-03
a6 1.082584067859D-03	a7 -2.740989886580D-04	a8 1.663374157798D-05

R(T) (cm**3/s) R3 H2 + H+

a0 -1.852351664804D+01	a1 2.697718272304D-01	a2 1.350651671297D-02
a3 -1.354211329590D-02	a4 -1.236691940121D-02	a5 1.289363581693D-03
a6 1.027842439916D-03	a7 -2.222408616640D-04	a8 1.252988405338D-05

R(T) (cm**3/s) R4 He + He

a0 -1.927232246647D+01	a1 1.490667894727D-01	a2 2.149231447853D-02
a3 -5.690616121964D-03	a4 -1.908223060123D-02	a5 1.394534352967D-03
a6 1.523437071234D-03	a7 -3.156990924124D-04	a8 1.763329693714D-05

Table 17: R(T)

OMEGA11 (cm**3/s) R1 H + H+

a0 -2.067495970296D+01	a1 -6.754454386651D-02	a2 -6.906186179718D-02
a3 -7.429922782229D-03	a4 -7.808813003874D-05	a5 -1.032158595103D-04
a6 -4.050666345184D-05	a7 1.836578913379D-05	a8 -1.377982388469D-06

OMEGA11 (cm**3/s) R2 H + He

a0 -2.203507049378D+01	a1 -6.666508829508D-01	a2 -7.301634332761D-02
a3 7.285987500237D-02	a4 -7.511137058200D-03	a5 -5.064240875152D-03
a6 1.170265885717D-03	a7 -7.290932193552D-05	a8 3.611435091385D-07

OMEGA11 (cm**3/s) R3 H2 + H+

a0 -2.058948378358D+01	a1 -3.091608300462D-01	a2 -1.157943457107D-01
a3 5.940618635367D-02	a4 9.580654599527D-03	a5 -5.467511099899D-03
a6 -2.415856443530D-04	a7 1.981931289049D-04	a8 -1.443879934691D-05

OMEGA11 (cm**3/s) R4 He + He+

a0 -2.167965486890D+01	a1 -5.460360301179D-01	a2 -1.181746519736D-01
a3 6.762120367287D-02	a4 2.761214449593D-03	a5 -5.300088703885D-03
a6 3.881535032205D-04	a7 7.237252600152D-05	a8 -7.356271943058D-06

Table 18: OMEGA11(T)

OMEGA22 (cm**3/s) R1 H + H+

a0 -1.970770010292D+01	a1 -4.750547016654D-02	a2 -6.717043480643D-02
a3 -5.020232904192D-03	a4 -1.897148429605D-03	a5 -5.978277546350D-04
a6 1.455101056679D-04	a7 6.113726187722D-06	a8 -1.495444636173D-06

OMEGA22 (cm**3/s) R2 H + He

a0 -2.119718118212D+01	a1 -6.047938325697D-01	a2 -1.105016966801D-01
a3 8.754381039703D-02	a4 -4.745795404802D-03	a5 -7.120538441431D-03
a6 1.286949073730D-03	a7 -3.373371121283D-05	a8 -3.452213060435D-06

OMEGA22 (cm**3/s) R3 H2 + H+

a0 -1.982520199889D+01	a1 -2.045986618368D-01	a2 -1.398594524973D-01
a3 5.709736784682D-02	a4 1.535016658865D-02	a5 -7.113316092217D-03
a6 -4.624966207800D-04	a7 2.996893330964D-04	a8 -2.193592594926D-05

OMEGA22 (cm**3/s) R4 He + He

a0 -2.086953660006D+01	a1 -4.470227740985D-01	a2 -1.654791308926D-01
a3 7.173876575209D-02	a4 1.094500514641D-02	a5 -7.279575206851D-03
a6 2.665521010922D-05	a7 2.035371868694D-04	a8 -1.639359039345D-05

Table 19: OMEGA22(T)

7 Appendix 1: Diffusion Cross Section

In this section we discuss the dependence of the diffusion cross section $\sigma^d(E_r)$ on the cut-off angle $\mid \chi_0 \mid$. We relate the diffusion cross section for the cut-off angles $\mid \chi_0 \mid = 0.5, 0.4, 0.3, 0.1, 0.05$ to that calculated for $\mid \chi_0 \mid = 0.01$ as reference value (Figs. 38 - 41). For R1 (Fig. 38) the influence of χ_0 is the greatest at large energies where χ is small. The same behaviour shows the diffusion cross section for the other collision processes for energies larger than E_{r0}. For small energies $E_r \leq E_{rc}$ the cut-off angle has no effect on the result. Deviations may occur between the two characteristic energies. But, however, $\mid \chi_0 \mid = 0.1$ seems to be a good approximation.

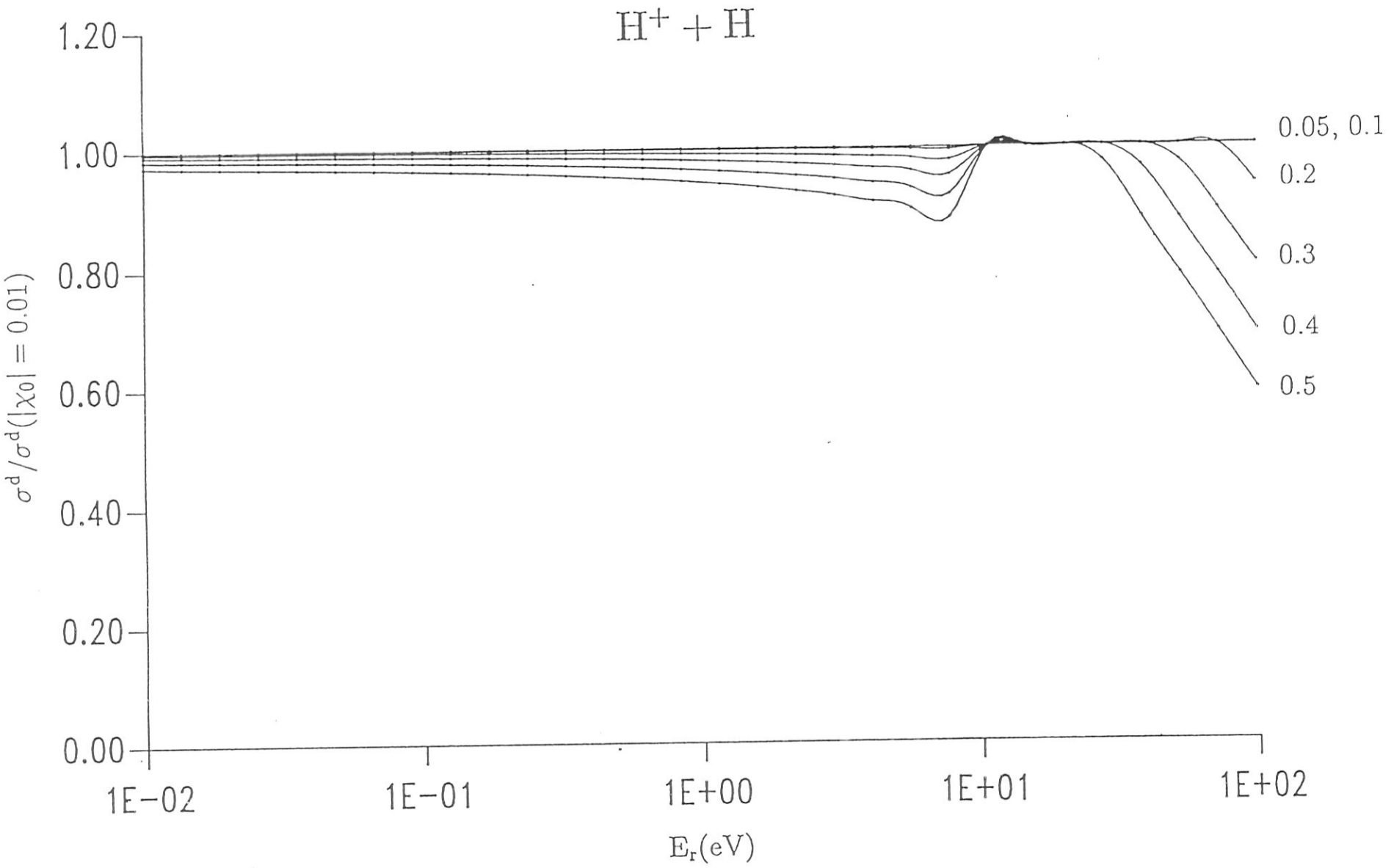

Figure 38: $\sigma^d/\sigma^d(|\chi_0| = 0.01)$ for R1 $H^+ + H$ as function of E_r for different $|\chi_0|$.

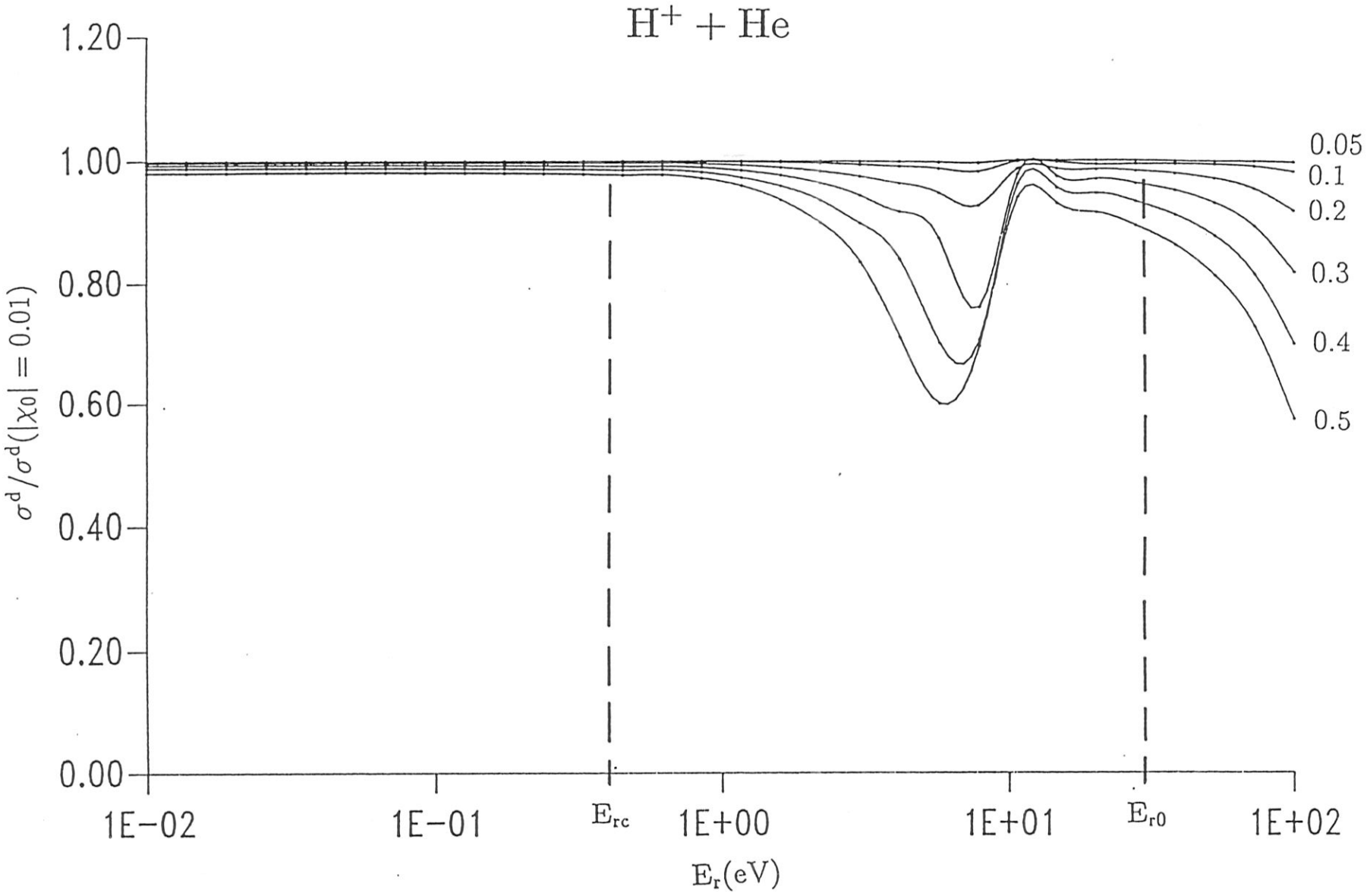

Figure 39: $\sigma^d/\sigma^d(\mid \chi_0 \mid = 0.01)$ for R2 $H^+ + He$ as function of E_r for different $\mid \chi_0 \mid$.

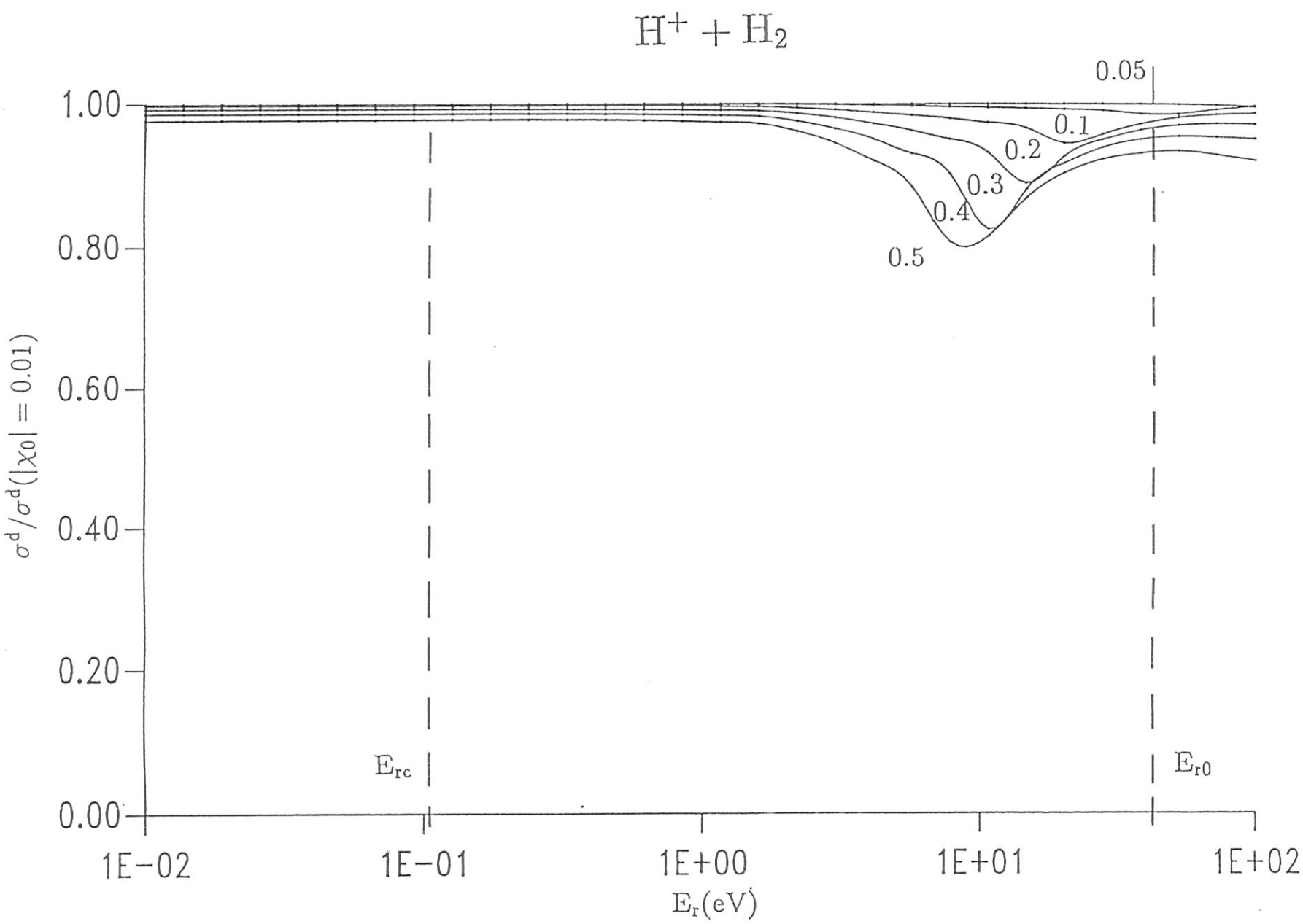

Figure 40: $\sigma^d/\sigma^d(\mid \chi_0 \mid = 0.01)$ for R3 $H^+ + H_2$ as function of E_r for different $\mid \chi_0 \mid$.

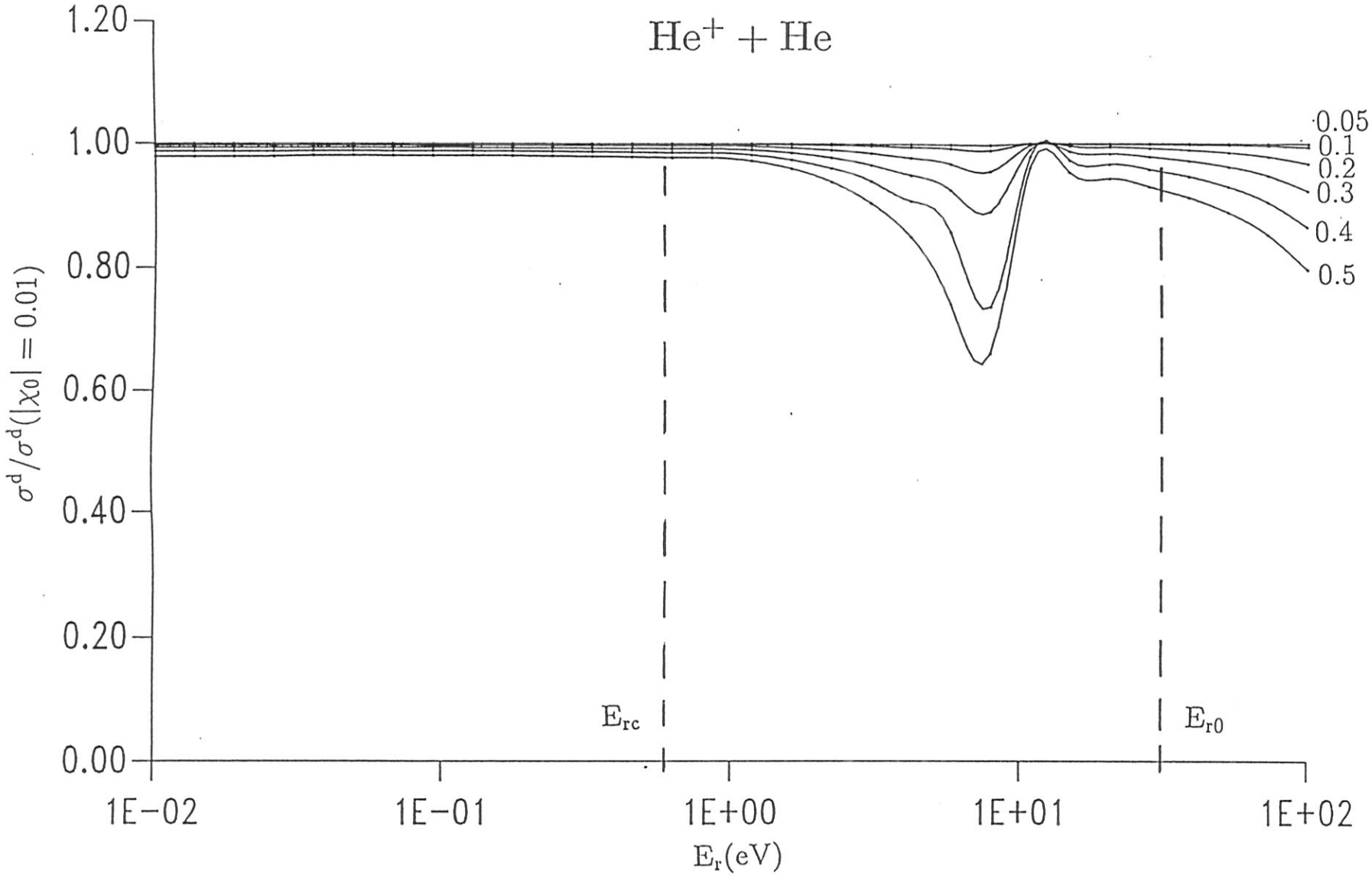

Figure 41: $\sigma^d/\sigma^d(\mid \chi_0 \mid = 0.01)$ for R4 $He^+ + He$ as function of E_r for different $\mid \chi_0 \mid$.

8 Appendix 2: Semi-Classical Approach

Given the fundamental quantum mechanical formulae for the calculation of the elastic cross sections (cf. e.g. [6]):

$$d\sigma/d\Omega = \sigma(\theta, E_r) = \mid f(\theta) \mid^2, \tag{114}$$

$$f(\theta) := \frac{1}{k} \begin{cases} \frac{1}{2i} \sum_{l=0}^{\infty} (2l+1)\ \exp(2i\eta_l)\ P_l(\cos\eta_l), & \theta \neq 0, \\ \sum_{l=0}^{\infty} (2l+1)\ \sin 2\eta_l\ \exp(i\eta_l), & \theta = 0, \end{cases} \tag{115}$$

$$\sigma^t(E_r) = 2\pi \int_0^{\pi} d\theta\ \sin\theta\ \sigma(\theta, E_r) = \frac{4\pi}{k^2} \sum_{l=0}^{\infty} \sin^2\eta_l \tag{116}$$

$$= \frac{4\pi}{k}\ \Im f(0). \tag{117}$$

with $k^2 = 2m_r E_r/\overline{h}^2$. $f(\theta)$ is the scattering amplitude, η_l the lth order phase shift. $P_l(\cos\theta)$ are Legendre's Polynomials.

We assume additionally the following WKB expression for the phase shifts (cf. [6]) as being valid:

$$\eta_l = k \left(\int_{r^*}^{\infty} dr \left[1 - \frac{V(r)}{E_r} - \left(\frac{l+1/2}{kr} \right)^2 \right]^{1/2} - \int_b^{\infty} dr \left[1 - \left(\frac{l+1/2}{r} \right)^{1/2} \right]^{1/2} \right). \tag{118}$$

Semi-classical methods compute cross sections (i) by means of the above formulae replacing there the sums by integrals and (ii) using appropriate approximations for the Legendre functions. The first assumption is justified when the number of contributing terms is large. The second assumption restricts the range of validity of the parameters for Legendre's polynomials. The most employed approximation (ii) which has often been described in the literature (cf. [6]),

$$P_l(\cos\theta) \simeq \left(\frac{2}{\pi l \sin\theta} \right)^{1/2} \cos\left[(l+1/2)\theta - \pi/4 \right], \tag{119}$$

is valid only for $l \sin\theta >> 1$.

The main results of this approximation are used here:

Identifying

$$E_r \equiv k^2\overline{h}^2/2m_r,\ L \equiv (l+1/2)\overline{h} \equiv m_r v_r b \equiv k\overline{h}b, \tag{120}$$

(L is the angular momentum)

$$\chi(b, E_r) = \frac{2}{k} \frac{\partial}{\partial b} \eta(b, E_r), \tag{121}$$

which relates the classical deflection function χ eq. (5) to the WKB phase shift eq. (118).

Because we want to calculate the total cross section σ^t only in order to justify are classical approach of section 2, especially the $\mid \chi_0 \mid = 0.1$ approximation, we use as the starting point of our semi-classical calculations not the scattering amplitude but the expression (116) in its integral form

$$\sigma^t(E_r) \cong 4\pi \int_0^\infty 2bdb \ \sin^2 \eta(b, E_r). \tag{122}$$

Contrary to the classical total cross section (7) the semi-classical one is weighted by the phase shift and is only divergent for potentials $V \sim r^{-a}, a \leq 2$ [16].

Because the fully WKB expression (118) for the phase shift is not so easy to be numerically computed, a simplified expression has often been used which results from eq. (118) for the case that b is sufficiently large so that $V(r)$ can be treated as a perturbation. The result is:

$$\eta \cong -\frac{k}{2E_r} \int_b^\infty dr \ V(r) \left(1 - b^2/r^2\right)^{-1/2}. \tag{123}$$

The philosophy of the following semi-classical approach is to use

(i) the exact relation (121),

(ii) the exact expression (5) for the deflection function χ and

(iii) the approximated expression (123) for the phase shift function η.

Case I: Repulsive potential

In Fig. 42 the qualitative behaviour of the phase shift η and the deflection function χ which are related to one another according to eq. (121) is displayed. η is like χ a one-to-one relation of b. For Case I it is always negative and increases monotonically to 0 for increasing b.

We compute the total cross section σ^t by means of eq. (122) and break up the integral into two parts as follows (cf. e.g. [19]):

$$\sigma^t(E_r) \cong 4\pi \left(\int_0^{b_4} 2bdb + \int_{b_4}^\infty 2bdb \right) \sin^2 \eta(b, E_r) \tag{124}$$

$$\simeq 4\pi \left[\frac{b_4^2}{2} + \int_{b_4}^\infty 2bdb \ \eta^2(b, E_r) \right] \tag{125}$$

with

$$b_4(E_r) := \{b : \eta(b, E_r) = \eta_0\}. \tag{126}$$

In the first integral $\sin^2\eta$ is replaced by its mean value $1/2$ and in the second one $\sin^2 \simeq \eta^2$. b_4 is calculated solving the eq. (126). η_0 has to be estimated by the last condition resulting in $\eta_0 \sim 1$. Then η indeed is small so that the approximation eq. (123) can be used.

In Fig. 43 classical and semi-classical results for the total cross section are shown for the collisions process R1 $H^+ + H$ for $\eta_0 \sim \pi/2$ and 1 which leads to a satisfactory agreement with the classical result for $\chi_0 \sim 0.1$. As known, the semi-classical cross section does not depend very strongly on the precise value of the the parameter η_0. But, however, it is somewhat larger than our classical result.

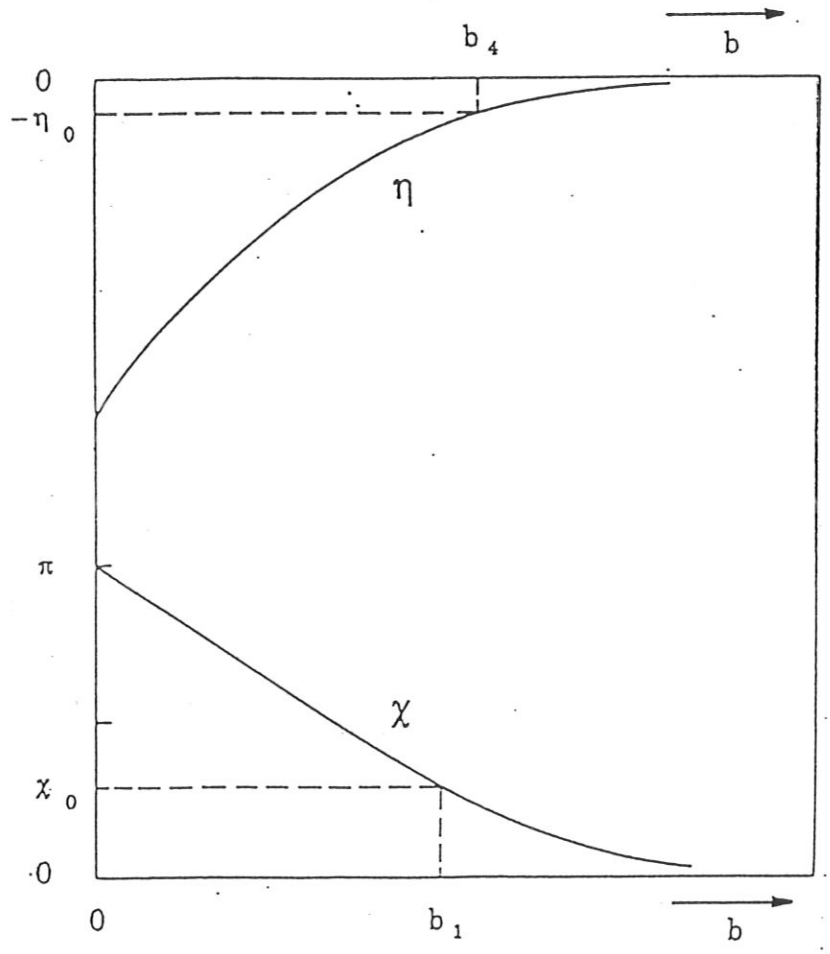

Figure 42: Qualitative behaviour of the WKB phase shift η and the classical deflection function χ for Case I (repulsive potential).

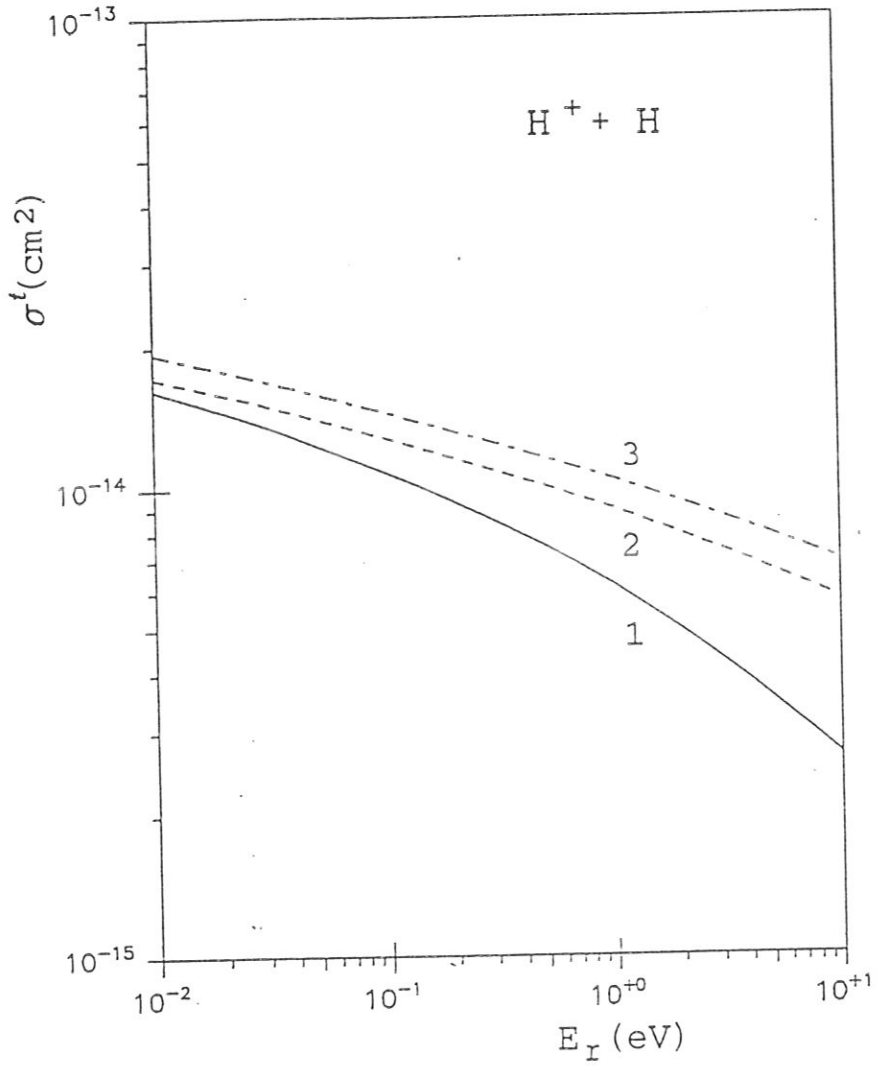

Figure 43: Classical and semi-classical total cross section calculations for elastic $H^+ + H$ collisions. 1 - classical for $\chi_0 = 0.1$, 2 - semi-classical for $\eta_0 = \pi/2$, 3 - semi-classical for $\eta_0 = 1$.

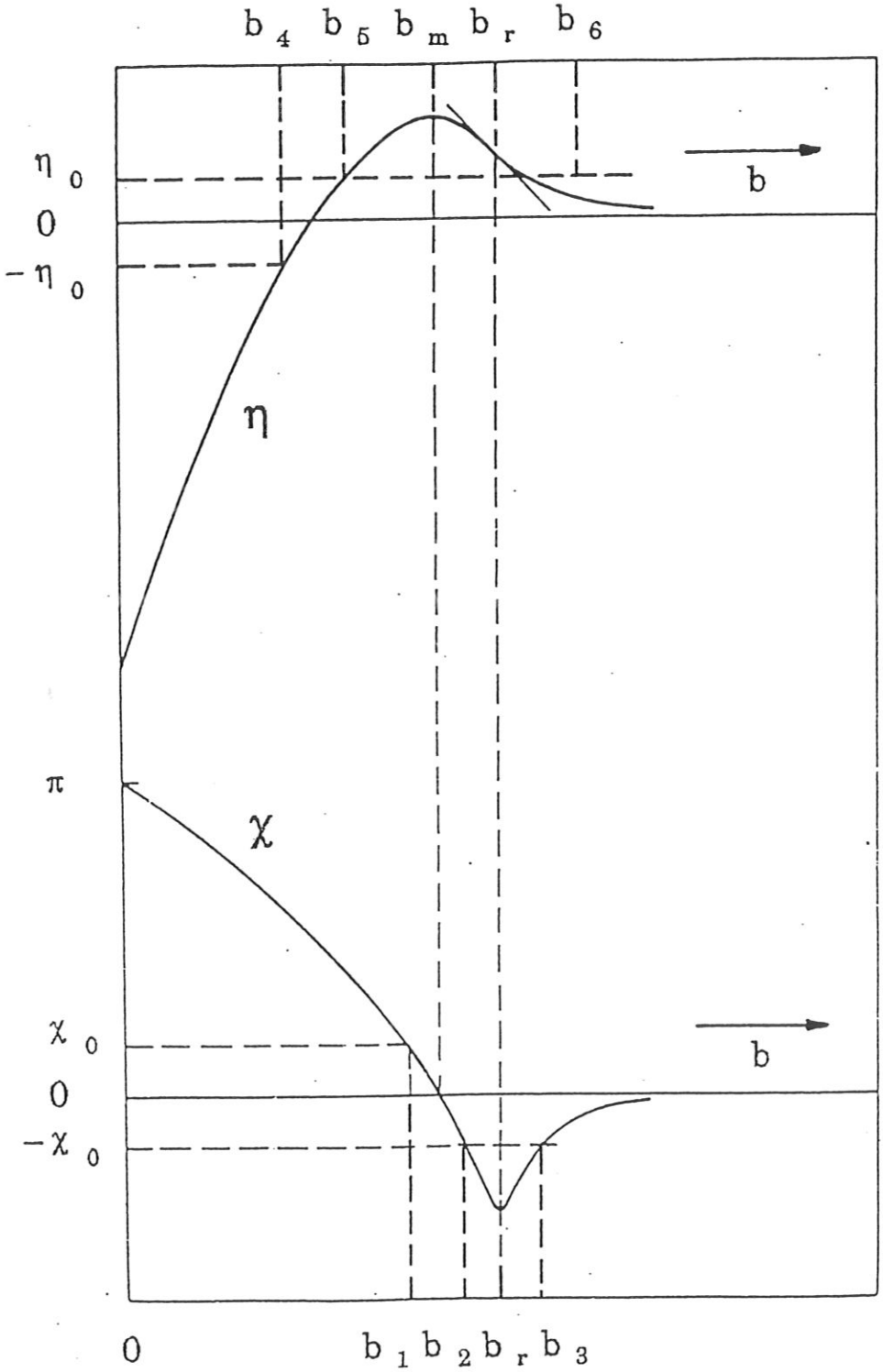

Figure 44: Qualitative behaviour of the WKB phase shift η and the classical deflection function χ for Case II (short range repulsive - long range attractive potential.

Case II: Morse-like potential

The qualitative behaviour of χ and η for Case II is shown in Fig. 44. η increases with increasing b from negative values, crossing the zero line to a maximium b_m which corresponds to the *glory* angle $\chi = 0$. Then it tends to $+0$ for $b \to \infty$.

The total cross section σ^t now results in

$$\sigma^t(E_r) \cong 4\pi \left(\int_0^{b_4} + \int_{b_4}^{b_5} + \int_{b_5}^{b_6} + \int_{b_6}^{\infty} \right) 2bdb \, \sin^2\eta(b, E_r) \tag{127}$$

$$\simeq 4\pi \left[\frac{1}{2}\left(b_4^2 - b_5^2 + b_6^2\right) - \int_{-\infty}^{\infty} bdb \, \cos 2\eta + \left(\int_{b_4}^{b_5} + \int_{b_6}^{\infty} \right) 2bdb \, \eta^2 \right]. \tag{128}$$

The first integral in eq. (128) can be calculated using the method of stationary phases. $\eta(b)$ can be expanded near the maximum b_m:

$$\eta(b, E_r) \cong \eta_m + \beta(b - b_m)^2, \; \beta = \frac{1}{2}\frac{\partial^2}{\partial b^2}\eta(b = b_m, E_r). \tag{129}$$

Calculating this integral we obtain the final expression for the total cross section σ^t:

$$\sigma^t(E_r) \cong 4\pi \left[\frac{1}{2}\left(b_4^2 - b_5^2 + b_6^2\right) - b_m\sqrt{\frac{\pi}{2 \mid \beta \mid}} \cos\left(2\eta_m - \frac{\pi}{4}\right) + \left(\int_{b_4}^{b_5} + \int_{b_6}^{\infty} \right) \eta^2(b, E_r) \right]. \tag{130}$$

The impact parameters $b_i(E_r)$ are defined as follows (s. Fig. 44):

$$b_i(E_r) := \{b : \mid \eta(b, E_r) \mid = \eta_0 \wedge b_4 \leq b_5 \leq b_6\}, \; i = 4, 5, 6; \tag{131}$$

and $b_5 \leq b_m \leq b_r$.

According to relation (121) it follows

$$\beta = \frac{k}{4}\frac{\partial}{\partial b}\chi(b = b_m, E_r). \tag{132}$$

b_m is the b value where $\chi = 0$. We expand χ near b_m

$$\chi \cong \frac{4\beta}{k}(b - b_m) \tag{133}$$

with (132). Then η follows by integration:

$$\eta = \eta_0 + \frac{\beta}{2}\int_{b_5}^{b} d\tilde{b} \, (\tilde{b} - b_m) \cong \eta_0 + \beta\left[(b - b_m)^2 - (b_5 - b_m)^2\right], \tag{134}$$

from which η_m can be obtained:

$$\eta_m \cong \eta_0 - \beta(b_5 - b_m)^2, \tag{135}$$

provided that this expansion is valid. Note that the relation (121) was used whose validity requires that one of the approximation eq. (119) which ceases to be valid for $\theta = 0$. But on the other hand we can χ expand near the rainbow point b_r which leads to

$$\chi \cong \chi_r + \gamma(b - b_r)^2, \gamma = \frac{1}{2}\frac{\partial^2}{\partial b^2}\chi(b = b_r, E_r) \tag{136}$$

and

$$\eta \cong \eta_0 + \frac{k}{2}\chi_r(b - b_6) + \frac{k\gamma}{6}\left[(b - b_r)^3 - (b_6 - b_r)^3\right] \tag{137}$$

from which η_m can also be calculated. If one does this, the Airy function Ai(x) which is the familar special function in the rainbow theory, will appear in the final expresssion for the cross section.

Consider at last the two limiting cases for estimating the cross section:

(i) b_6 large (rainbow case):

$$\sigma^t \simeq 4\pi\left[\frac{b_6^2}{2} - b_m\sqrt{\frac{\pi}{2 \mid \beta \mid}}\cos\left(2\eta_m - \frac{\pi}{4}\right)\right]. \tag{138}$$

(ii) $b_5 \simeq b_m \simeq b_r \simeq b_6$ (glory case)

$$\sigma^t \simeq 4\pi\left[\frac{b_4^2}{2} + \int_{b_4}^{\infty} 2bdb\ \eta^2(b, E_r)\right] \tag{139}$$

which indeed is the result (125) for Case I so that this case is also included in our final expression (130).

In Fig. 45 classical and semi-classical cross section calculations for the collision process R2 $H^+ + He$ are shown for the same parameters as in Fig. 43. The differently calculated results agree rather satisfactorily.

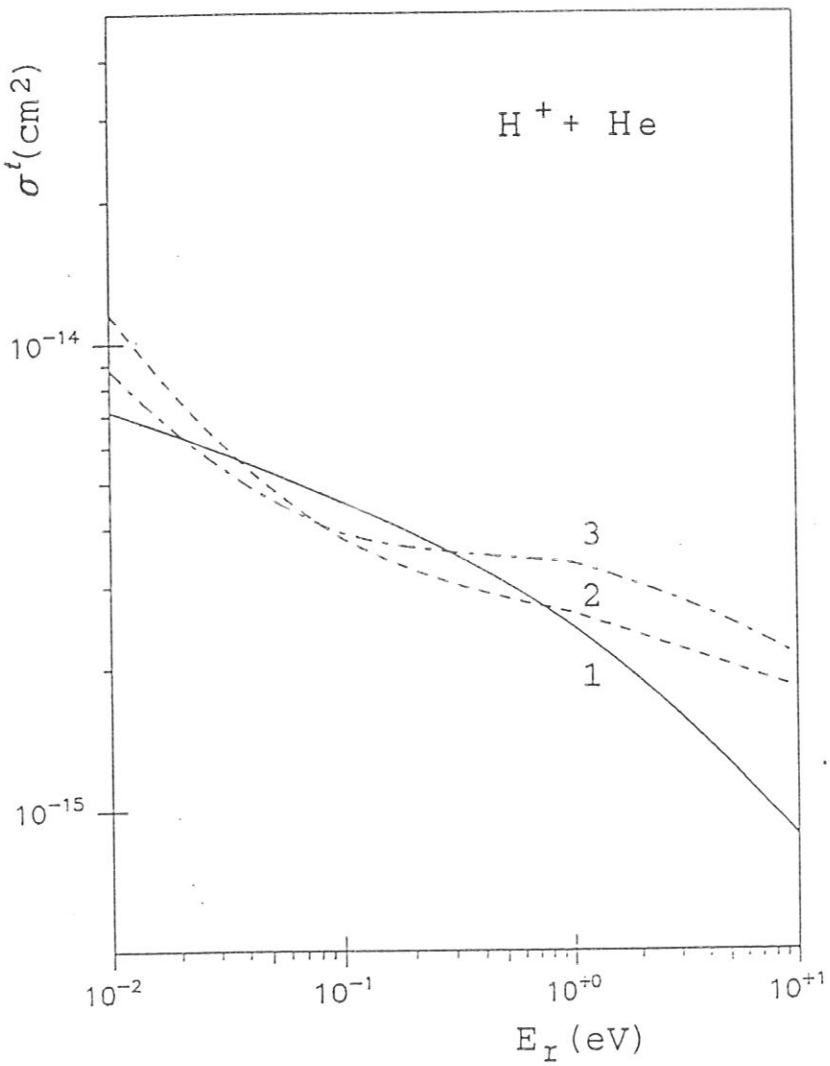

Figure 45: Classical and semi-classical total cross section calculations for elastic $H^+ + He$ collisions. 1 - classical for $\chi_0 = 0.1$, 2 - semi-classical for $\eta_0 = \pi/2$, 3 - semi-classical for $\eta_0 = 1$.

9 Concluding Remarks

The aim of this report is to provide data for elastic collisions between neutral particles and ions in such a format that they may easily be implemented in neutral gas transport codes.

We derived a complete and consistent set of data on the basis of the classical theory of binary collisions. This applies at first to the following quantities: classical deflection angle χ, total, diffusion and viscosity cross sections. Because the potentials, used in this paper, have an infinite range, the total cross section becomes infinite. So a cut-off angle $\mid \chi_0 \mid = 0.1$ was introduced to obtain a finite value. This result was obtained by evaluating the diffusion cross section (considered as the physically more relevant quantity with regard to transport effects) for a decreasing sequence of cut-off angles until it does not change significantly anymore. Furthermore, a semi-classical approach for calculating the total cross section was developed which supports the above choice. However, this problem could be dealt with more rigorously in a quantum mechanical treatment only.

Polynomial fits to the cross sections are presented together with asymptotic representations. These results were used to calculate collision rates (i.e. Maxwellian averaged momentum and energy exchange rates) that enter both kinetic and hydrodynamic transport models. Fits to those integrals which determine these rates are also given.

Though this report is concentrated on elastic collisions in hydrogen-helium plasmas, both methods of solution and algorithms may also be applied to other collision processes.

Data and data fits will be made avalaible by the authors on request.

Acknowledgements

The authors would like to thank Dr. D. Reiter (Jülich) for many valuable suggestions and critical comments to this paper. We also gratefully acknowledge M. Dewitz, P. Börner and B. Küppers for their assistance during the preparation of this report.

References

[1] H.H. Abou-Gabal, G.A. Emmert, Nucl. Fusion 31(1991)407.

[2] M. Abramowitz, I.A. Stegun (eds.), Handbook of Mathematical Functions, New York 1968.

[3] P. Bachmann, D. Reiter, Max-Planck-Institut Report IPP 8/1 (May 1992).

[4] P. Bachmann, D. Reiter, A.K. Prinja, J. Nucl. Mat. 196-198(1992)865

[5] G.A. Bird, Molecular Gas Dynamics, Oxford 1976.

[6] M.S. Child, Molecular Collision Theory, Academic Press 1974.

[7] E. Cupini, A. De Matteis, ENEA Report RT/TIB/87/33.

[8] E. Cupini, A. De Matteis, IL NUOVO CIMENTO 11D(1089)1489.

[9] V.E. Golant, A.P. Zhilinsky, I.E. Sakharov, Fundamentals of Plasma Physics, John Wiley Sons, New York 1980

[10] G. Haas, D. Düchs, J. Ehrenberg, et al., EPS Berlin 1991, Contr. Papers III-101; G. Haas, P. Bachmann, D. Düchs, et al., J. Nucl. Mat. 196-198(1992)481

[11] F.J. de Heer, in: M.R.C. Mc Dowell, A.M. Ferendeci (Eds.), Atomic and Molecular Processes in Controlled Thermonuclear Fusion, New York 1980, p. 351.

[12] O. Hirschfelder, C.F. Curtiss, R.B. Bird, Molecular Theory of Gases and Liquids, Wiley, New York 1954.

[13] R.K. Janev, W.D. Langer, K. Evans Jr., D.E. Post Jr., Elementary Processes in Hydrogen-Helium Plasmas, Springer-Verlag 1987.

[14] H. Kastelewicz, R. Schneider, D. Reiter, et al., Contrib. Plasma Phys. 32(1992)456.

[15] Z. Kopal, Numerical Analysis, London 1961.

[16] L.D. Landau, E.M. Lifschitz, Lehrbuch der theoretischen Physik, Band III, Quantenmechanik, Akademie-Verlag, Berlin 1965.

[17] E.A. Mason, J.T. Vanderslice, Phys. Rev. 114(1959)497.

[18] H.-U. Mittmann, H.-P. Weise, A. Ding, Z. Naturforsch. 26a(1971)1112

[19] N.F. Mott, H.S.W. Massey, The Theory of Atomic Collisions Collisions, Clarenden Press, Qxford 1965

[20] H.M. Mott-Smith, Phys. Fluids 3(1960)721.

[21] M.L. Watkins, P.H. Rebut, Proc. Inter. Conf. on Plasma Physics, 19th EPS, Innsbruck 1992, 16C, II-731

[22] A.V. Phelps, J. Phy. Chem. Ref. Data 19(1990)653

[23] D. Reiter, Report JÜL-1947 (1984);
D. Reiter, Report JÜL-2599 (1992).

[24] D. Reiter, P. Bachmann, A.K. Prinja, Contrib. Plasma Phys. 32(1992)261

[25] D. Reiter, J. Nucl. Mat. 196-198(1992)80

[26] R. Schneider, D. Reiter, H.P. Zehrfeld, et al., J. Nucl. Mat. 196-197(1992)810

[27] R. Schneider, B. Braams, D. Reiter, et al., Contrib. Plasma Phys. 32(1992)450

[28] K. Suchy, in: Handbuch der Physik, Band XLIX/7, p. 57, Berlin, Heidelberg, New York, Tokyo 1984.

[29] H.-P. Weise, H.-U. Mittmann, A. Ding, A. Henglein, Z. Naturforsch. 26a(1971)1122